INVESTIGATION ON STRATERGIES TO MINIMIZE IMPACTS OF GLOBAL TEMPERATURE RISE ON AIR CONDITIONING COOLING LOAD DEMAND OF EXISTING BUILDINGS

Serasinghe S.V.I.R.V.

208051X

Degree of Master of Philosophy

Department of Mechanical Engineering

Faculty of Engineering

University of Moratuwa

Sri Lanka

December 2024

DECLARATION

I declare that this is my own work, and this thesis/dissertation does not incorporate without acknowledgement any material previously submitted for a degree or diploma in any other University or Institute of higher learning and to the best of my knowledge and belief it does not contain any material previously published or written by another person except where the acknowledgement is made in the text. I retain the right to use this content in whole or part in future works (such as articles or books).

Signature: Date: 2024/11/17

The above candidate has carried out research for the MPhil thesis/dissertation under my supervision. I confirm that the declaration made above by the student is true and correct.

Name of the supervisor: Dr. N. A. I. D. Nissanka

Signature of the supervisor: ………………………… Date: ……2024/11/30…

Name of the supervisor: Dr. M. A. Wijewardane

Signature of the supervisor: ………………………… Date: …2024/11/30……

ACKNOWLEDGMENT

I would like to thank my supervisors Dr. Indrajith D. Nissanka and Dr. Anusha Wijewardane for giving me this opportunity and for their patience and support in keeping me on track to complete this degree. My gratitude goes towards Dr. Inoka Manthilake for chairing my progress review panel and the valuable advice. I thank the Department of Mechanical Engineering, and the academic and non-academic staff for giving me support during this degree. My appreciation also goes out to my family and friends for their encouragement and support all throughout my studies.

My special thanks goes to Mr. Sameera Jayarathne and Mr. L. D. Jaysuriya of Central Environment Authority, Sri Lanka for providing outdoor temperature data. Also, I would like to acknowledge Ms. Thuthiprabha, Mr. Thalangama and Mr. Parakrama from Western Provincial Council, Sri Lanka for granting permission to collect data in their building premises.

The research project leading to this thesis was funded by Senate Research Committee (SRC) grant of the University of Moratuwa, Sri Lanka (Grant no: SRC/LT/2020/09).

ABSTRACT

Energy demand for building air conditioning and heating account for a significant fraction of the global electricity demand. With global average temperatures projected to increase throughout the 21st century, building energy demand and consumption are slated to also increase. Even though climate resilient building energy management has been identified as a key research area to date, there have been a very little studies conducted to estimate the sensitivity of electricity demand for air conditioning to the climate variability. Most of the energy efficient building codes are mainly focused on new buildings, while the existing buildings pose a significant threat to the building air conditioning energy loads. The localized studies are important in this regard, as the air conditioning loads significantly vary with the local ambient conditions. The impacts of climate change on building air conditioning energy demand for existing buildings can be reduced by establishing future energy demand patterns and by effective usage of passive cooling strategies. Hence, this study focused on investigating the current demand for building air conditioning in selected existing buildings and forecast energy demand for predicted future climate scenarios to establish the electricity demand patterns and investigate effectiveness of passive cooling strategies to counteract the effects of climate change on cooling energy usage of existing buildings. The study used data driven black box and hybrid grey box models to predict the indoor temperature using RCP emission scenarios. The model results were then used to predict the cooling demand increase for the selected building zones. It was observed that cooling demand can increase on average by 20% and 50% by 2035 and 2090 respectively while the suggested mitigation tactics are able to reduce the demand increase by approximately 30%. The knowledge gained by the investigation will have a significant importance in terms of mitigating climate change challenges and identifying counteracting measures in neutralizing climate effect in building cooling energy in different climate environments.

Keywords: Climate change, Building energy, Cooling energy demand mitigation, Energy demand prediction, Global warming

TABLE OF CONTENTS

LIST OF FIGURES

LIST OF TABLES

LIST OF ABBREVIATIONS

Abbreviation	Description
ACCA	Air Conditioning Contractors of America
ACH	Air Changes per Hour
ANN	Artificial Neural Networks
ARI	Air conditioning and Refrigeration Institute
ARX	Autoregressive with Exogenous Input
ASHRAE	American Society of Heating, Refrigerating and Air-Conditioning Engineers
CDD	Cooling Degree Days
CEA	Central Environmental Authority
CFD	Computational Fluid Dynamics
CIBSE	Chartered Institute of Building Services Engineers
CLTD/CLF	Cooling Load Temperature Difference/Cooling Load Factor
COP	Coefficient of Performance
EPW	EnergyPlus Weather
FAR	First Assessment Report
GAST	Global Average Surface Temperatures
GDP	Gross Domestic Product
GHG	Greenhouse Gasses
HB	Heat Balance
HDD	Heating Degree Days
HDKR	Hay-Davies-Klucher-Reindall
HVAC	Heating Ventilation and Air Conditioning

IES VE	Integrated Environmental Solutions Virtual Environment
IPCC	Intergovernmental Panel on climate Change
LPD	Lighting Power Density
MAE	Mean Absolute Error
MPC	Model Predictive Control
MSE	Mean Squared Error
NARX	Nonlinear Autoregressive with exogenous input
NRMSE	Net Root Mean Squared Error
PMV	Predictive Mean Vote
RCP	Representative Concentration Pathways
RH	Relative Humidity
SCLF	Solar Cooling Load Factor
RMSE	Root Mean Squared Error
RNG	Re-Normalization Group
RTS	Radiant Time Series
SC	Shading Coefficient
SCLF	Solar Cooling Load Factor
TAR	Third Assessment Report
TETD/TA	Total Equivalent Temperature Difference/Time Average
Toe	Ton of oil equivalent
UHI	Urban Heat Island
WFR	Wall to Floor Ratio
W-L-R	Wall to Length Ratio
WWR	Wall to Window Ratio

LIST OF APPENDICES

CHAPTER 1

INTRODUCTION

Energy consumption for buildings is a significant portion of the global energy demand. It is reported that building energy accounts for 46% of total electrical energy consumption in Sri Lanka, out of which 51% is utilized for HVAC (Heating, Ventilation and Air Conditioning) [1]. Sri Lanka being a country near the equator, a region which is predicted to have high impacts of global warming in the 21st century, will have to face significant climate change impacts especially in the energy sector. The demand increase for the domestic energy sector due to socio-economic factors also poses a high threat in this regard [2], [3]. Studies have shown that the increase in cooling demand and the decrease in heating demand will be highly dependent on the geographical location of the country [4], [5]. The Intergovernmental Panel for Climate Change (IPCC) in its sixth assessment report predicted several emission scenarios and in each of these scenarios, the frequency of hot days, hot nights, and heat waves are predicted to increase [6]. As a consequence, the HVAC energy demand is also slated to increase in the 21st century.

The impact of climate change is more prominent in tropical areas where most of the population resides and have fast-growing dense urban areas. Colombo city of Sri Lanka is a perfect example of a fast-growing city with lots of old architecture situated in this hot and humid climate zone. It is estimated that in this region the maximum temperature can reach up to 40 °C and the energy demand in South and Southeast Asian coastal cities is predicted to increase by 40 times in 2100 compared to 2000 [7].

Most of the previous research focused on reducing building energy consumption due to temperature rise is mainly focused on introducing energy efficient air conditioning systems by innovative use of coolant gases like refrigerant grade propane. Furthermore, government policies are being established in efforts to make the new constructions more energy efficient and sustainable. The Colombo area, with its rich architecture, have a majority of existing buildings that were built in the last century before the existing energy-efficient building codes came into effect. Hence, these building strategies and building codes have not been applied to many of the existing buildings which would have a considerable proportion of energy demand in the next few decades [8].

Air temperature is found to be the most significant weather variable which affects the cooling energy demand. With all the future climate scenarios predicted to increase global temperature, the study of climate change impacts on cooling energy demand is an important topic to investigate especially for existing buildings [9]. Thus, current research is focused on studying the impacts of climate change on the cooling energy demand of existing buildings and investigate the methods to minimize or counteract the adverse impacts of climate change. The buildings were analyzed under several climate change scenarios. The effects of cooling load mitigation tactics are numerically calculated, and computational tools were used to determine the efficiency of those methods in mitigating the future building cooling energy demand.

The major parameters contributing to the cooling load inside the building were identified through the literature review. Since climate change has a direct impact on Global Average Surface Temperatures (GAST), and outdoor temperature being one of the major influencing factors in cooling load inside a building, the future cooling load calculations and predictions were decided to be based on outdoor temperature. Two types of modelling techniques were used to predict the indoor temperature of the building with respect to the ambient outdoor temperature. The first model is a data driven model based on NARX type neural networks and the second model is data driven and physics-based hybrid model. The models were calibrated for each selected building zone and the model results from two models were compared. To validate the results from the models and to train the data-driven models, several buildings were selected, and the indoor and outdoor data (indoor temperature and relative humidity, outdoor temperature and relative humidity) were logged. The developed models were then used with existing climate change predictions to predict future cooling loads in selected buildings. Two climate change predictions: RCP 4.5 (intermediate scenario) and RCP 8.5 (worst-case scenario) were used to predict the indoor temperature and future cooling load variations of the selected buildings.

It was concluded that both models showed significant accuracy in the indoor temperature predictions of the zones. All selected zones showed significant cooling load increase predictions of up to 30% and 50% (on average) by RCP 4.5 and 8.5 climate change scenarios by 2090 which will have significant impacts on the sustainability of the electrical infrastructure of the region unless properly managed. Furthermore, the suggested modifications and cooling demand mitigation tactics showed a potential to reduce the expected increase of cooling load by up to 30% in some of the zones. It was observed that improved solar designs will have significant improvement in most of the building zones used in the study. Furthermore, there is potential in some zones for demand offset using thermal mass optimization and some zones were observed to be benefited from natural and induced ventilation to increase occupant thermal comfort. The results from the study and the developed models can be used widely in future research in developing passive cooling strategies to mitigate climate impacts on the building cooling energy demand increases in tropical countries. Developing the models for several building architectural types is important in generalizing the model outputs to the specified area. By this, a more generalized outlook on the future energy requirements for building cooling in the area can be obtained which will be useful in sustainable energy directives.

CHAPTER 2

LITERATURE REVIEW

2.1 Sri Lanka Energy Sector

Sri Lanka is a country with a high energy density (economic output per unit energy used) which recorded the highest energy density among countries having per capita GDP between $3,000 and $4,500 [1]. This energy is predominantly produced by nonrenewable sources mainly petroleum products and coal as depicted in Figure 2.1 [1]. One of the key issues faced by the energy sector in the country is that a major component of energy production comes from the sources that are imported into the country [2]. In year 2017, Sri Lanka consumed 12,850 kilotons of oil equivalent. (Ton of oil equivalent is 10 Giga calories or 41.84 Giga Joules) [3].

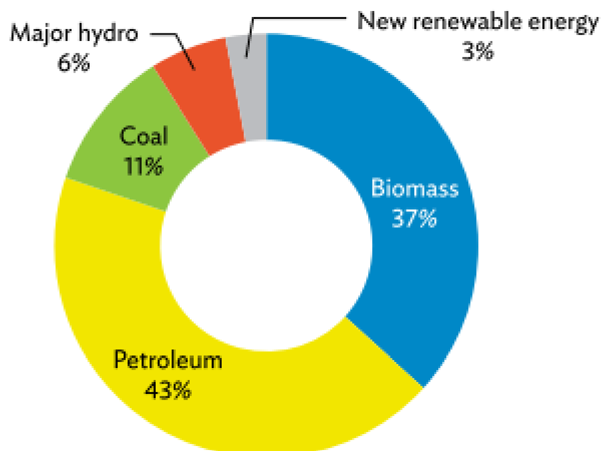

Fig. 2.1: Energy production of Sri Lanka for 2015 [1]

By observing the primary energy supply in Sri Lanka (Figure 2.2) historically, the increase in the energy demand has been compensated by increasing the power generation through thermal power plants such as coal and petroleum posing a significant threat to the environmental system in Sri Lanka [1]. Thermal power plants are one of the main contributors of increased carbon dioxide levels in the world contributing to the global warming [4].

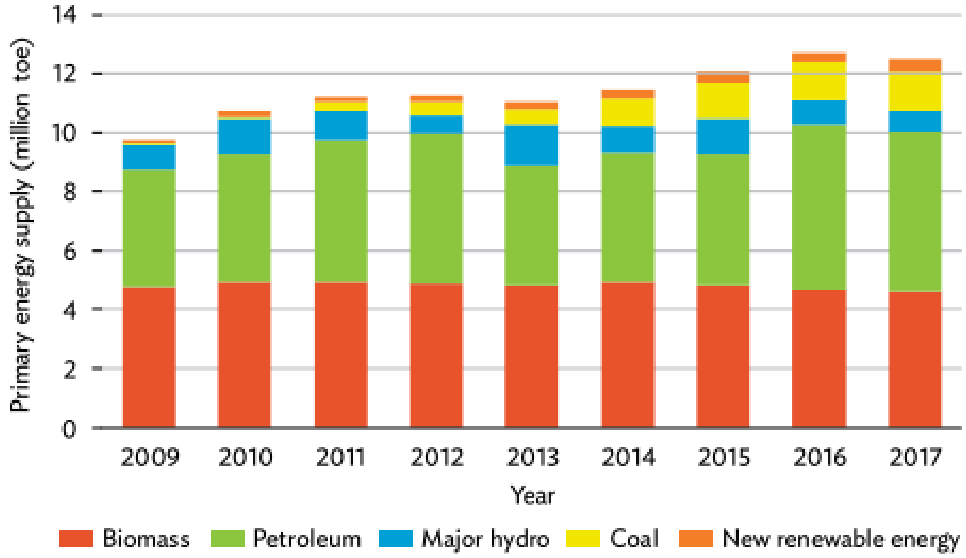

Fig. 2.2: Energy production of Sri Lanka for 2015 [1]

Figure 2.3 shows a detailed breakdown of the energy consumption in Sri Lanka. Currently, the building sector in Sri Lanka is observed to consume 46% of the total energy generation [10]. The industrial sector and the transport sector trail behind with 25% and 29% of energy consumption, respectively. More than 50% of the building energy consumption in Sri Lanka in 2018 was occupied by HVAC systems as calculated by the electricity bills and end-use electricity breakdown [5].

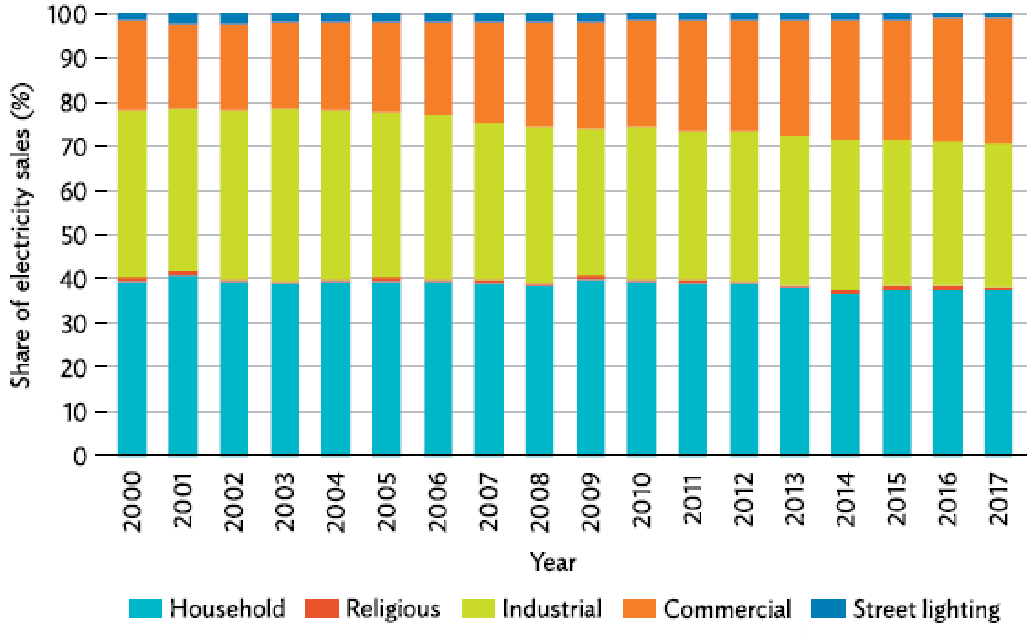

Fig. 2.3: Sri Lanka energy consumption patterns [11]

Figure 2.4 shows the energy demand growth of Sri Lanka over the past 15 years. Sri Lankan government is targeting to reduce this energy demand growth by 2% through conservation of energy and efficient use by 2025. To achieve this target the efficiency of energy use in buildings in Sri Lanka is a key factor, where building cooling is the main contributor for the building energy consumption [2].

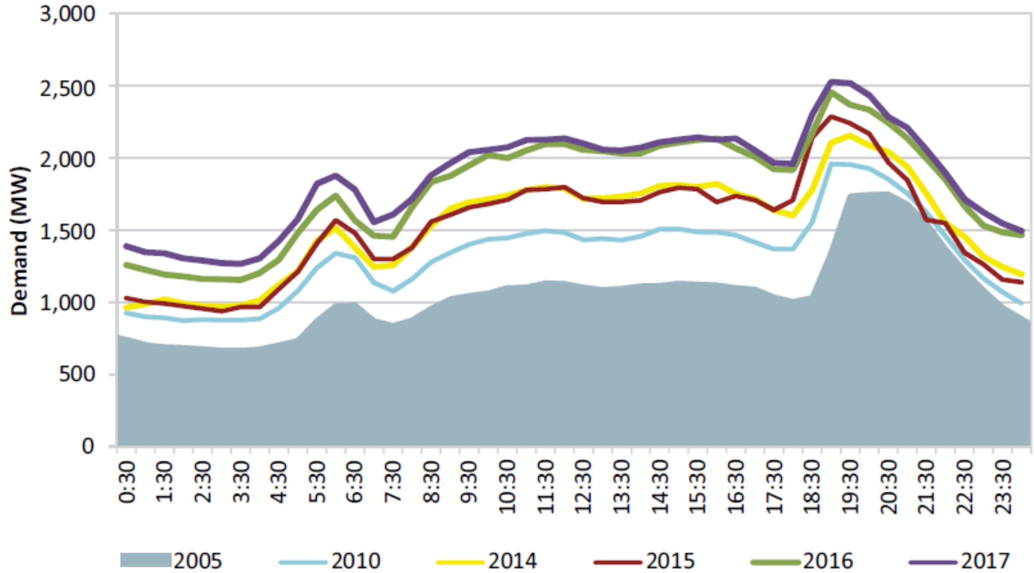

Fig. 2.4: Sri Lanka energy demand curve variation [11]

2.2 Factors affecting building cooling demand

Building cooling energy requirements depends on various factors as illustrated in Figure 2.5. Most of these factors are determined at the pre-construction stage of the building. In Sri Lanka, areas which are categorized as low latitude and hot-humid areas, the main factor that affects building cooling demand is found to be the solar radiation load [6].

The effect of outdoor temperature is also prominent in building cooling energy demand. This outdoor temperature is seemingly uncontrollable by humans in the short term. However, in a longer duration, the climatic conditions will be affected by human behavior in terms of climatic change and its mitigation. A controlled climate change is one of the major governing factors that will impact the controlling of energy consumption for space cooling in the long run.

The building envelope is the next major contributing factor to cooling energy demand. The building envelope is defined as the physical barrier between the exterior unconditioned and interior conditioned environments of the building. The building envelope includes walls, windows, doors, insulations, roof, etc. The easiest way to increase the energy efficiency of buildings is to improve the building envelope. Most of the passive cooling strategies improve the building envelope to reduce the cooling energy demand. The airtightness of a building envelope is most important in this regard. Tight buildings have low air infiltration into the building which will reduce the cooling energy demand. Some passive cooling strategies attempt to transfer air through the building envelope to exhaust hot air inside the building when no air conditioner is in use [7].

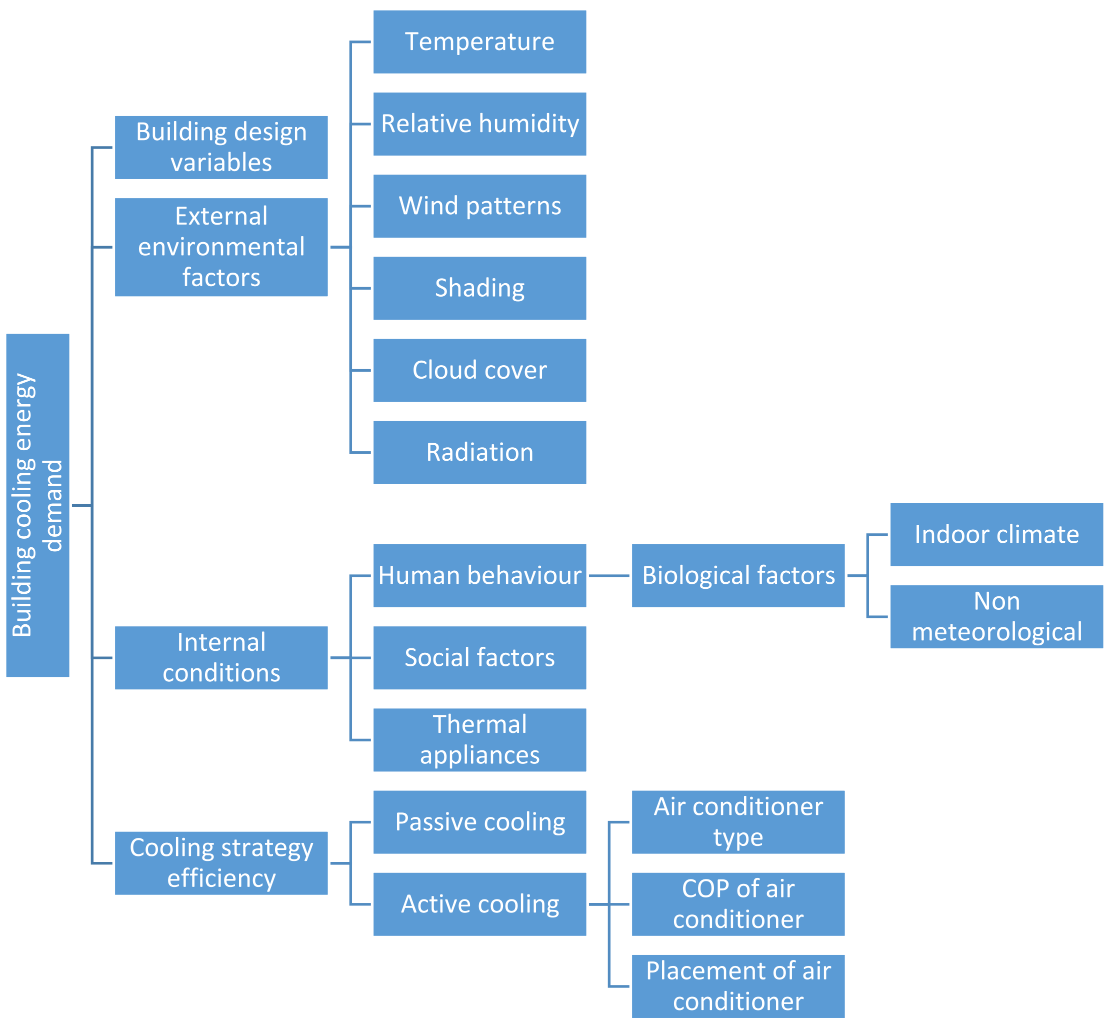

Fig. 2.5: Factors affecting building cooling energy demand

2.2.1 Building design variables

The building design variables/parameters and surrounding buildings also have an impact on the cooling load of the building. The following section discusses those variables and their effects.

- Building orientation/ type/ shape
  - For hot and high radiation climates, the impact of building shape is an important factor in cooling energy demand. A circular building shape with a width to length (W-L) ratio of 1:1 is found to be the optimum shape of the building. If it is a rectangular shape, the building should be in a North-South orientation to reduce the cooling load as can be observed from Figure 2.6 [8].
  - To reduce direct solar heat gain, it is recommended to use the short axis of the building in a North to South orientation so that less area of walls would be exposed to direct sunlight [9].

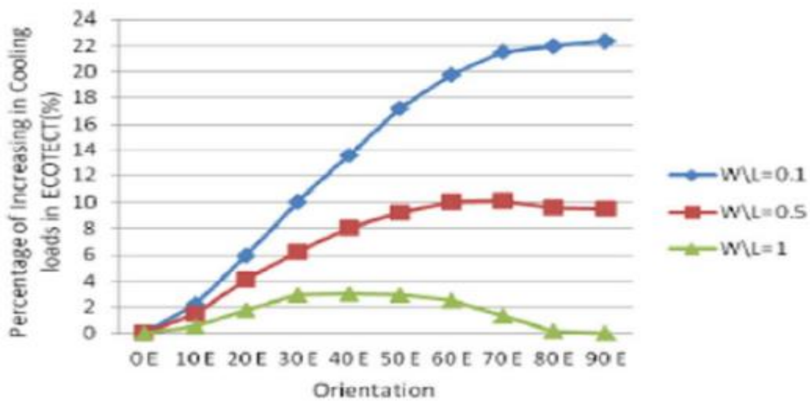

Fig. 2.6: Change in building cooling energy with the orientation of the building and W/L ratio [18]

- Grouping of buildings/ density
    - In urban areas it is observed that the mean temperature is higher than other areas. This is traced back to the urban heat island (UHI) effect. Figure 2.7 shows the comparison of the average variation of buildings in urban areas and suburban areas. It is clear from Figure 2.7 that urban areas show higher average temperatures than suburban areas. This is caused due to high building density in the area which obstructs the solar heat radiation reflection and is trapped among the buildings. Also, the heat rejection from air conditioner outdoor units (condenser fans) is a major factor affecting the urban heat island effect [11]. This effect is mainly counteracted by using urban forests and rooftop forests in building which is becoming an increasing trend in the developing countries.

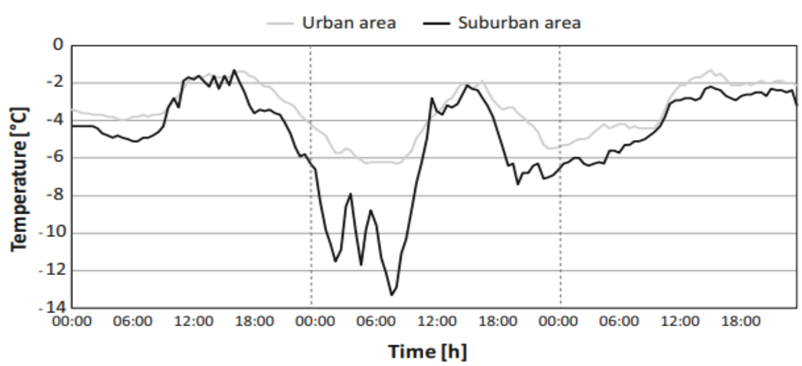

Fig. 2.7: Variation of average cooling loads in urban and suburban areas with the time of the day [20]

- Building Area and Wall to Floor Ratio (WFR)
    - Buildings with higher WFR have a high capacity to gain external loads as the walls are the main transmitter of external heat to the building interior.

Buildings with higher areas have shown little sensitivity to outside conditions due to the high thermal mass [8].

- Window to wall ratio (WWR)
    - Building glazing is the weakest thermal component of a typical building envelope mainly due to the high U value [8]. WWR value is calculated by dividing the glazed area by the exterior envelope area. It is found that a WWR higher than 0.3 contributes to too much heat gain inside the building [12].
- Number of floors
    - With an increased number of floors, the floors situated in the middle have shown to gain less heat from the roof or top of the floor as it is not directly exposed to outdoor conditions whereas the top floor of the building usually shows higher cooling loads [8].
- Building materials and insulation
    - Use of high reflectivity materials for outdoor surfaces reflects most of the incoming radiation from the sun. These reflective materials combined with good heat insulators can prevent both conductive and radiative loads from entering the building.
- Surface coverage
    - Most of the green building codes have implemented urban forests on top of the building roof in an effort to counteract the heat island effect and also block incoming solar radiation [11].

2.2.2 External environmental factors

Outdoor temperature and relative humidity are the main contributing external environmental factors to building cooling energy demand. Although wind patterns do not directly contribute to the building's cooling demand, the wind direction will affect the building’s ventilation and internal air circulation [13]. The wind patterns also affect the cooling towers of the air conditioning systems used in the building changing the efficiency of the air conditioner [13] [14]. Further, the cloud cover and shading directly affect the amount of solar radiation approaching the building which will reduce heat gains into the building [15].

2.2.3 Internal environmental factors

Internal loads of a building are mainly due to the occupants and the appliances in the building. Most electrical appliances add a sensible load into the building while some equipment like water heaters add latent heat load as well. The occupants add latent and sensible heat to the building. This occupancy load is hugely dependent on non-meteorological factors such as: clothing, activity level, posture, exposure, age, sex, nutrition, and health conditions.

Furthermore, the thermal comfort of the occupants is a driving factor for the air conditioning set temperature. ASHARE 55 standards provide a fixed range of thermal comfort values calculated by Fanger's PMV correlation. PMV is the predictive mean vote given by the ASHRAE seven-point scale (Table 2.1). These values are obtained through occupant surveys inside the building [16].

TABLE 2.1: ASHRAE 7 POINT SCALE FOR THERMAL COMFORT

Value	N
+3	Hot
+2	Warm
+1	Slightly warm
0	Neutral
1	Slightly cool
2	Cool
3	Cold

The PMV value depends on six variables,

- air temperature
- mean radiant temperature
- air velocity
- air humidity
- clothing resistance
- activity level

Although a fixed range of thermal comfort is specified by ASHRAE, it is observed that the thermal comfort sensation depends on social factors due to adaptive thermal comfort where residents in hot and humid countries tend to set the air conditioner set values to higher temperatures than relatively colder countries (adaptive approach). Sri Lanka Sustainable Energy Authority(SEA) has identified that air-conditioned spaces should be designed for dry bulb temperatures of 25° C ± 1.5° C and relative humidity of 55 % ± 5 [17].

2.3 Cooling demand calculations

Cooling demand calculations in a building are done through building energy models. There are different approaches to building energy models. These methods can broadly be categorized into three types. In estimating the required air conditioner capacity, cooling load calculations play an important role. Cooling demand calculation is mainly based on the principle that the heat flow rate is not instantaneously converted to loads. When radiant heat is incident on a room surface, some of the heat is absorbed, this absorbed heat is later emitted by the surface. This phenomenon is named as the radiative delay. Therefore, heat addition to a building does not immediately increase the building temperature. This is due to the thermal mass of the building components. This time lag of thermal addition can delay the peak cooling load of the building by a few hours from the peak outside conditions. There are several methods that try to calculate the thermal load considering this time lag [18][10].

2.3.1 White box, physics-based models

The white box models are physics-based models that calculate the heat transfer and heat gains of a building or a zone through empirical equations. White box models are based on a comprehensive understanding of the physical processes governing energy use in buildings. These models use detailed mathematical representations of a building's physical characteristics, such as its geometry, construction materials, and systems for heating, ventilation, and air conditioning (HVAC) [19], [20]. By incorporating these elements, white box models can accurately simulate how energy flows through a building, how it interacts with the environment, and how energy is consumed by various systems and occupants. White box models rely on well-established principles of thermodynamics, fluid dynamics, and heat transfer. They often require substantial data input and computational resources to simulate complex interactions between the building and its environment accurately.

- The development of white box models involves creating a detailed description of the building, often referred to as the building's "digital twin." This description includes:
    - Geometric Information: The building's size, shape, orientation, and layout, which influences how it interacts with external environmental factors such as sunlight, wind, and temperature.
    - Material Properties: The thermal properties of construction materials, including insulation, windows, walls, and roofs, which affect heat transfer and energy retention.
    - HVAC Systems: The specifications and operational characteristics of heating, cooling, and ventilation systems, which are critical for maintaining indoor comfort and air quality.
    - Occupant Behavior: Patterns of occupancy, equipment usage, and other activities that influence energy demand within the building.

Building energy white box models are established types of models. There are numerous software solutions that take in detailed descriptions of the building to calculate the thermal environment of a building. Some of these include EnergyPlus, IESVE and TRNSYS [19], [20]. The advantage of using white box models is that these types of models do not require any operational data of the building (Eg : Indoor environment data like indoor temperature) and therefore can be used during the design phase. The major disadvantage is the vast knowledge needed on the construction of the building, its HVAC systems and weather conditions. These models are also at a disadvantage as these models are highly dependent on assumptions that make up equations for the heat transfer processes which introduce an inherent error into the system equations or the model. These models are also highly computationally extensive requiring high computational power and engineering time to set up and run. [21], [22], [23]

Most available software and previous studies in the literature use one of the following methods to calculate heat transfer and heat addition to a building or a building zone.

- Total equivalent temperature difference/Time average (TETD/TA)
- Cooling load temperature difference/Cooling load factor (CLTD/CLF)
- Transfer function method
- Heat balance (HB) and Radiant time series (RTS)
- Using air conditioning manuals

TETD and CLTD methods are mostly manual methods that are used in the design phase of a building to calculate a conservative cooling load value. HB method is the most accurate and RTS method is a simplified method of the HB method. Heat load can also be calculated by using manual of the Air conditioning contractors of America (ACCA) and Air Conditioning and refrigeration institute (ARI) where, Manual J is for residential applications and manual N is for commercial applications [18].

TETD/TA and CLTD/CLF methods use a similar procedure and the same structure of equations for calculations. The main difference between the two methods is the factors used to calculate the time lag. The TETD method uses a more time-based approach to calculate the factors while the CLTD method uses a thermal mass-based approach to calculate the time lag. Both these values are given in ASHRAE fundamental tables and have been derived by the heat balance method [24][25][26].

CLTD/CLF method is a manual calculation method that uses data from ASHRAE standards tables to calculate the radiant delay of the building. The method can be optimized for indoor and outdoor temperatures using a simple Equation [16], [26], [27], [28], [29], [30].

Heat load through the roof, windows, and external walls

As the CLTD values from 2017 ASHRAE fundamental tables are developed for internal temperature of 25.5 °C and mean outdoor temperature of 28 °C, these table CLTD ($CLTD_T$) values should be adjusted to different outdoor and indoor temperatures changing with the climatic conditions of the country using Equations 1 and 2 [25],

$$Q_1 = U * A * \mathrm{CLTD}_C \tag{1}$$

$$\mathrm{CLTD}_C = \mathrm{CLTD}_T + (25.5 - \mathrm{T}_R) + (\mathrm{T}_M - 28) \tag{2}$$

where,

T_M - mean outdoor temperature

T_R - desired air-conditioned room temperature.

U - thermal transmittance

A - area of the surface concerned

$CLTD_C$ - corrected cooling load temperature difference.

The heat due to solar radiation

The heat gain due to solar radiation is calculated based on *SCLF* (Solar cooling load factor) and *SC* (Shading coefficient), using Equation 3,

$$Q_2 = A * (SCLF) * SC \tag{3}$$

Heat load from occupants

Heat gain from the occupants can be calculated using Equations 4 and 5,

	Sensible heat load:	$Q_3 = N_O * q_S * CLF$	(4)
	Latent heat load:	$Q_4 = N_O * q_L * CLF$	(5)

where,

q_S – sensible heat load from a typical person

q_L - latent heat load from a typical person

N_O - average number of occupants in the area.

Sensible and latent heat load from a person depends on the activity level of the person.

Load due to lighting appliances

The heat load due to lighting loads can be calculated using the standard *LPD* (Lighting Power Density) per unit area values as given in Equation 6,

$$Q_5 = (LPD) * A * F_U * F_B * (CLF) \tag{6}$$

where,

F_U - usage factor

F_B - ballast factor

CLF - Cooling Load Factor

A - area of the room

Load due to other electrical appliances

Heat load due to the other appliances can be calculated using Equation 7 based on CLF value,

$$Q_6 = W * \ F_U * F_R * (CLF) \tag{7}$$

where,

W - total heating load

F_U - usage factor

F_R - radiant factor

2.3.2 Black box: data-driven models

Black box data-driven models sit on the opposite end of the spectrum to white box physics-based models. These types of models do not require any data on the building construction or characteristics and do not rely on any physical thermodynamic and heat transfer equations [31]. These models are trained in the operational data of the building and therefore the model performance depends heavily on the quality and quantity of operational data collected from the building. These models can range from very simple regression based models to state of the art Neural Network Models [32], [33].

The development of black box models typically involves the following steps:

- Data Collection: Gathering extensive historical data on energy consumption, weather conditions, building occupancy, and other relevant factors. This data serves as the foundation for training the model.
- Data Preprocessing: Cleaning and preparing the data to ensure its quality and relevance. This may involve handling missing values, normalizing data, and selecting appropriate features.
- Model Training: Applying machine learning algorithms to preprocessed data to identify patterns and relationships. Common algorithms used in black box

modeling include linear regression, decision trees, support vector machines, and neural networks.

- Model Validation and Testing: Evaluating the model's performance using a separate dataset to ensure its accuracy and generalizability. Metrics such as mean absolute error (MAE), root mean square error (RMSE), and R-squared are often used to assess model performance.

The main advantage of black box models over physics-based white box models is that these models do not require details about the building construction. The building construction data (materials of construction, actual dimensions of construction etc) are very difficult to accurately calculate which are required for physics-based models. Additionally, the heat gain from occupants and internal gains are also very difficult to calculate accurately and are mostly calculated through empirical equations for physics-based models [34], [35], [36], [37]. When using a data-driven model, as the models are trained with actual building data, the uncertainties of these calculations are not present. The actual operation of the building is captured through actual operational data reducing the need for assumptions. The downside of these methods is that these methods usually require quality data in a higher quantity [38]. It is known that the quality and quantity of the data is a main factor in the accuracy of these models. Additionally, the state of the art neural network models require good setting up and are highly computationally intensive both in model training and model evaluations [39]. Another disadvantage is that the black box models being pattern recognition models work well when the model is used to interpolate the results and the model performance is not guaranteed when extrapolating the results. Therefore, these models work well in predicting operation of the building within the limits of the training data set and any extreme events which are not available in the training data set are likely to be less accurate when predicted by black box models.

2.3.3 Hybrid grey box models

Hybrid grey box models are a combination of both black box and white box models. These kinds of models combine advantages from both white box and black box models. These models usually contain a simplified low-order model of the system. Therefore, these models only capture the important or most prominent heat transfer dynamics of the system through the physical equations, but also the building operational data set through the collected data. Therefore, gray box models do not have empirical errors in assumptions made in physical equations used in physics-based models. These models being low order, simplified models take a fraction of time to evaluate when compared to physics-based models [21], [40], [41], [42]. This is advantageous in predictive control applications and therefore these models are becoming increasingly popular in the field of building energy modelling. These models require high computational power when training the model but require very little computational power when evaluating the model or when the model is being used for predictions [34], [36], [37]. These models require less weather-related data and therefore are low reliant on detailed weather files making these models very useful in future energy predictions as these models are less affected by the uncertainties in weather predictions [40], [43]. Although the applications and advantages of grey box models in the advancement of building energy models are evident, this is a relatively new topic of discussion and there are several challenges and limitations in the literature in the context of grey box models as identified in [22].

The development of grey box models involves the following key steps: [21], [41], [44]

- Physical Representation: Incorporating fundamental physical principles and equations to describe the building's thermal behavior. This includes aspects such as heat transfer, thermal mass, and HVAC system performance. The physical representation ensures that the model captures the essential dynamics of the building's energy consumption.
- Empirical Data Integration: Utilizing historical data to calibrate and refine the physical model. This data-driven component helps account for factors that may be difficult to model purely through physics, such as occupant behavior, equipment usage patterns, and specific operational conditions.

- Parameter Estimation: Combining the physical and empirical components to estimate model parameters. Techniques such as system identification, statistical regression, and optimization algorithms are used to fine-tune the model, ensuring it accurately reflects real-world energy consumption patterns.
- Model Validation and Testing: Evaluating the model's performance using a separate dataset to verify its accuracy and generalizability. This step ensures that the grey box model provides reliable predictions for various scenarios and conditions.

2.4 Climate change effects on building energy demand

Figure 2.8 shows the energy balance for Earth. In a long-term scenario, the earth and its atmosphere absorb solar energy from the sun and radiate back into space after some time. About half the incoming energy is absorbed by the earth and is transferred back into space. During this process, this energy is absorbed by the atmosphere and the air in contact with the surface becomes warmer. This energy is absorbed by the greenhouse gases in the atmosphere and radiated back into Earth and some to space. The more the greenhouse gases are present in the atmosphere, the more energy is retained inside the earth's atmosphere and therefore not all incoming energy is radiated back to space. This excess energy causes global warming [45][46][47].

Global warming and climate change impacts the cooling energy demand in a building by two major factors,

1. Increase of the GAST (Global average surface temperature)
2. Increase in frequency of hot days

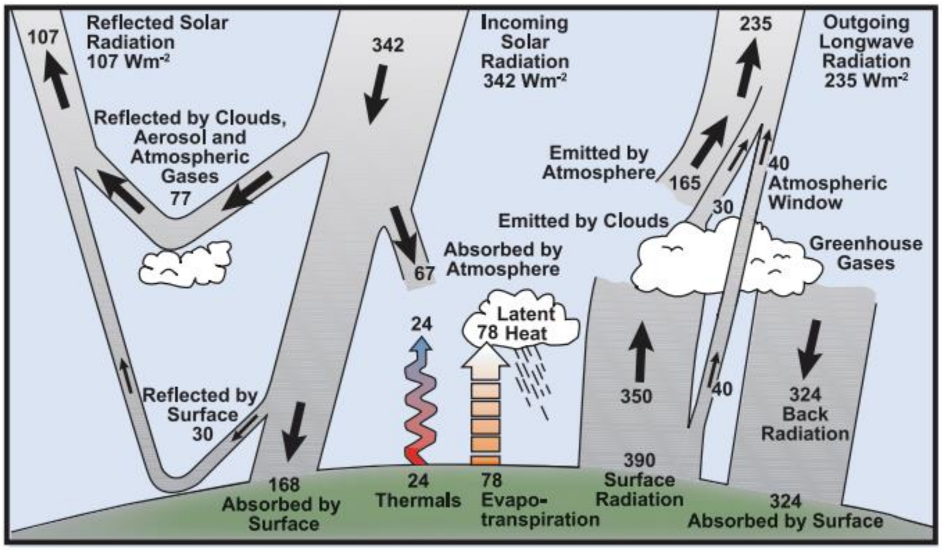

Fig. 2.8: Heat balance of earth. When energy absorbed is greater than energy emitted, global warming is increased [28]

The world has experienced an increase in global average surface temperature (GAST) for the past years (Figure 2.9). The IPCC assessment reports provide the predicted future climate change from the historical data (Figure 2.10) [46][48].

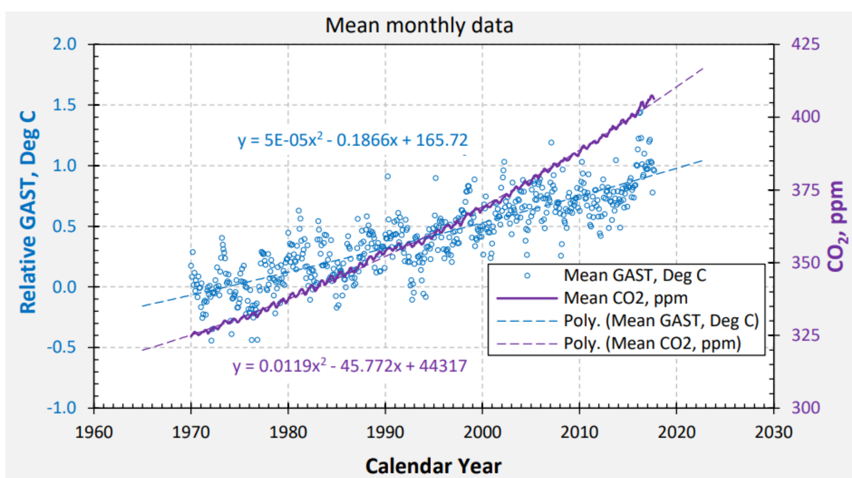

Fig. 2.9: Historical climate data patterns of carbon emissions and GAST [29]

Up to 2005, the observed climate change has followed the upper limit of the path specified by the IPCC TAR (Third Assessment report) and the lower limit of the IPCC FAR (First assessment report). To eliminate these differences, IPCC has introduced several emission scenarios from 2006 onwards. These scenarios are the Representative Concentration Pathways (RCP) which are used to develop climate change scenarios. These RCPs are distinguished by the radiative forcing (difference between solar irradiance absorbed by earth and the amount of energy radiated back to space) value of the different emission conditions by the year of 2100 [48]. Figure 2.14 shows the comparison of different emission scenarios predicted by IPCC.

RCP 2.6 – Radiative forcing of 2.6 W/m^2 considered to be one of the best-case scenarios. Surface warming will be less than 2 °C by the year 2100.[49]

RCP 4.5 – One of the two intermediate scenarios predicted with radiative forcing of 4.5 $W/m^{2.}$ Emissions peak by 2040 and then decline. Surface warming will be less than 3°C by the year 2100.

RCP 6.0 – One of the two intermediate scenarios predicted with radiative forcing of 6 $W/m^{2.}$ Surface warming will be less than 3.5°C by the year 2100.

RCP 8.5 – Worst case scenario predicted with radiative forcing of 8.5 $W/m^{2.}$ Surface warming will be less than 5°C by the year 2100 [45][50][48].

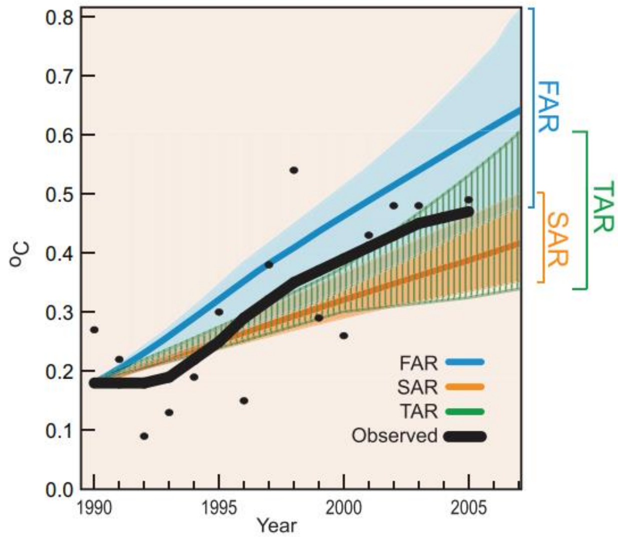

Fig. 2.10: Historical temperature variation with climate change predictions according to IPCC FAR, SAR and TAR (First Assessment report, Second Assessment report, Third Assessment report) [29]

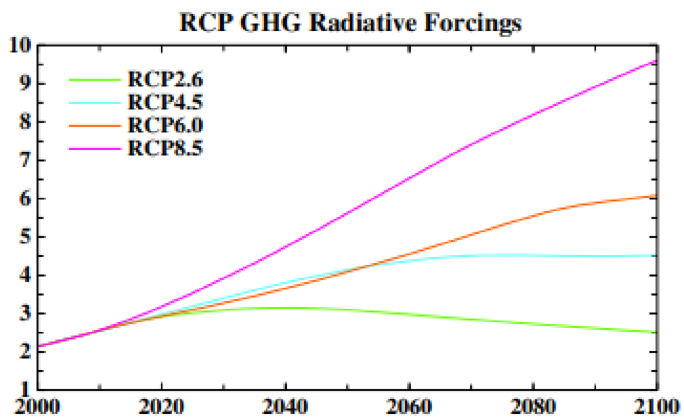

Fig. 2.11: Comparison of different emission scenarios [29]

Figure 2.12 shows the predicted average global surface temperatures under different emission scenarios.

South Asian region is categorized as the world's second most in risk area for electrical infrastructure. This has been calculated by the population growth and the vulnerability of the electrical infrastructure to climate change [51][52].

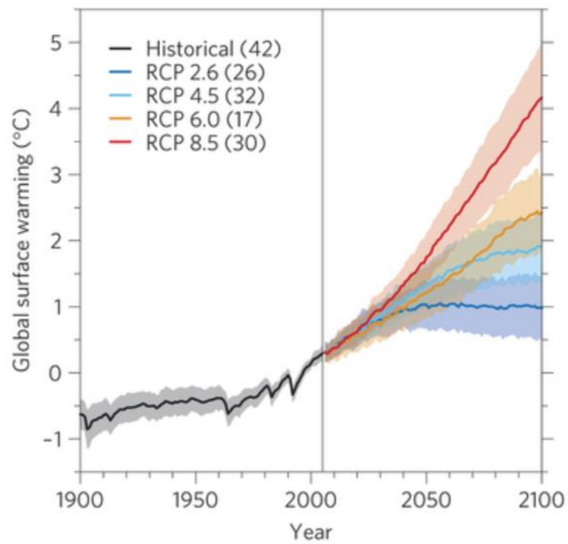

Fig. 2.12: Global surface warming prediction according to IPCC fifth assessment report with different climate change scenarios [29]

The effect of climate change on buildings is generally characterized by observing the demand change of buildings with respect to the change in Cooling Degree Days (CDD) values over the period considered. CDD is the measurement of annual or monthly periods where the ambient temperature was above a set point [53], which can be calculated using Equation 8,

$$CDD = \sum_{1}^{d} \left(\frac{\sum_{1}^{24}(T_A - T_P)}{24}\right) \tag{8}$$

where,

d is the number of days in the concerned time period,

T_A is ambient temperature,

T_P is the set point temperature which is measured hourly

The Indian subcontinent region has shown the highest number of CDD in 2010. The CDD values have shown a rapid increase of 30% in the past 30 years, and they are predicted to increase by a further 30% in the next 30 years. Figure 2.13 shows the CDD values of 2010 while Figure 2.14 shows the predicted CDD increase in the regions of the world [51].

2.5 Impact of climate change for buildings

Energy consumption predictions for cooling in buildings depend mainly on two factors,

1. Impact due to climate change
2. Impact due to socio-economic status and development [54][55]

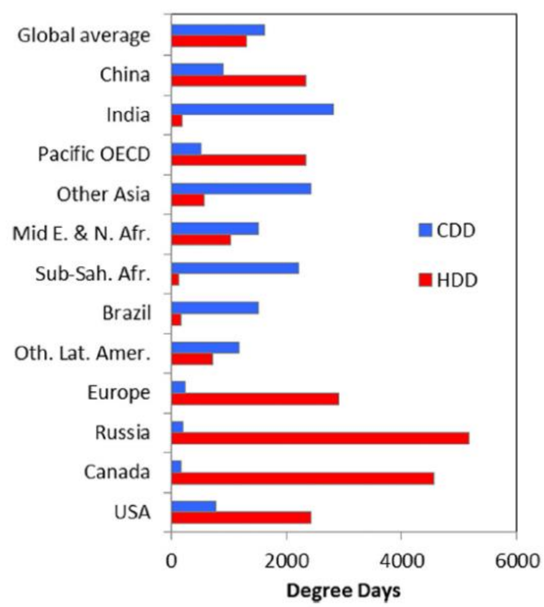

Fig. 2.13: Cooling degree days (CDD) for different parts of the world in 2010 [34]

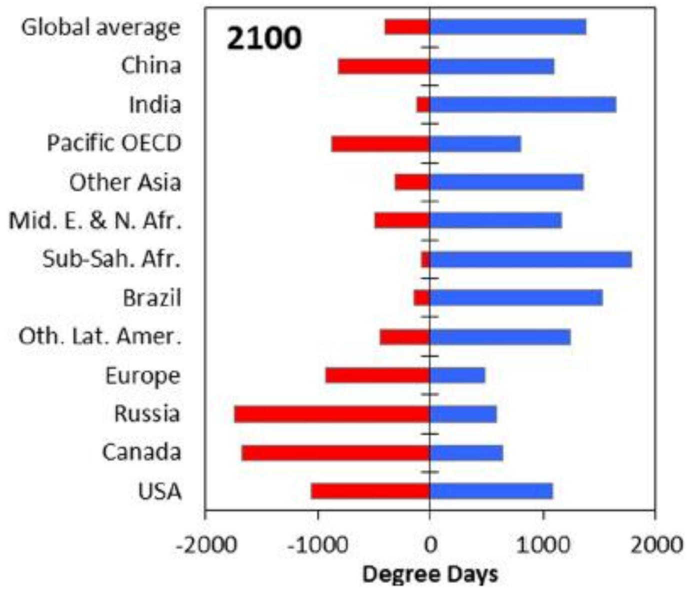

Fig. 2.14: Predicted change of CDD and HDD for different parts of the world [34]

To predict the climate change effect on buildings, six climate categories are identified [56],

1. Warm-humid - 15°N and South of the equator, e.g. Lagos, Mombassa, **Colombo**, Jakarta etc.
2. Warm-humid Island - equatorial and trade wind zones, e.g. Caribbean, Philippines and Pacific Islands etc.
3. Hot-dry desert - 15° to 30° North and South, e.g. Baghdad, Alice Springs, Phoenix etc.
4. Hot-dry maritime desert - latitudes as (3), coastal large landmass, Kuwait, Karachi etc.
5. Composite Monsoon - Tropic Cancer/Capricorn, Lahore, Mandalay, New Delhi etc.
6. Tropical uplands - Tropic Cancer/Capricorn, 900 to 1200 meters above sea level (plateau and mountains), Addis
7. Ababa, Mexico City, Nairobi etc.

A framework to calculate the effect of climate change on per capita expenditures for space heating has been established in the literature as given in Equation 9 [57][58],

$$E_C = f d_C P_c \tag{9}$$

where,

E_C = per capita expenditure for space cooling

f = floorspace per capita

E_C = energy consumption per unit floorspace

E_p = price of a unit of energy

The demand (d_C) is calculated based on the principle that the consumers demand more energy services with the service becoming more affordable until energy satiation is reached [59][60], which is given in Equation 10,

$$d_C = k_C(CDD.\tau.R + IG)(1 - \exp(-\frac{\ln 2}{\mu_C}\frac{i}{P_C})) \tag{10}$$

where,

k_C is a caliberation coefficient

CDD is the annual cooling degree days value

τ is the combined average thermal conductance (U value)

R is the average surface to floor area

IG are the internal gains in the building

i is the per capita income of the country

μ_C is a parameter defining a degree of demand satiation which is regional dependent.

In equation 10, CDD, τ, R and IG terms directly capture the effect on energy demand due to various physical parameters including climate change while i and μ_C terms capture the demand change due to change of energy price and income of the country.

A fixed climate scenario is generally used which assumes that there is no change in climatic conditions as the reference scenario. RCP emission scenarios are then compared to the fixed climate scenario. In the fixed climate scenario, it is assumed that there is no effective change in the CDD values at a country level [61].

Figure 2.15 shows the per capita cooling demand predictions in the fixed climate scenario. Even without the effect of global warming, India and other Asia regions show a huge spike in energy demand.

When compared with the RCP 8.5 climate change scenarios, it is observed that the energy demand per person increase will almost double between the RCP 8.5 scenario and the fixed climate scenario (Figure 2.16) [62][63].

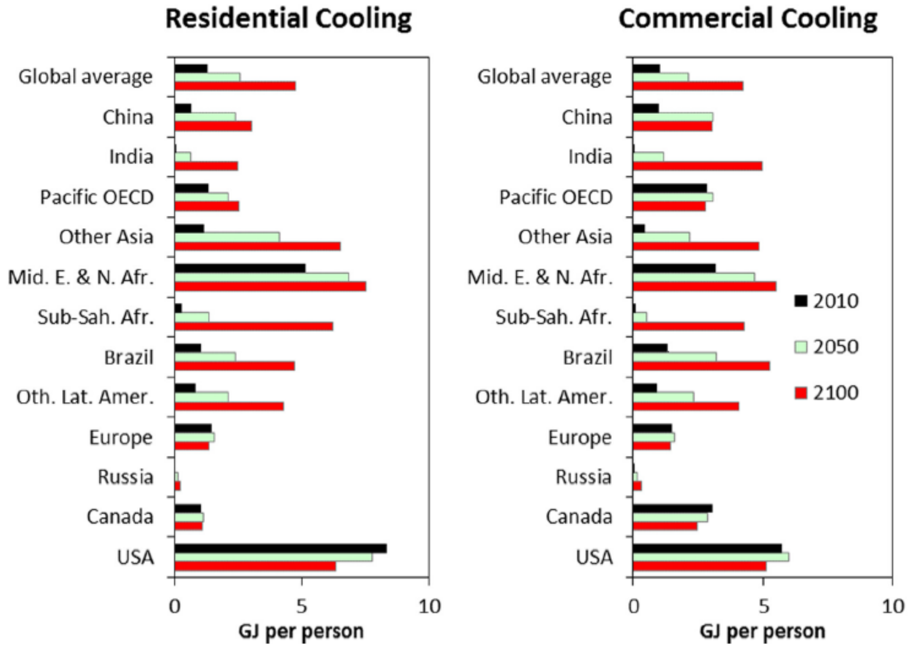

Fig. 2.15: Predicted increase of energy consumption per capita in 2050 and 2100 under fixed climate scenario for residential buildings (left) and commercial buildings (right) [34]

It is estimated that the net global building energy expenditures increase on the order of 0.1% of global economic output for a 2 °C increase in global mean surface temperature. Also, the cooling energy requirement will increase by 10% per 1 °C increase in global surface temperature. In the USA 48% of total energy demand is through climate change factors. But it is also noted that the Phoenix metropolitan area of the USA will have only 25% of the total cooling energy demand increase due to climate change factors. The remaining 75% is due to population growth and city expansion. A study by Rogner (2007)[64] showed that the energy demand for air conditioning in these areas could increase up to 40 times in the year 2100 with an average annual rise of 7%. The difference in these results suggests that the impact of climate change on building energy demand is highly localized. [6] Although Sri Lanka can be geographically approximated to follow the same physical climate change parameters as India, the socio-economic factors and the change in city architecture make it difficult to approximate the same values of India to the demand patterns for Sri Lanka. Therefore, a localized study of climate change impacts is important to predict the demand patterns for Sri Lankan urban areas [58].

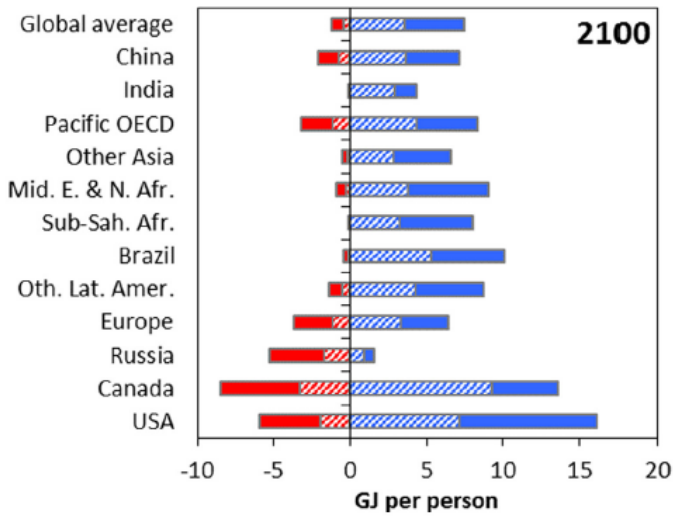

Fig. 2.16: Predicted increase of energy consumption per person by 2100 under RCP 8.5 scenario [34]

2.6 Cooling energy demand increase mitigation

Several passive cooling and adaptive measures are discussed in the literature to reduce the impact of cooling load increase on power production in different countries. The most efficient of these methods is implemented at the construction stage of the building. Passive strategies require no energy input. Most prominent passive and low energy cooling strategies include,

- Natural and night-time ventilation
  - Removes hot air and supplies cold air directly when incoming air is cool and clear of contaminants. Naturally ventilated buildings can have higher interior set points than mechanically ventilated buildings. This is because the natural cooling effect of air motion increases the thermal comfort. For example, at an outdoor temperature of 30 °C, naturally ventilated rooms with operable windows can have internal temperatures of 27 °C while

mechanically ventilated rooms require internal temperatures to be around 25 °C for the same thermal comfort sensation.

  - Natural ventilation is generally achieved through courtyards, atria, wind towers, operable windows, and solar chimneys
  - Mechanical or natural ventilation at night-time can cool down the thermal mass of the building at night. Due to radiative delay, this cooling down of thermal mass at night will result in lower cooling load peaks during the day. In California, more than 40% of the houses require no daytime mechanical cooling and can keep daytime peaks to less than 26°C if the houses are cooled at night.
  - One major setback of this method is that there can be condensation occurring when the moist daytime air meets the night-cooled indoor surfaces

- Evaporative cooling
  - There are two types of evaporative cooling
    - Direct cooling– water is evaporated directly into the air stream to be cooled
    - Indirect cooling – a secondary air stream is used; water evaporates into the secondary air stream. The two air streams go through a heat exchanger which prevents moisture from being added to the supply air

- Underground earth piping
  - In climates having a good year-round variation in temperature, heat sinks underground can be used to reject heat. An air duct is buried underground, and air is circulated to cool the air (Figure 2.17) [65][66].

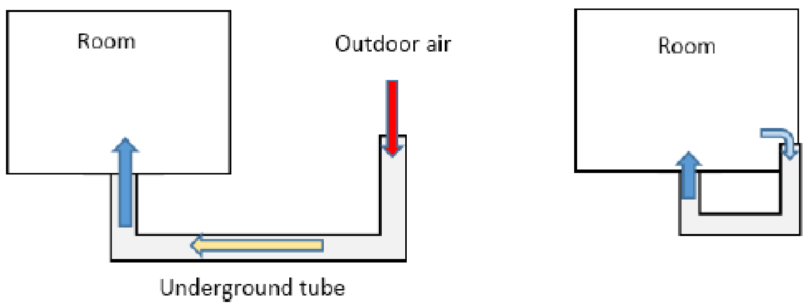

Fig. 2.17: Underground tube cooling method [47]

- Desiccant dehumidification
    - In mechanical air conditioning systems, the coil temperature is set to a low value. When moist air meets the coil, the moisture in the air is condensed on the coil. This induces a latent load on the coil where energy is expended in the latent transformation of water vapor. To reduce this latent energy consumption, desiccants can be used to remove the moisture before the air meets the cooling coil. Solar energy can be used to regenerate the desiccant. In hot and humid countries, some systems combining evaporative cooling with desiccant systems are a viable solution [67][68][54].

- Highly efficient ventilation and cooling systems
    - The use of a high COP (coefficient of performance) air conditioning system is a key factor in reducing energy consumption. COP is calculated by dividing the cooling power of the air conditioner by the input power to the air conditioner. A typical split type air conditioner COP ranges from 2.2 to 3.8, however, these values are generally lower in tropical countries like Sri Lanka. For larger buildings, centralized air conditioning systems like chillers are more efficient with COP values up to 7.9. However, these

systems require additional energy to pump the chilled water and circulate air [69].

  - Alternative cooling strategies that are different from the traditional air conditioning systems are also efficient in some applications.
    - Radiant chilled ceiling cooling – The room ceiling is cooled by cooling pipes and lightweight panels. Because water has high effectiveness in transporting heat than air, this method can provide significant energy savings. Nearly 10% of European countries have adopted this strategy as an alternative cooling strategy. Water-side direct cooling strategies can also be implemented in these systems where the chiller is bypassed and the cooled water from cooling towers is directly used [65].

- Displacement ventilation
  - These ventilation systems usually use turbulent mixing of room air and ventilation air. In displacement ventilation, ventilation air is introduced to the room at low velocities. The diffusers are located near the floor and this cold air absorbs the internal heat of the room and rises exiting through vents at the top of the room. This method is implemented in Northern Europe and North America [66].

There are some other passive techniques which can also be used in controlling the building cooling load which are listed below,

- passive solar design
- high-efficient lighting and appliances
- daylighting
- insulation materials and techniques
- high-reflective building materials and multiple glazing.
- self-shading [70]

- height-to-floor-area ratio optimization
- optimizing thermal mass to minimize interior temperature peaks
- increasing the solar reflectivity of roofs and horizontal or near-horizontal surfaces around buildings
- planting shade trees
- cogeneration and district cooling [66][71]

2.7 Advancements in indoor temperature modelling

Indoor temperature has been identified as a key parameter that affects the air-conditioning energy demand /cooling load of a building. It was identified from the literature review that there are two types of modelling approaches that has been used to establish a relation between indoor temperatures and outdoor ambient conditions which are,

- models based on physical principles,
- data driven modelling using machine learning techniques.

Models based on physical principles are developed using existing heat transfer equations and on most occasions, they are difficult to solve analytically and require numerical solutions. These numerical models are complex and require high computing power due to the high number of parameters involved with detailed descriptions of the building characteristics or the envelope. Comparatively, data-driven models are less complex and can be simplified by eliminating less significant parameters. Some studies have also used a combination of these two types of models. Data driven models are based on data collection and analysis which predict the indoor temperature of zones in buildings using different pattern recognition techniques. The advantage of using a mathematical model-based prediction is the ability to generalize the model prediction for buildings in the area that were not used for the data collection.

While white-box models are detailed numerical/empirical representations of the building, the modeling using white-box models has major assumptions. It is very difficult to collect the actual data from the building (e,g, heat conductance of envelope elements, actual construction properties, actual heat added by occupants and equipment). Most of these are calculated through equations derived through physical principles or through experimental means. Therefore these formulations introduce higher uncertainties to the model. Additionally, these types of models require a detailed weather file. These types of models are useful in the design stage of the building as no operational data are available. In existing buildings where operational data are available, most studies in the literature prefer a data-driven type of model (black box or grey box). Since these models are trained with actual building operational data, the actual heat dynamics of the building are captured well by these kinds of models. Another advantage is that the models can be developed in a used case base scenario where the inputs of the models can be decided based on the data available and the end use of the models. Therefore, a detailed weather file is not needed which makes these models very useful in model predictive scenarios where the models are used for future energy predictions of the building. The grey box models have a slight edge over the black box models in this case as the hybrid property of the model means that the model has a physical basis and is not completely data-driven. The physical basis of the model means that the model can be used to extrapolate the data. Therefore, grey box models can be used to evaluate extreme conditions which are not available in the training data set while black box models are confined within the range of the training dataset. Grey box models also take a fraction of time to run when compared to physics-based or black box models.

The grey box models are developed to capture the dynamic behaviour of heat transfer into a building zone [72]. In transient heat transfer of buildings, the temperature profiles were assumed to be sinusoidal in most of the models. Together with the autoregressive nature of the temperature signals, there was a significant delay in the heat addition to the thermal mass of the building and the related temperature change in the building [73]. Some of the models have attempted to capture this autoregressive dynamic behavior by incorporating the time delay into the models. Grey box model structures estimate parameters by using a historical data set [74][75], which is obtained by mainly two methods. The first method is to create an artificial data set using a white box or a physical model of the building. The second method is through a manual data collection of the building itself to create a required data set [76], [77], [78]. Some studies have also created data sets by conducting step response tests on model buildings. The second method of manual data collection although is time-consuming however, it captures the building dynamics more efficiently than an artificial data set created based on physical models [79]. Comparatively, both type of models: black box models and gray box models have their advantages and disadvantages in different applications/building zones. Nevertheless, there have been no systematic studies conducted in the literature to properly compare the accuracy of these models in their applications in tropical climate regions.

In recent decades, with the advancement of machine learning techniques data driven modeling has been popularly used for building energy research. The models developed by data-driven techniques can also be generalized by sampling the buildings in the area using different architectural types. The data collected is used to develop models and the models can be generalized if data collected are from different architectural type samples. However, to generalize to a certain region, these models require a large set of data collected over different types of buildings in the region. Due to the practical limitations of collecting data on different buildings by sampling the buildings in the Colombo area, especially due to the inability to access the buildings due to the pandemic situation, it was decided to develop data-driven models based on selected few buildings. These data driven models cannot be generalized for the region as these models are developed zone-specific and can be only used for predictions within the zone. However, once model is formulated it can be trained for any given building if the indoor and outdoor condition data are available. The data-driven model can then be used to predict the future indoor conditions and cooling load conditions under different future climate scenarios.

2.8 Research gap

The world is currently on a path of increasing global warming. The effect of global warming in hot and humid countries like Sri Lanka is prominent. Together with the global warming impact, the improvement of the socio-economic status of the country has put Sri

Lanka in the high-risk tier of the electrical infrastructure of the country. The building energy sector has been identified as a key area that consumes almost half of the country's power generation and it is slated to increase in the next several decades. Therefore, identifying the energy demand patterns for buildings, both residential and commercial is important to improve the electrical infrastructure of the country. These energy demand patterns can be used to predict the future energy demand of buildings, using computational tools. There are new building codes to ensure that the new constructions are energy efficient and sustainable, however, most of the existing buildings were constructed before the implementation of these codes and pose a significant threat to the electrical infrastructure of any tropical country. Although there has been research conducted in this regard all around the world to predict the climate change impact on building energy consumption, the results of these studies are highly localized due to various factors such as geography, population growth, building architecture etc. Furthermore, most of these studies are conducted in developed countries like USA and Europe with limited studies conducted in India and Mexico regions. There are only a few studies have been conducted in conditions like Sri Lanka both in geometrical conditions and socio-economic conditions. Development of data-driven models; especially grey box models is highly dependent on the geographical area. The type of building varies vastly from country to country and the thermal performance varies vastly from climatic region to climatic region. Therefore, the application of data-driven methodology of models from different climate regions and a different building stock to a vastly different type of building stock in a different climatic area is irrational. Different countries have developed grey box modelling methods for their building stocks and other countries are following the trend with little to no such method being presently developed for hot and humid climatic regions. Thus, the present study aims to address this research gap by analyzing the energy demand patterns of selected existing buildings located in Colombo city and its suburbs to establish future energy demand patterns. Further, the study expects to evaluate the climate change impacts on the future building energy demand and the effectiveness of passive cooling techniques to mitigate those effects.

2.9 Aim

This study aims to investigate the predicted energy demand for future climate scenarios in selected existing buildings and to investigate the effectiveness of passive cooling strategies to minimize the effects of climate change on the cooling energy usage of existing buildings in tropical regions.

2.10 Objectives

- To identify current energy demand patterns for air conditioning and ventilation in selected existing buildings and establish the relationship with ambient temperature and relative humidity changes
  - The sensitivity of the building to outdoor air conditions and the effectiveness of the building's thermal envelope are to be quantified. The change in cooling energy demand with short-term meteorological variables is to be studied using the heat balance method. The energy demand patterns for different conditions such as different types of thermal envelopes of buildings, different groupings of buildings, and different end-use of buildings are to be studied. The impact of different factors that affect cooling load are to be identified for different buildings. Since the Colombo area has a variety of buildings changing from geometrical locations to different types of architecture, several buildings should be selected to represent the Colombo sub-urban area.

- To develop methods to predict the future cooling energy demand pattern for existing buildings using future climate scenarios
  - The future cooling energy demand for existing buildings is to be predicted using the identified cooling energy demand patterns. All climate change scenarios introduced by IPCC are to be taken into consideration. The

prediction will be made by developing a grey box and black box model for selected existing buildings.

- To investigate the application of different passive cooling methods to reduce the predicted extra cooling energy demand in existing buildings.

- .
    - The cooling energy demand increase can be controlled by using passive cooling methods as well as low-energy ventilation methods. The effectiveness of different mitigation tactics is to be evaluated for selected buildings and the energy savings are to be calculated. Furthermore, the possibility of using and combining different passive cooling strategies in buildings in Colombo is to be identified through computational simulations with a focus on identifying the best passive cooling strategy/strategies for the selected geographical region

CHAPTER 3

METHODOLOGY

3.1 Overview

This section of the thesis discusses the methodology used to achieve the above research objectives. The research was conducted in main three stages. In the first stage, the existing buildings under current climatic conditions were analyzed to establish the current energy demand patterns and their relationship with the key weather-forcing parameters. Several sample buildings were selected and the energy demand patterns with short-term meteorological variability were studied for the selected buildings. In the second stage, the identified demand patterns were used to predict energy demand in future climate scenarios. In the third and last stage, different passive cooling strategies were evaluated to study their effectiveness in mitigating the climate change effects. Computational analysis was used to identify the effect of different passive cooling strategies and to establish the most suitable passive cooling strategy for the selected buildings. The selected strategies were analyzed to calculate and quantify the money saved through electricity bills over a 10-year period.

Stage 1: Literature review, data collection, and model development

- Literature review
    - A comprehensive literature review was conducted to identify the effect of climate change on existing buildings and establish critical parameters. Furthermore, different cooling load calculation procedures were studied and parameters affecting cooling energy load in buildings were identified. Studies relating to cooling demand patterns in buildings with the weather parameters in the published literature were studied, especially, the effect of climate change on tropical countries was studied to understand the severity of climate change impacts. Different passive cooling strategies used around the world were studied and the possibility of using these strategies to mitigate climate

change effect in climate conditions similar to Sri Lanka was studied through literature.

- Data collection
    - Several suitable sample buildings were selected considering the parameters affecting cooling load identified through literature. The buildings were selected to represent different building types identified. The indoor temperature and relative humidity data were logged. The outdoor weather conditions: the outdoor temperature and relative humidity data were also collected during the same period. Thermal comfort surveys were conducted to measure the thermal comfort of the occupants. Equipment surveys listed in the ASHRAE handbook were used to identify the internal loads of the buildings. In the data collection, the data logger placements were identified such that the data logger was not directly exposed to any heat sources identified in the literature.

- Data analysis
    - The collected data was used to establish a relation between the outdoor data and indoor conditions. Simple linear or non-linear models were used to establish the connection between identified parameters. One-dimensional linear methods, Autoregressive models with exogenous variables (ARX), Artificial Neural Network (ANN) models, and Nonlinear Artificial Neural Network models (NARX) were tested to predict the indoor temperature. Models of the type MPC (model predictive control) which allow to predict of the parameters for the next time step using the values of the current time step were used when predicting future energy consumption scenarios. Mean absolute error (MAE), Mean square error (MSE), and Root mean square error (RMSE), were used with separate testing and validation data to calculate the effectiveness of the numerical models used.

- Additionally, data-driven and physics-based hybrid models were developed for each building zone and compared with the model results from data-driven black box models
- Heat balance calculation software was used to calculate the indoor conditions using non-simplified heat balance calculations. The model predicted indoor condition calculations, measured values, and the values obtained through the calculation software were compared to optimize the model.
- Collected data from 2010 in a selected building was used in the model to predict the outputs for 2020-2021. The collected actual data in 2021 were used to test the model results

- Stage 2: Prediction of futuristic energy demand patterns and climate change impacts Study of climate change effect
  - The established numerical model was used to predict the indoor conditions and cooling energy demand for the selected areas in this stage. The prediction model was one step ahead or a two-step ahead model as literature has identified that making the model more complex will not have a significant increase in model reliability. The outdoor conditions for the prediction model were calculated using the existing climate change models published by the IPCC [80].
  - Different climate change models predicted by different emission scenarios until 2100 by IPCC were used to identify the outdoor conditions in the selected areas.
  - The IPCC predicted outdoor conditions were also used in the heat balance calculation software and the numerical model output and the heat balance calculation software output were compared.

Stage 3: Evaluation of the effectiveness of different adaptive measures to reduce the cooling energy demand

- Analysis of adaptive measures
    - The effectiveness of adaptive measures such as passive ventilation, heat storage materials, and solar designs in mitigating the climate change effects under different climate scenarios was studied. Computational analysis and thermo-fluid simulations were used for this analysis. The computational simulations used existing flow simulation software ANSYS fluent and simple numerical codes established based on cooling load calculations. The effect of mitigation tactics was modeled in the selected areas using the cooling load calculation software IES VE and thereby the amount of cooling energy demand reduced was calculated. Different combinations of passive cooling strategies were tested and the best passive cooling strategies for the selected areas were established. The selected strategies were then modeled to calculate the amount of electricity load saved and quantify the economic benefit in terms of money saved through electricity bills in a 10-year time span. Additionally, an estimate of the payback period for a 1,000,000 LKR initial investment was calculated.

A detailed discussion of the three stages of the methodology and the methods used for the different stages are provided in the subsequent sections of this chapter**.**

3.2 Initial data collection

The data collection from a wider range of buildings is vital in establishing a relationship between outdoor conditions and building cooling energy requirements. As discussed above, for both physics-based models and data-driven models, experimental data collection is critical in model validation and training of the model. In physics-based models, the collected data can be used to validate the model and then it can be generalized to other buildings. However, due to the limited accessibility and limited equipment availability mainly three accessible buildings located in Colombo and its suburbs were selected for data collection. In the selection of the buildings, it was tried to select buildings with saliently different features to make the data collection more versatile. The details of the selected sample buildings are given below

- Western Provincial Council building, Battaramulla, Sri Lanka,
    - This building is a relatively newer building, which started construction in 2015 and was commissioned in 2016. The building is situated in Battaramula, Sri Lanka, in an area where most government office buildings are currently being shifted. This newly constructed building was selected for the initial study because of heat addition due to infiltration of air caused by the aging of the building is minimal. Also, the building has minimal disturbances caused by greenery, and the shadowing of the building from surrounding structures.
- Sumandasa building, University of Moratuwa,
    - This is an older building constructed more than 40 years ago, which is situated in the University of Moratuwa, Sri Lanka. The importance of this building is that this building has been designed for natural ventilation with many passive cooling techniques to reduce the heat addition into the building zones from the external environment. However, in recent years certain parts of the building have been mechanically ventilated. Thus, this gives an example of an existing building which has been affected by climate change impacts.
- Building of Department of Electronic and Telecommunication Engineering, University of Moratuwa

- A relatively older building than the Western Provincial Council building, however relatively new compared to the Sumanadasa building and built for mechanical ventilation. The building has non-air-conditioned internal corridors which connect mostly air-conditioned rooms in the building.

Several zones in the buildings were selected for the data collection and analysis based on the number of occupants, air-conditioned/non-air-conditioned space, and west and east-facing windows etc. The zones were selected to have the most variety possible. The zones were selected such that they are non-air conditioned as much as possible such that the data collected inside the zones are solely dependent on the natural heat additions and heat rejections. The details of the zones selected in the three buildings are given in Table 3.1.

For the initial round of calculations and predictions of future cooling load data were collected from building 01 from 2020/09/14 to 2020/11/25 (Access to the building after this date was restricted due to the lockdown in the country). The predictions of cooling loads of the building for 2050 and 2090 were calculated based on the current cooling load conditions and a simple linear climate change model.

TABLE 3.1: INFORMATION OF THE SELECTED BUILDINGS AND IDENTIFIED ZONES FOR DATA COLLECTION

	Building 1	Building 2	Building 3
Location of the building	Battaramulla, Sri Lanka	University of Moratuwa, Sri Lanka	University of Moratuwa, Sri Lanka
Built year	2017	1973	2001
Building application	Office space	Laboratories and Classrooms	Laboratories and classrooms
Designed cooling method	Mechanical cooling	Natural ventilation with external shadings and courtyards	Mechanical cooling
Description of Zones	Zone 1.1- Deck on the top floor of the building with a West facing unshaded window, No internal loads, Not air conditioned Zone 1.2 – Office area on first floor, Air conditioned Zone 1.3 – Cafeteria on the first floor with large floor area, Not air conditioned	Zone 2.1 – Machinery laboratory on first floor. Not air conditioned. Many heat dissipating machinery are used. Zone 2.2 – Classroom on first floor. Not air conditioned. Not been in use during data collection and therefore no internal loads. High furniture mass factor Zone 2.3 – Break room on top floor. Not air conditioned. Small floor area	Zone 3.1 – Office area on third floor with shaded windows. Not air conditioned Zone 3.2 – Break room on the third floor. Low exposure to outdoor conditions through external walls Not air conditioned

3.3 Initial cooling load predictions for building 01 using a linear climate change model

The data collected from three zones of building 1 (Western Provincial Council building): zones: zone 1.1- timber deck, zone 1.2-office, and zone 1.3- cafeteria were used for the initial analysis.. HOBO U12-012 Temperature and Relative Humidity (RH) data loggers were used to collect the indoor temperature and RH data. The technical specification of the data logger is given in Table 3.2. The position of data loggers and the floor plans with the building orientations are shown in Figure 3.1. The shading coefficient of windows is estimated using the guidelines given in the ASHRAE pocket guide for air conditioning [30]. A survey of the equipment inside selected zones was conducted to identify the internal loads as depicted in Annex II. The usage factors and radiant factors of the equipment were adapted from ASHRAE fundamentals [81].

TABLE 3.2: SPECIFICATIONS OF THE DATA LOGGER

Property	Details
Description	Temperature, Relative Humidity, and Light Intensity standalone data logger with external channel for an external sensor
Memory	40,000 measurements
Sampling range	1 second to 18 hours, user-selectable
Battery	Typical one year, user replaceable CR 2032
Range	Temperature - -20° to 70°C (-4° to 158°F) Relative humidity - 5% to 95% RH (non-condensing) Light intensity – For general purpose indoor measurements - 1 to 3000 foot-candles (lumens/ft2) typical 0-32,300 lumens/m2 External input - 0 to 2.5 VDC
Accuracy	Temperature - ± 0.35°C from 0° to 50°C (± 0.63°F from 32° to 122°F) Relative humidity - ± 2.5% typical, 3.5% maximum, from 10 to 90% RH Light intensity – For general purpose indoor measurements External input - ± 2 mV, ± 2.5% of absolute reading
Resolution	Temperature - 0.03°C @ 25°C (0.05°F @ 77°F) Relative humidity - 0.03% RH External input - 6mv

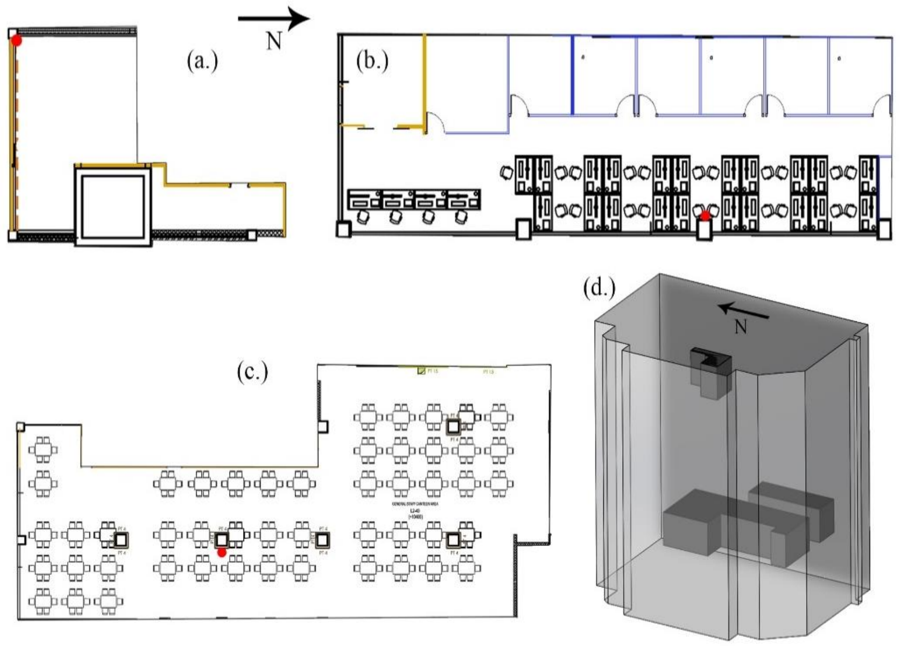

Fig. 3.1: Floor plans and position of rooms in the building. (a) Timber Deck, (b) Office, (c) Cafeteria and (b) position of rooms in building in the building. Location of the data loggers are marked in red dots

3.3.1 Calculation of cooling load

For cooling load calculations, the CLTD/CLF (Cooling Load Temperature Difference / Cooling Load Factor) method was used. Equations 11- 17 were used to calculate the cooling load from different internal and external sources.

Heat load through the roof, windows, and external walls were calculated using Equation 11,

$$Q_1 = U * A * \mathrm{CLTD}_C \tag{11}$$

where, U is the thermal transmittance according to the 2017 ASHRAE fundamentals, A is the area of the surface concerned, $\mathrm{CLTD_C}$ is the corrected cooling load temperature difference. As the CLTD values from 2017 ASHRAE fundamental tables were provided for an internal temperature of 25.5°C and mean outdoor temperature of 28°C, these table CLTD ($CLTD_T$) values has been adjusted using the Equation 12 to be used in the Sri Lankan weather conditions.

$$\mathrm{CLTD}_C = \mathrm{CLTD}_T + (25.5 - \mathrm{T}_R) + (\mathrm{T}_M - 28) \tag{12}$$

where, T_M is the mean outdoor temperature and T_R is the desired air-conditioned room temperature. The heat due to solar radiation (Q_2) can be calculated by using Equation 13 where, A is the surface area concerned, $SCLF$ and SC are the solar cooling load factor and shading coefficient according to 2017 ASHRAE fundamentals. Heat load from occupants can be calculated by using Equations 14 and 15 which gives the sensible heat load (Q_3) and latent heat (Q_4) load, respectively. q_s and q_L are the sensible and latent heat load from a typical person according to activity level as given in the 2017 ASHRAE fundamentals [82] and N_O is the average number of occupants in the area. Load due to lighting appliances (Q_5) was calculated using the standard LPD (Lighting Power Density) per unit area values given in the 2017 ASHRAE fundamentals [83]. Equation 16 was used to calculate the heat gain by lighting, where the F_U is the usage factor, F_B is the ballast factor and CLF is the Cooling Load Factor given in the ASHRAE fundamentals 2017. A is the area of the room concerned. Loads due to other electrical appliances (Q_6) were calculated by using Equation 17 where W is the total heating load, F_U is the usage factor and F_R is the radiant factor as indicated in the Annex II.

$$Q_2 = A * (SCLF) * SC \tag{13}$$

$$Q_3 = N_O * q_S * CLF \tag{14}$$

$$Q_4 = N_O * q_L \tag{15}$$

$$Q_5 = (LPD) * A * F_U * F_B * (CLF) \tag{16}$$

$$Q_6 = W * F_U * F_R * (CLF) \tag{17}$$

3.3.2 Determining the desired internal temperature for cooling load calculations

An internal set point should be established to calculate the cooling loads of the zones selected. Although standard internal temperature set points are given by ASHRAE, people in hot and humid tropical regions are more comfortable in higher set points than people in relatively colder countries where the standards are used [16].

To address this, a survey was conducted at zone 1.3-cafeteria to calculate the thermal comfort level of the occupants and the average Clo values of the clothing of the occupants. The survey is attached in Annex I. The survey was prepared according to ASHRAE 55 [84]. The survey results were only taken from occupants who spent more than 5 minutes in the cafeteria area and were seated down in a cafeteria table. The survey results were calculated for time intervals of 8.00 a.m. – 10.00 a.m., 10.00 a.m. – 12.00 p.m., 12.00 p.m. – 2.00 p.m., and 2.00 p.m. – 4.00 p.m. The results were used to calculate the thermal insulation of occupants (clo values) and obtained the average clo value separately for men and women using Equation 18. $I_{cl,\ active}$ is the calculated clo value and I_{cl} is the clo value due to clothing and M is the metabolic rate due to activity level.

$$I_{cl,active} = I_{cl} * (0.6 + \ 0.4/M) \tag{18}$$

The thermal comfort sensations of the occupants were calculated as the PMV (Predicted Mean Vote) value and were recorded using the survey with ASHRAE 7-point scale (-3 – too cold, -2 – cold, -1 – slightly cold, 0 – comfortable, 1 – slightly warm, 2 – warm, 3 – too hot).

3.3.3 Calculation of sampling intervals

According to the literature, for data-driven models, sample intervals have a clear influence on the model performance. Using studies published by Ljung and Underwood [85] there are three steps in practice to calculate the sampling intervals in data collection:

- Apply a step increment to the input signal
- Find the dominant time constant – (i.e. time taken by the response to reach 63.21% of the apparent overall change)
- Ideal sampling frequency is 10% of the dominant time constant.

The issue with these methods is the inability to isolate a signal input to apply a step increment to the input in a practical scenario. Therefore, during the current study, two other alternative methods were considered in calculating the sampling interval[86],

1. Estimation of the difference between the outdoor temperature peak time and the indoor temperature peak time and take sample interval as $1/10^{th}$ of this value.
2. Use an accurate software which uses the heat balance method to calculate dominant time constant. The software should have the ability to provide dynamic input variables.

The data collected from each zone of the selected buildings were used to calculate the variation of indoor and outdoor temperature for an average day. The difference between the times of day for the peak of the indoor and outdoor temperatures was calculated and they were used to determine the time constants.

In the second method, IES VE software was used to calculate the ideal sampling intervals. The selected zones were modelled using the modelling tool in the IES VE software. All variables were set to constant values. All outdoor temperature parameters were set at constants assuming the time to be 12.00 am on 1st January 2020. This eliminates any load change due to sun travel. A preconditioning period of 12 hours was used with an outdoor temperature of 25^{o}C and relative humidity of 80%. A step increase of 5^{o}C was given as the input. The transient time model was used to calculate the variation of indoor temperature and the time taken to reach 63.21% of the indoor temperature after being stabilized (indoor temperature 24 hours later) was used to calculate the sampling interval required. The calculated ideal sampling intervals from the two methods are given in Table 3.3.

TABLE 3.3: CALCULATED IDEAL SAMPLING INTERVALS FOR THE ZONES

Zone	Time constant (using measured values)	Time constant (Using simulated values)
Zone 1.1	8 minutes 3 seconds	6 minutes 43 seconds
Zone 1.2	10 minutes 23 seconds	6 minutes 52 seconds
Zone 1.3	11 minutes 5 seconds	9 minutes 37 seconds
Zone 2.1	10 minutes 58 seconds	7 minutes 32 seconds
Zone 2.2	8 minutes 21 seconds	7 minutes 38 seconds
Zone 2.3	7 minutes 49 seconds	4 minutes 12 seconds
Zone 3.1	9 minutes 42 seconds	10 minutes 33 seconds
Zone 3.2	11 minutes 34 seconds	6 minutes 32 seconds

Most of the calculated sample times were close to 10 min, thus a constant sampling interval of 10 minutes was used in data analysis and modelling of the selected zones.

3.4 Data collection

Room internal temperature and relative humidity were logged for buildings two and three from 2021/02/15 to 2021/03/28 and for building one from 2020/09/14 to 2020/11/25. An additional data logger was used to log the outdoor temperature and relative humidity values for the same duration. The time period for data collection was 6 weeks and sampling intervals of one minute. Ten data points were averaged to get a data set with sampling intervals of 10 minutes.

The indoor data loggers were positioned in the locations indicated by red dots in Figure 3.2. The data loggers have been placed such that they were not directly exposed to sunlight or any other heat-emitting device. An equipment survey was carried out to estimate the internal heat gains of the zones. The zone geometrical parameters and internal loads are given in Table 3.4.

TABLE 3.4: PROPERTIES OF THE SELECTED ZONES.

Property	Zones							
	1.1	1.2	1.3	2.1	2.2	2.3	3.1	3.2
Type of room	Viewing deck	Office	Cafeteria	Machine lab	Lecture room	Break room	Office	Break room
Floor area (m^2)	25.49	52.39	652.62	179.47	46.23	12.14	32.57	36.36
External wall area (m^2)								
North	0	0	0	116.69	24.78	0	0	4.9 **
East	0	49.38	0	0	0	0	0	0
South	0	14.45	37.62	0	0	0	15.3*	0
West	20.04	0	17.67	0	0	10.26	0	0
External window area (m^2)								
North	0	0	0	37.8	8.4	0	5.83	2.98
East	0	28.21	0	0	0	0	0	0
South	0	8.35	34.85	0	0	0	0	0
West	19.81	0	15.21	0	0	6	0	0
Internal wall area (exposed to air-conditioned space) (m^2)	0	16.46	206.18	47.18	24.64	0	32.31	0
Internal wall area (exposed to non-air conditioned space) (m^2)	66.17	49.38	46.9	115.18	48.86	37.96	45.92	88.37
External wall area/Total wall area	0.233	0.492	0.179	0.418	0.252	0.213	0.164	0.052
External Window area/Total External wall area	0.99	0.573	0.905	0.324	0.339	0.585	0.380	0.608

Note - * indicates walls facing southwest, ** indicates walls facing northeast

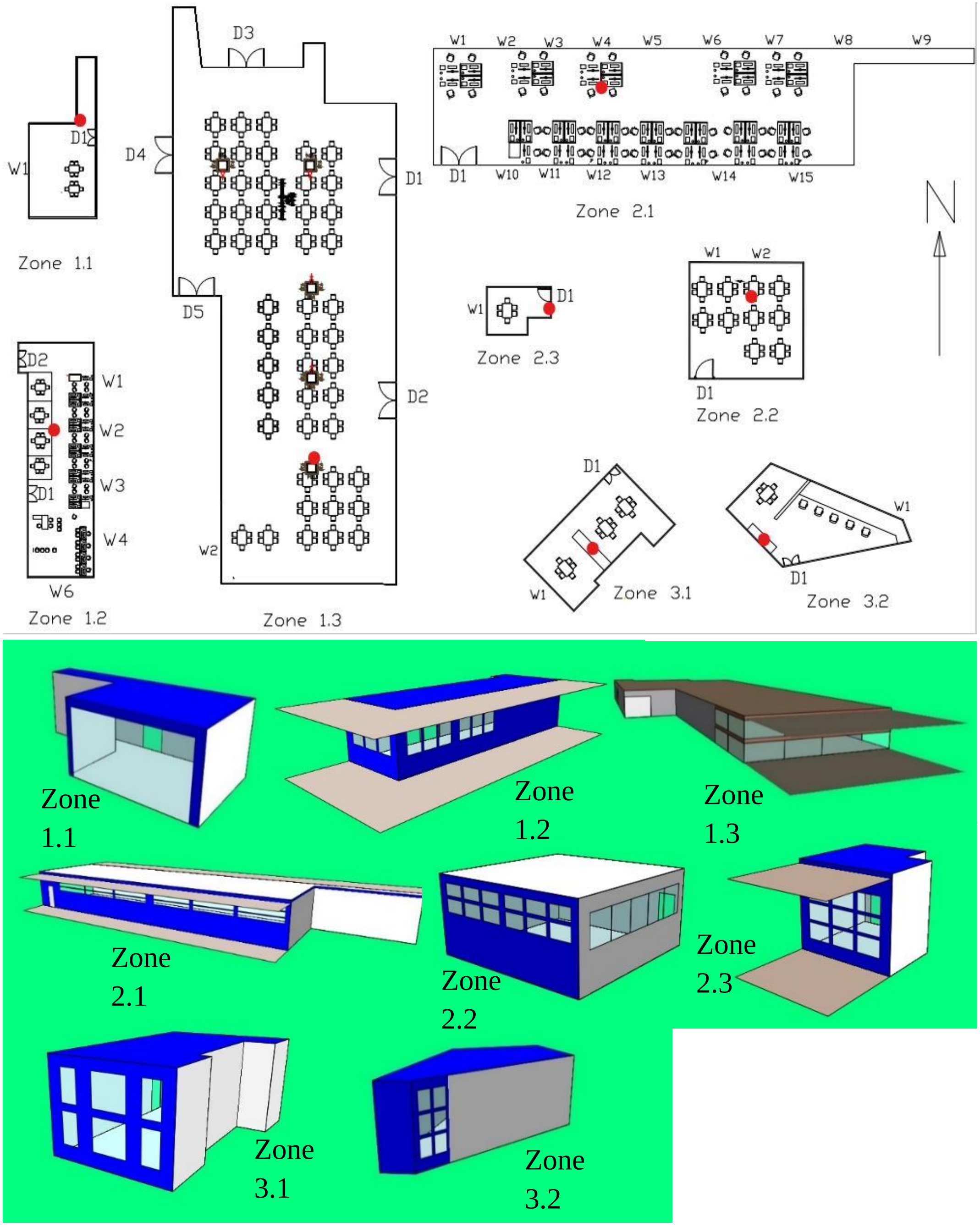

Fig. 3.2: Plans and elevations of the selected zones. The red dots indicated in the plan represent the positions of the data loggers

3.5 Neural network model (Black box model)

NARX (Non-linear auto-regressive with exogenous input) neural network modelling was used to analyse eight selected zones of three buildings, discussed in section 3.4. Indoor temperature and relative humidity were identified as the model outputs or predictions, and outdoor temperature and relative humidity were used as the external inputs or predictors of the model. The collected data from the eight zones were used to train and validate the model. Furthermore, the models were tested for data sets of 2010 and 2021 for accuracy for one of the zones (zone 3.2).

A total of 6048 data points including indoor temperature, indoor relative humidity, outdoor temperature and outdoor relative humidity have been obtained during data collection per single zone. Out of the total data collected, data from four weeks (4032 data points) have been used to train the NARX model and other two weeks (2016 data points) have been used to test the models. The established NARX models for the eight zones were then used with predicted outdoor temperatures of year 2090 to calculate the corresponding indoor temperature variation. The NARX model was used to predict future values of a time series *y(t)* according to a set delay time (*d*). The model can be written mathematically in the form indicated by Equation 19.

$$T_i(t) = f(T_i(t-1), \ldots, T_i(t-d), T_o(t-1), \ldots, T_o(t-d), RH_o(t-1), \ldots, RH_o(t-d), RH_i(t-1), \ldots, RH_i(t-d)) \quad (19)$$

where, t indicates the time step of the time series and the meaning of the other variables are given below;

$T_i(t)$ – Measured indoor temperature (^oC)

$T_o(t)$ – Measured outdoor temperature(^oC)

$RH_i(t)$ – Measured indoor relative humidity (%)

$RH_o(t)$ – Measured outdoor relative humidity (%)

t – Time of day (minutes)

$T_p(t)$ – Predicted indoor temperature(^oC)

The model used the past values of itself ($T_i(t-1), \ldots, T_i(t-d)$) and the past values of some different time series ($RH_o(t)$, $T_o(t)$) for the prediction. Therefore, the inputs to the neural network were $RH_o(t)$, $RH_i(t)$ and $To(t)$ and $T_i(t)$ was the target time series of the model.

Two feed-forward multilayer neural networks were trained for each zone to predict the one-time step ahead values of indoor temperature and indoor relative humidity[87]. Each network consists of three exogenous (external) inputs and one output. The study used one hidden layer with ten hidden neurones to predict the one-time step head values. The hidden neurones were of logsig (sigmoid) type. The optimization study was conducted by changing the number of hidden neurones, however increasing the number of neurones has not shown any significant change in the results. The model used one feedback input in the network with one-time step delay. The neural networks to predict the temperature values and RH values were created using MATLAB with 1000 epochs of training. The developed model outputs the predicted indoor temperature values at a one-time step ahead (10 minutes ahead) by using the current time step indoor temperature, indoor relative humidity, outdoor temperature, outdoor relative humidity and time as inputs to the network. The layout of the NARX network is shown on Figure 3.3.

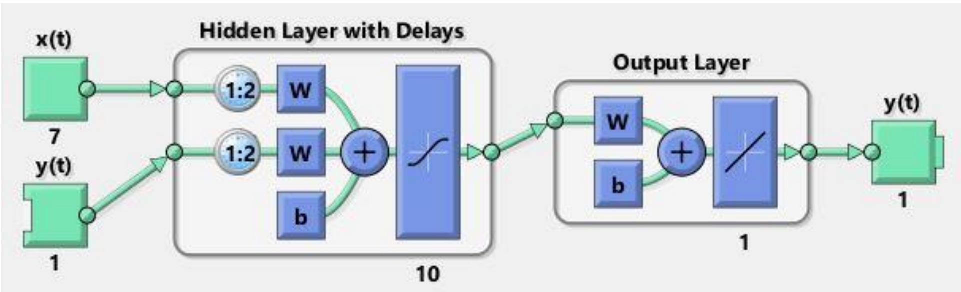

Fig. 3.3: Layout of the Neural network of the NARX model

In training the neural network, the collected data points (temperature and RH) have been divided into three categories: where 70% of the collected data were used for model training, 15% for model validation and the rest for testing during model training.

MATLAB neural network modelling toolbox enables to training of the networks using three algorithms. The networks were tested with all three algorithms, and it was observed that Levenberg-Marquardt algorithm showed the highest accuracy with low computing time. The networks were also tested by changing the delay interval but no significant change in model accuracy was observed by using higher delay intervals. Therefore, one-step-ahead prediction models were trained for all zones.

The weights of the neural network were modified during the training stage comparing the predicted values to the actual targets. The training was stopped by checking the generalization from the validation stage. Testing during training was conducted to analyse the performance during training and validation of the network. After training, the additional data of two weeks were used as a testing data set for the network. Because the data sets were selected at random when training the model, for the same input data set, the performance of the network changes every time when the network is trained. Therefore, each data set was trained ten times and the network showing the best performance was selected for the analysis.

3.5.1 Network performance

The network performance has been evaluated using the coefficient of correlation (R) and Mean Squared error (MSE). MSE was calculated using Equation 20.

$$MSE = \frac{1}{n}\sum_{k=2}^{n+1}(T_P(k) - T_i(k))^2 \tag{20}$$

The R and MSE values were calculated for both the training stage (training, validation and testing during training) and the testing stage.

3.6 Grey box model introduction

Therefore, the present study compared the performance of a simplified NARX model and a dynamic grey box model which are both based on data collected in eight selected zones in three different buildings located in Colombo, Sri Lanka.

IPCC (Intergovernmental Panel for Climate Change) in its 7th report have predicted the change in global average surface temperatures considering two different emission scenarios. These scenarios are the Representative Concentration Pathways (RCP) which are distinguished by the radiative forcing value of the different emission conditions. The established models are used to predict the indoor temperature of the selected zones for 2090 under RCP 4.5 and RCP 8.5 climate change scenarios [48], [49], [50], [88].

3.6.1 Network performance

In the present study, a grey box model which is formulated based on Newton's cooling law was used. In this model, the rate of heat loss from the object is directly proportional to the temperature difference between the object with its surroundings which is modeled according to Newton's Cooling Law as given in Equation 21,

$$\frac{dQ}{dt} = hA(T_o - T_{env}) \tag{21}$$

where, dQ/dt is the rate of heat loss from the object, h is the coefficient of heat transfer, A is the effective surface area for heat transfer of the object and the surroundings, T_o and T_{env} are the temperature of the object and the surrounding environment, respectively.

Equation 21 is written based on the rate of heat transfer. The heat capacity equation (Equation 22) was used to convert Equation 23 to express in terms of the rate of change of temperature as,

$$\frac{dQ}{dt} = C * \frac{dT}{dt} \tag{22}$$

To model the building zone using the above set of equations, the selected zone was assumed to be a lumped thermal mass, where the entire zone was considered as a single mass of thermal object with uniform indoor temperature. The internal thermal convection effect was neglected during the calculation. Therefore, indoor temperature was considered as the object temperature in the equations and outdoor temperature was considered as the environment temperature of the model. It was assumed that outdoor temperature is uniform throughout all the surfaces of the zone exposed to external conditions.

$$\frac{dT_{in}}{dt} = \frac{U}{C}(T_{in} - T_{out}) \tag{23}$$

where, T_{in} and T_{out} are indoor and outdoor temperatures, respectively (in Kelvin) and overall heat loss coefficient $U=hA$ (measured in W/K). As the entire zone was assumed as a single lumped thermal mass, the addition of thermal energy into the system in the form of internal energy sources through equipment utilized in the building was included in the equation as,

$$\frac{dT_{in}}{dt} = \frac{1}{C}[U(T_{in} - T_{out}) + E] \quad (24)$$

where, E is the thermal energy added to the system by equipment used inside the zone.

Solar irradiance on the external surfaces of the building envelope is a major contributing factor to the thermal energy transferred through the envelope into the building's thermal mass. In literature, studies have used isotropic sky models and anisotropic diffusion sky models to calculate the global horizontal irradiance and the radiation power on building envelope surfaces [77]. Isotropic diffuse radiation of the sun, ground reflected diffuse radiation and beam radiation are considered in isotropic diffuse sky models. Literature shows that isotropic diffuse sky models underestimate 10-15% radiation power values compared to anisotropic diffuse models. The anisotropic diffuse models take into account the circumsolar diffuse and horizon brightening effects which are significant for vertical building envelopes. Hence this study used Hay-Davies-Klucher-Reindall (HDKR) anisotropic sky diffuse model in calculating solar irradiance of the external surfaces. The different diffused radiation components used in the model are illustrated in Figure 3.4 [89].

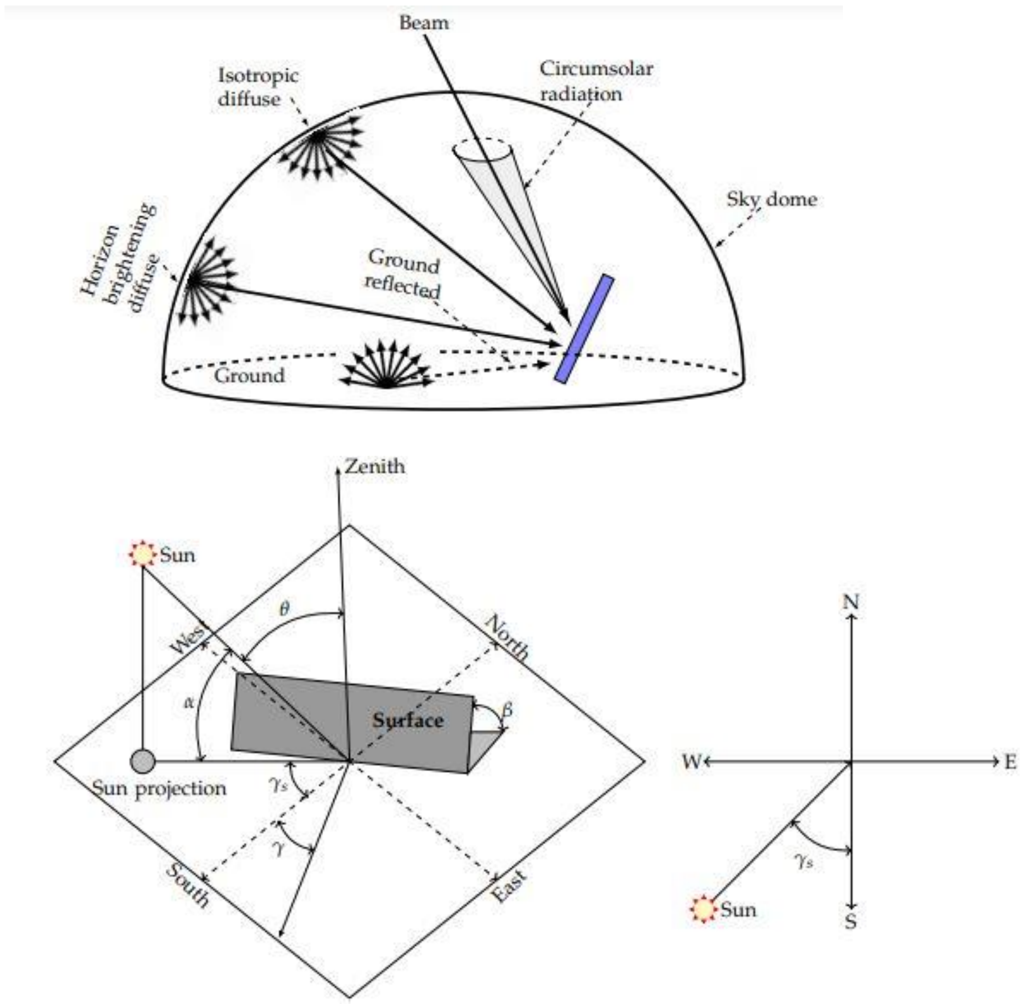

Fig. 3.4: Components of radiation considered in HDKR model and angles considered [86]

HDKR model calculates the radiation incident on an inclined surface using Equation 25 [86],

$$I_T = (I_b + I_d)R_b + I_d(1 - A_i)\left(\frac{1 + \cos(\beta)}{2}\right) X \left[1 + f sin^3(\frac{\beta}{2})\right] + I_{gh}\rho_g(\frac{1 - \cos(\beta)}{2}) \tag{25}$$

where, I_T is the total radiation incident on the inclined plane, I_b and I_d are beam and diffuse radiation, A_i is the anisotropy index, $R_b$is the geometric factor, $\beta$is the angle of inclination of the plane relative to horizontal plane, $f$is the cloudiness index, $I_{gh}$is the total radiation incident on a horizontal ground plane and ρ_g is the albedo of ground.

For building envelope study, the walls and windows of the building are vertical and therefore β is taken as 90^{O}. This simplifies Equation 25 to,

$$I_T = (I_b + I_d)R_b + I_d(1 - A_i)\left(\frac{1}{2}\right) X\ [1 + 0.3535f] + I_{gh}\rho_g(\frac{1}{2}) \tag{25}$$

Anisotropy index (A_i) is calculated by using Equation 27, where *I* is the extraterrestrial radiation. All values were calculated according to the latitudes and longitudes of the selected region for study as given in [9],

$$A_i = \frac{I_b}{I} \tag{27}$$

Considering θ as the beam radiation incident angle on a tilted surface, geometric factor R_b was calculated using the Equations 28, 29 ,and 30 [79],

$$\begin{aligned} cos\theta = {} & sin\,\delta\, sin\,\emptyset\, cos\,\beta - sin\,\delta\, cos\,\emptyset\, sin\,\beta\, cos\,\gamma \\ & + cos\,\delta\, cos\,\emptyset\, cos\,\beta\, cos\,\omega + cos\,\delta\, sin\,\emptyset\, sin\,\beta\, cos\,\gamma\, cos\,\omega \\ & + cos\,\delta\, sin\,\beta\, sin\,\gamma\, sin\,\omega \end{aligned} \tag{28}$$

$$cos\theta_Z = sin\,\delta\, sin\,\emptyset + cos\,\delta\, cos\,\emptyset\, cos\,\omega \tag{29}$$

$$R_b = \frac{cos\theta}{cos\theta_Z} \tag{30}$$

where, $\theta, \omega, \gamma, \theta_Z, \emptyset$ are the incidence angle, hour angle, surface azimuth angle, zenith angle and latitude angle, respectively.

The declination angle (δ) is calculated by using Equation 31,

$$\delta = 23.45\, sin\left[360\left(\frac{284 + n}{365}\right)\right] \tag{31}$$

where, *n* is the number of the day of the year.

For a building envelope, the hourly solar radiation absorbed by the building envelope (Q_r) was calculated by using Equation 32 as [79],

$$Q_r = I_t S_i \alpha_i \tag{32}$$

where S_i is the surface area and α_i is the index representing surface radiation absorptivity and transmittance.

The total radiation absorbed by the building envelope into the considered room (P) was calculated by the summation of the above Q_r value of Equation 32 averaging over the time interval considered in the model. The calculated solar radiation heating power or the total radiation absorbed by the building envelope (P) can be included in Equation 24 to obtain a refined model for rate of change in indoor temperature as given in Equation 33.

$$\frac{dT_{in}}{dt} = \frac{1}{C}[U(T_{in} - T_{out}) + E + P] \tag{33}$$

The first-order differential equation given in Equation 33 was discretized by Euler's method to obtain a predictive model equation where the indoor temperature was calculated using past values of indoor temperature (Equation 34). Δt is the time delay or the time step size considered.

$$\begin{aligned} T_{in}(t) - T_{in}(t-1) \\ = \frac{\Delta t}{C}[U[T_{in}(t-1) - T_{out}(t-1)] + P(t-1) + E(t-1)] \end{aligned} \tag{34}$$

Although the main heat energy input into the system were considered in the above model formulation, there are some other un-modelled parameters such as air infiltration and internal heat gains which may affect the indoor temperature of the zones. Therefore, to account for these un-modelled parameters few additional parameters *x1, x2, x3, …* were introduced into the model. To account for the autoregressive nature of the model and the dynamic time delay of variable change to indoor temperature increase, a calculated delay time was introduced to the model (Equation 34). Using these corrections Equation 34 becomes,

$$\begin{aligned} T_{in}(t) = x_1 \Big[& T_{in}(t-d) \\ & + \frac{\Delta t}{C}[x_3 U[T_{in}(t-d) - T_{out}(t-d)] + x_4 P(t-d) \\ & + x_5 E(t-d)] \Big] + x_2 \end{aligned} \tag{35}$$

where, d is the number of delay time steps, $T_{in}(t)$ is the indoor temperature during the current time step, and $T_{in}(t-d)$ is the indoor temperature in d number of previous time step.

3.6.2 Evaluation of model performance

The model performance was analyzed by calculating the Root Mean Square error (RMSE) (Equation 36) and the Normalized Root Mean Square error (NRMSE), (Equation 37). Both these represent the measure of the difference between the predicted indoor temperatures from the above model and the actual measured indoor temperature values.

$$RMSE = \sqrt{\frac{1}{n}\sum_{i=1}^{n}\left[T_{i-m}(t) - T_{i-p}(t)\right]^2} \tag{36}$$

$$NRMSE = \frac{RMSE}{Range\ of\ measured\ indoor\ temperature\ distribution} X\ 100\% \tag{37}$$

where, T_{i-m} is the measured indoor temperature, T_{i-p} is the model predicted indoor temperature and n is the total number of time steps.

Although RMSE and NRMSE values evaluate the accuracy of the predicted values compared to the observed data, both these statistical indicators fail to capture the correlation between input and output variables which is important when identifying a suitable model. To check the correlation, Pearson correlation coefficient (R) was calculated for the models using Equation 38.

$$R = \frac{n\sum_{i=1}^{n}\left[T_{i-m}(t) - T_{i-p}(t)\right] - \left[\sum_{i=1}^{n}[T_{i-m}(t)]\right].\left[\sum_{i=1}^{n}\left[T_{i-p}(t)\right]\right]}{\left[n[\sum_{i=1}^{n}[T_{i-m}(t)]^2] - [\sum_{i=1}^{n}[T_{i-m}(t)]]^2\right].\left[\ n\left[\sum_{i=1}^{n}\left[T_{i-p}(t)\right]^2\right] - \left[\sum_{i=1}^{n}\left[T_{i-p}(t)\right]\right]^2\right]} \tag{38}$$

3.6.3 Parameter identification

Simulated annealing algorithm was used to identify the parameters in the model. Simulated annealing is a stochastic algorithm which is used for parameter identification using minimizing and optimizing an objective function. According to the literature, the annealing algorithm minimizes to a global minimum, however it was reported that it could also be minimized to local minimums resulting in incorrect solutions [90], [91]. Hence a probability function was used in the present study to escape local minimums by not accepting the seemingly best solution and scanning for other solutions. If no better solutions are observed, the best solution is presented as the parameter values which gives the minimum value for minimizing or objective function. In the present analysis, the error function was used as the objective function.

Existing literature showed that initial estimations of parameters have a significant impact on the model performance. Therefore, rough estimations of the parameters were calculated by the *pattern search* algorithm in the MATLAB Optimization toolbox. This rough estimation was then used with the *simulated annealing* algorithm in the same toolbox to further refine the results. Furthermore, the identified parameters were used as starting points for the *fminunc* algorithm in the Global optimization toolbox to find the local minimum.

3.6.4 Model validation

The data collected were used to estimate the parameters for the gray box model. The physical parameters (*U* and *C*) required for the model were calculated as guided by ASHRAE Fundamentals 2017 [81]. Overall *U* value was calculated by averaging the *U* value over the surface area of each component given in Table 3.4. Estimation of heat capacity was done considering the age of the building, type of construction, thermal mass of furniture and equipment in the zone, and the zone floor area.

Previous studies have shown that the time delay taken in parameter identification has a significant impact on the accuracy of the predictions [77], [92]. Different studies have used different methods to calculate the time delay with most being a trial-and-error method of calculations. Most of these studies have sampling intervals of one hour and therefore use time delays of one or two time steps. For this study, the time delay was estimated by analyzing the collected data. The time delay was set to be equal to the time lag of peak outdoor temperature and peak indoor temperature assuming that the difference in peak temperatures is a better representation of the dynamic time delay of the building thermal mass. The averaged *U* and *C* values with the calculated time delays used for the model for the zones are given in Table 3.5. Cloudiness index (*f*) for calculating radiation intensity was estimated from the data of cloud cover obtained by the Central Environmental Authority (CEA) of Sri Lanka.

TABLE 3.5: OVERALL U, C AND TIME DELAY FOR ZONES

Zone	U (kW/K)	C (kJ/K)	Measured time delay of peak temperatures (minutes)	No. of delays time steps
Zone 1.1	0.84	105,240	81	8
Zone 1.2	3.24	1,547,811	104	10
Zone 1.3	1.21	804,125	107	11
Zone 2.1	1.15	912,885	98	10
Zone 2.2	1.94	624,852	80	8
Zone 2.3	0.22	245,251	72	7
Zone 3.1	1.13	548,723	88	9
Zone 3.2	0.83	400,258	111	11

The collected data was used to calculate the x_1, x_2, x_3, x_4, x_5 parameters and validation using a four-fold cross validation method [86]. The collected data sets were divided into four folds. Three of the folds were used for identification and the remaining fold was used for model validation. Each data set was used to calculate four instances of the parameters changing the folds used for validation and identification in the manner shown in Figure 3.5. RMSE was used as the objective or minimizing function for the simulated annealing algorithm. Time discontinuity was taken into account by pre-processing and smoothening the input data as in two instances, the validation data set is in the middle of the identification data set. Model performance was evaluated for each identification and validation steps using RMSE, NRMSE and R values.

Fold 1	Fold 1	Fold 1	Fold 1
Fold 2	Fold 2	Fold 2	Fold 2
Fold 3	Fold 3	Fold 3	Fold 3
Fold 4	Fold 4	Fold 4	Fold 4

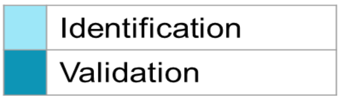

Fig. 3.5: Four fold cross validation

3.7 Prediction of indoor temperature and cooling load using developed models

The cooling load of a space is affected by both internal and external heat gains. Although the rise in internal temperature is the tangible outcome of the outdoor heat gain, calculating the cooling load based on indoor temperature is a more practical outcome in designing HVAC systems in tropical regions. The main sources of heat for a typical area of a building are heat gain through conduction, solar transmission, infiltration, internal loads such as lighting, and also the delayed heat addition due to thermal mass inside the building. In the present study, the cooling loads of the selected zones of the three selected buildings have been calculated using the cooling load calculation software tool IES VE. IES VE software provides two methods to mathematically model the dynamic heat transfer and calculate the thermal load of an area. The first method uses the ASHRAE heat balance method. The external temperatures have been acquired by the standard dry bulb temperature and wet bulb temperature values of a specific location given in the ASHRAE database. The second method is a dynamic simulation using the heat balance method which allows to calculate heat load in hourly basis. This also allows to create a custom outdoor temperature database. This analysis used the second method with an outdoor temperature database made using the collected outdoor temperature data as used in heat load simulations. The created models have been used to predict the indoor temperature of the selected zones for the years 2035 and 2090. Outdoor conditions required for the models were obtained using the RCP 4.5 and 8.5 emission scenarios [48], [50], [93], [94]. The maximum, minimum, and daily variation of the outdoor conditions for years 2035 and 2090 has been obtained using the WeatherShift™ tool which uses morphing techniques to estimate future climate conditions [95]. The related simulation weather file (EPW) has been selected from the closest geometrical location to Colombo, Sri Lanka.

The cloud cover and internal thermal additions due to equipment in the zones were considered to be the same as in 2020 for the grey box model. The same month of the year was used to calculate the parameters required for the radiation power input in the grey box model. NARX models were converted to their closed-loop form to calculate the indoor temperature predictions as this gives more accurate predictions as observed during testing.

3.8 Evaluation of cooling methods

Several passive cooling and adaptive measures are discussed in the literature to reduce the impact of cooling load increase on power production in the country. The most efficient of these methods is implemented at the construction stage of the building. Passive strategies require no energy input. The cooling methods selected to be evaluated in this study are,

- Natural and night-time ventilation
  - Removes hot air and supplies cold air directly when incoming air is cool and clear of contaminants. Naturally ventilated buildings can have higher interior set points than mechanically ventilated buildings. This is because the natural cooling effect of air motion increases the thermal comfort.
  - Natural ventilation is generally achieved through courtyards, atria, wind towers, operable windows, and solar chimneys
  - Mechanical or natural ventilation can cool down the thermal mass of the building at night. Due to radiative delay, this cooling down of thermal mass at night will result in lower cooling load peaks during the day.
  - One major setback of this method is that there can be condensation occurring when the moist daytime air meets the night-cooled indoor surfaces
- Optimized solar design

One of the major sources of heat for buildings is through solar radiation. The external surfaces of the buildings absorb solar energy in the form of heat. This is the major reason for the buildings to have high indoor temperature peaks in the noon. Building optimization to reduce the absorption of solar heat is identified to be one of the major methods to reduce the total heat gain into the occupied spaces in buildings.

- Optimizing thermal mass to minimize interior temperature peaks

Thermal mass is the mass of the building which absorbs the heat energy from sources. Higher thermal masses require higher heat energy to raise their temperature, while it also sustains the temperature for a longer time duration. Increasing the thermal mass reduces the daytime peaks of buildings, however, it increases the night-time temperature. This strategy, when combined with night-time passive cooling strategies, has high effectiveness in reducing the cooling energy required.

Previous research has shown that the natural ventilation, passive thermal design, and optimizing thermal mass are the most effective methods usable in hot and humid climate conditions like Sri Lanka. Hence, these three methods were selected through the literature review to further analyze.

Due to high humidity and relatively high cooling load, desiccant dehumidification and evaporative cooling are not effective solutions for cooling the selected buildings. Tactics like height-to-floor area optimization and underground earth piping should be implemented during the design phase of the buildings. These methods are therefore overlooked as the research is focused on existing buildings. The efficiency of lighting appliances and the air conditioning or ventilation systems require no further study as the energy saving done by using efficient appliances has a direct influence on energy consumption.

3.8.1 Optimizing thermal mass to minimize indoor temperature peaks

The optimization of thermal mass has two direct effects on the thermal load of a zone.

1. An increase in thermal mass reduces the indoor temperature peaks. However, it increases the time the peak indoor temperature is retained.
2. The time lag between the indoor and outdoor temperature increases with increasing thermal mass.

This effect can be observed in the collected data in the zones. Zones with high C values (Effective heat capacity) showed relatively lesser peaks and a larger lag between indoor and outdoor temperatures.

Thermal mass optimization is majorly combined with night-time ventilation in some cities. The high thermal mass inside zones has enough time to cool down during the low temperatures of night and the heat addition from the daytime of the next day will show relatively low peaks due to the increased thermal mass. For effective night-time ventilation, the night-time air should have low humidity. Therefore, night-time ventilation in the humid Colombo area is not very effective.

3.8.2 Optimized Solar Design

The variation of indoor temperature with changing α_i values of Equation 17 were calculated for each zone. Optimized solar design contains the use of reflective coatings, high radiation insulations, and shading of glasses. The different transmittance values used in the study are given in Table 3.6.

3.8.3 Natural and induced ventilation

Natural ventilation is a strategy for increasing the thermal comfort of the occupants rather than reducing the peak indoor temperature of the zone. Research has shown that naturally ventilated buildings can have indoor temperature set points of around 2^{o}C higher than that of mechanically ventilated buildings [66]. The cooling effect from the motion of air tends to give occupants a higher cooling sensation than that of a stagnant air environment having the same temperature. Therefore, it is important to have effective air circulation throughout the zones for the natural ventilation strategies to be effective.

The evaluation of the effectiveness of natural and induced ventilation analysis was carried out through CFD simulations by ANSYS Fluent. The indoor temperature and air velocities of zones were used to calculate the thermal sensation of the occupants and compared with the results from the survey conducted. The validation of the CFD model for the evaluation was carried out by re-enacting the simulations published in [96] [97] [98].The target of the validation experiment was to determine the accuracy of the discretization scheme, numerical method, grid size, turbulence model, and time step.

In the validation simulation, supply air is from a vent which is situated in the upper corner of the room. The exhaust air is from a vent which is situated in a bottom corner. The supply and exhaust are in opposite corners of the room. The temperature of the airflow is controlled and is considered as isothermal. The air inlet is at the top corner with a height of 3 cm while the outlet is 8cm as given in Figure 3.6.

TABLE 3.6: EMISSIVITY FOR DIFFERENT SOLAR DESIGNS USED

Design	Emissivity	Design	Emissivity	Design	Emissivity
Aluminum Foil	0.04	Concrete	0.85	Lime wash	0.91
Aluminum Commercial Sheet	0.09	Concrete, rough	0.94	Marble White	0.95
Aluminum Highly Polished	0.039 - 0.057	Concrete tiles	0.63	Masonry Plastered	0.93
Aluminum paint	0.27 - 0.67	Glass smooth	0.92 - 0.94	Mild Steel	0.20 - 0.32
Asbestos board	0.96	Glass, pyrex	0.85 - 0.95	Oil paints, all colors	0.92 - 0.96
Black lacquer on iron	0.875	Granite, natural surface	0.96	Plaster	0.98
Black Enamel Paint	0.8	Gypsum	0.85	Plaster, rough	0.91
Brick, red rough	0.93	Iron polished	0.14 - 0.38	Roofing paper	0.91

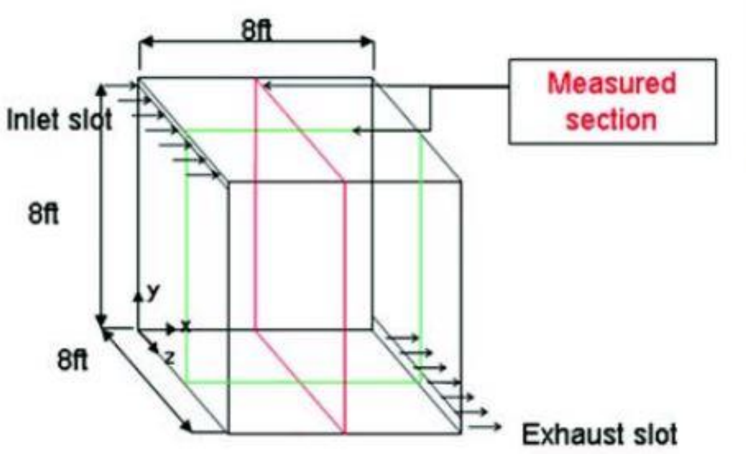

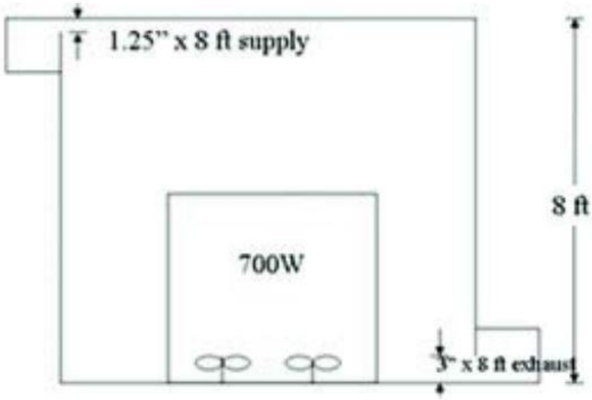

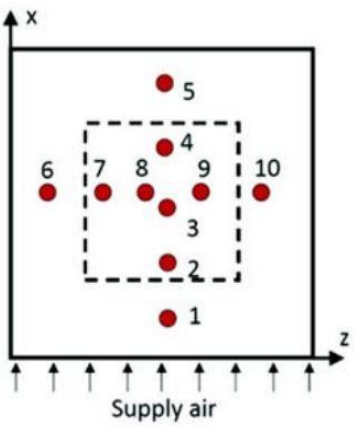

Position	Coordinate (x inch, y inch)	Position	Coordinate (x inch, y inch)
1	(0.2286, 1.2192)	6	(1.2192, 0.2286)
2	(0.6858,1.2192)	7	(1.2192, 0.6858)
3	(1.1430,1.2192)	8	(1.2192, 1.1430)
4	(1.6002,1.2192)	9	(1.2192, 1.6002)
5	(2.0574,1.2192)	10	(1.2192, 2.0574)

Fig. 3.6: Zone selected for validation simulation and measurement positions [78]

The grid for the simulation was created as non-uniform, with lower grid sizes near the walls and heat addition surfaces. The turbulence model used is Re-Normalization Group (RNG) k-ε model. According to the literature this model has high accuracy and low computational times in simulating enclosed spaces. All cases used a second-order upwind discretization scheme for calculation except for pressure for which the PRESTO scheme was used. When the normalized residual sum reached $1x10^{-5}$ for all variables ($1x10^{-7}$ for energy), the solution was considered as converged. Boussinesq approximation was used in body force approximation for gravity.

Room boundaries for the simulations were defined as given below:

A velocity inlet boundary was defined for the air supply. The temperature and air velocity with normal direction were defined. Outflow boundary condition was defined for exhaust air. The exhaust air parameters were unknown at the start of the solution but were calculated using the flow inside the zone. Walls, ceiling, and floor were defined as wall boundaries, at which a uniform heat flux was defined.

The indoor temperature variation of the zones was simulated in two stages,

1. Natural ventilation; all doors and windows are open
2. Induced ventilation; use of ceiling fans inside the zones

Zone 1.1 was not used for the simulations as the zone does not have any operable windows and the door is always closed as this is an unused zone. The simulation was done with the outdoor conditions for an average day during the data collection period. Hourly simulations per day were carried out per zone.

Radiation solar heat flux on building envelope elements were calculated using HDKR radiation model used in the development of the grey box model. Hourly average solar heat flux was used as the heat gains into the zone through walls. The equipment and the sensible heat gain from the equipment used inside the zones were included in the simulations. It was assumed that equipment like computers is only operable during working hours (8.00 a.m to 5.00 p.m).

The modelling of the building zones and equipment was done through SolidWorks. Wind velocity for natural ventilation was taken by the average wind velocity values around the buildings obtained through Central Environmental Authority of Sri Lanka. The inlet and outlets of the zones for CFD simulation were selected considering the direction of airflow during the data collection period. Internal doors were kept as velocity outlets for the simulation.

For simulations with induced ventilation, ceiling fans with a 1200 mm sweep radius were used. It was assumed that one ceiling fan covers a 10 m^2 floor area. The ceiling fan is hung 300 mm from the ceiling while the ceiling fan operates at 100 CFM (169.9 CMH) only during working hours (8.00 a.m. to 5.00 p.m.). The hourly average indoor temperature and average flow velocities (1.0 m height from the floor) were analyzed to find the results of using natural and induced ventilation. Flow velocities together with indoor temperatures were used to calculate the PMV using Fanger's PMV correlation as a measure of the thermal comfort of occupants inside the zones. Clothing insulation values were taken from the survey results.

3.8.4 Cost benefit analysis

The predicted energy savings through the above-discussed methods were analyzed to calculate the economic benefit of each method in terms of money saved. For this, baseline grey box models were compared with the grey box models implemented with energy-saving methods. Since the cost of the methods is variable and cannot be predicted (different methods such as whitewashing external walls or aluminum cladding can change with many different factors such as labour cost, equipment cost and also the placement orientation and even accessibility of the external walls), a cost benefit analysis to calculate the money saved was used instead of calculating a payback period. A payback period was then calculated for different hypothetical costs of implementation for each building.

The analysis was done on several selected zones in the selected buildings. The impact of the cooling strategies suggested are for the zones selected and are different from zone to zone. For example, the building interior zones will have no benefit or reduction in cooling load when optimized solar designs are used but moving air by induced ventilation by fans. Therefore, the percentage decrease of cooling load calculated was generalized to the building considering the building area, position, and orientation of the different zones of the building and predicted occupancy in each area. As there is no calculated baseline of the total cooling load, only a calculated percentage decrease of cooling load from each strategy is calculated for the whole building while the quantified colling load decrease and the related economic benefit is calculated zone-wise. Since the impact of some strategies such as optimized solar designs is time-dependent (high savings when solar loads are higher), a dynamic calculation of electrical energy saving was calculated through the time domain and was averaged. It was assumed that the air conditioners operated on only during the working hours of weekdays when calculating the economic benefit or the money saved.

When converting from the calculated cooling load reduction to economical savings, the cooling load reduction had to be converted to electrical load savings. The COP (Coefficient of Performance) was used to convert from cooling load reduction to electrical energy saved. The COP is dependent on various factors such as the type of equipment used, its efficiency, and outdoor conditions. It was assumed that the zones in Sumanadasa building and ENTC building in the University of Moratuwa are cooled using multiple standalone split air conditioning systems. The cafeteria in Western Provincial Council building is currently being cooled using a central air conditioning system and the office area is cooled using multiple split air conditioners. The timber deck area is not currently air conditioned, however, it is assumed that this area will be cooled using a similar split-type air conditioner for cost calculations. A COP of 3.6 is rated for the split air conditioners installed at the office zone in Western Provincial Council building and this was used as the theoretical COP for the calculations. The COP of the centralized air conditioning system at the Western Provincial Council building can vary in a wide range from as low as 3 to as much as 7. A typical COP of 5 is used for the electrical energy-saving calculations at this zone.

The cost for electrical energy usage was calculated by the tariff structures posted by PUCSL (Public Utilities Commission of Sri Lanka). Under the government building category of tariff structure, an energy charge of 14.55 LKR/kWh is posted for customers where the contract demand exceeds 42 kVA. This electricity charge is used to calculate the economic benefit or money saved from the reduction in electrical energy usage. A moderate rise of electricity cost is assumed which is a potential rise of electricity cost by around 4-5% annually. Using these assumptions, the potential of money to be saved over the next 10 years for the selected zones was calculated. Additionally, a payback period for an implementation cost of 1,000,00 LKR was also calculated.

CHAPTER 4

RESULTS AND DISCUSSION

This chapter of the thesis discusses the results from the experimental study and the simulation results based on both data-driven modelling as well as the physics-based Grey box model. Further the results of the climate change impacts on the future energy and the effectiveness of different mitigation strategies are presented.

4.1 Results of the initial cooling load predictions for Building 1

As discussed in section 3.2, at the initial data collection temperature and relative humidity values of building 1 were collected for 6 weeks. Figure 4.1 shows the variations in the indoor temperatures and outdoor temperatures throughout the month of August 2020. The highlighted days are the government holidays during this period where the majority of internal loads (load due to occupants, load due to equipment and lighting) were eliminated as can be observed by Figure 4.2 which shows the variation of calculated cooling load and outdoor temperature throughout the month. When building a relationship to understand the sensitivity of the building zones to the outdoor temperature, the ratio of external walls to internal walls, external wall to window ratio and the shading coefficient are important. Observing these values for the selected building which are given in Figure 4.2 and the trend of indoor temperature with time and cooling load with time, it was clear that the timber deck with the highest wall-to-window ratio with very less shading coefficient has the highest sensitivity to outdoor temperature. The timber deck showed a high variation of indoor temperatures following the trend of outdoor temperature while the cafeteria area which has a low external wall ratio has a more stable indoor temperature trend with a slight sensitivity to outdoor temperature. It can also be observed that although the office area was air-conditioned, it showed a high sensitivity to the outdoor temperature due to the high ratio of external walls and high ratio of windows.

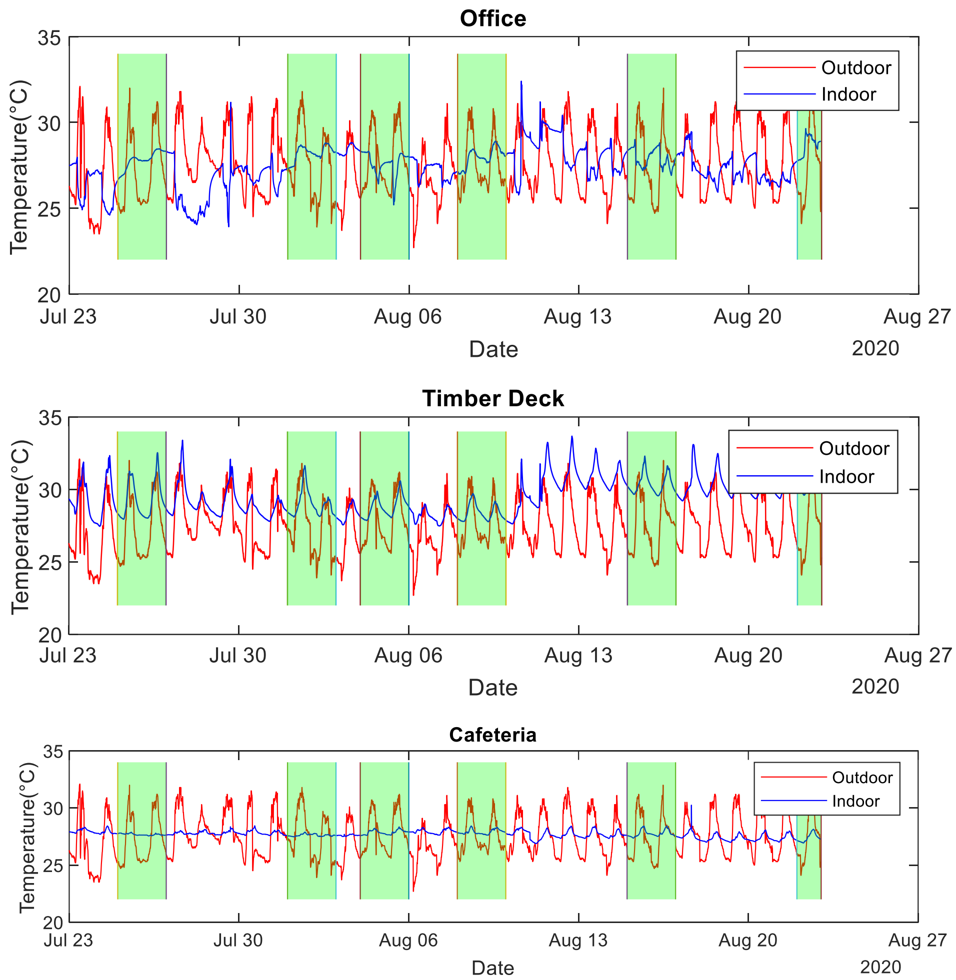

Fig. 4.1: Indoor temperature and outdoor temperature variation with time: (a) Office, (b) Timber Deck and (c) Cafeteria

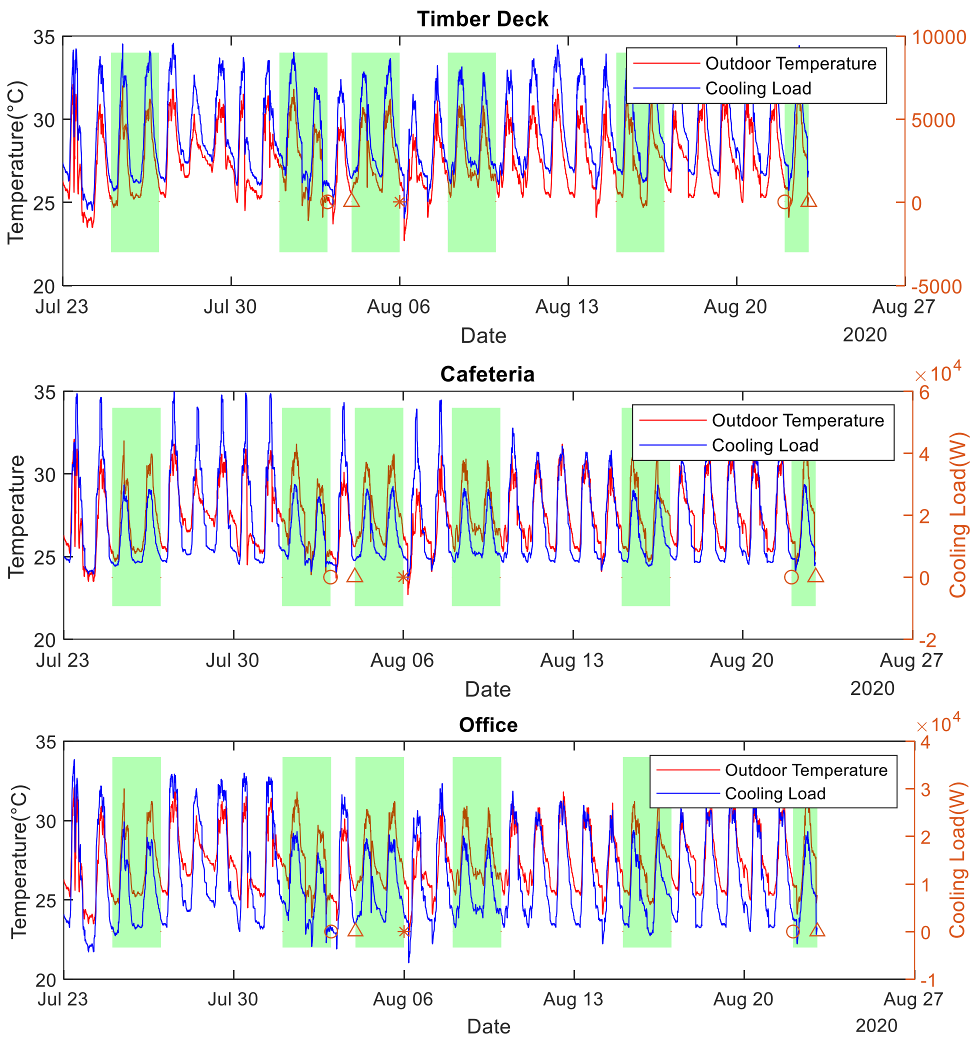

Fig. 4.2: Cooling Load and outdoor temperature variation with time for (a) Timber Deck (b) Cafeteria and (c) Office

4.1.1 Time lag between maximum outdoor temperature and cooling load

The internal cooling loads of the three zones were further analyzed to establish a relation between the total cooling load, external loads, and the outdoor conditions by selecting outdoor conditions of an average day of the month. The variation of external loads, total load, and outdoor temperature during the time of the day are shown in Figure 4.3.

As can be seen from Figure 4.3, there are no internal loads in timber deck and therefore the total loads follow the variation of outdoor temperature. The peak cooling load of timber deck was observed at 2.15 p.m. on an average day. The external window of the timber deck was facing the west direction and the highest heat gain from surfaces exposed to west direction were at the time window of 1.00 p.m. – 3.30 p.m. as indicated by the CLTD values in the ASHRAE handbook. The external windows of the office area were facing the east direction, and the peak external load of the office area was observed at 11.35 a.m. The CLTD values of walls facing the east side are high at the time window of 9.30 a.m. – 12 p.m. which results in a high heat gain into the building during this period.

As indicated in the work by [99] the indoor temperature lags behind the peak heat gain into the building. The average indoor temperature variation of the office area decreases at around 8.00 a.m. which is the office starting time when the air conditioners are turned on, following this variation, a sudden peak can be seen at 3.15 p.m. which is explained by the lag of peak heat transfer into the building and the indoor temperature increase. The same phenomenon can be observed in the timber deck where the peak heat gain is at 12.15 p.m. and the indoor temperature peaks at 2.20 p.m.

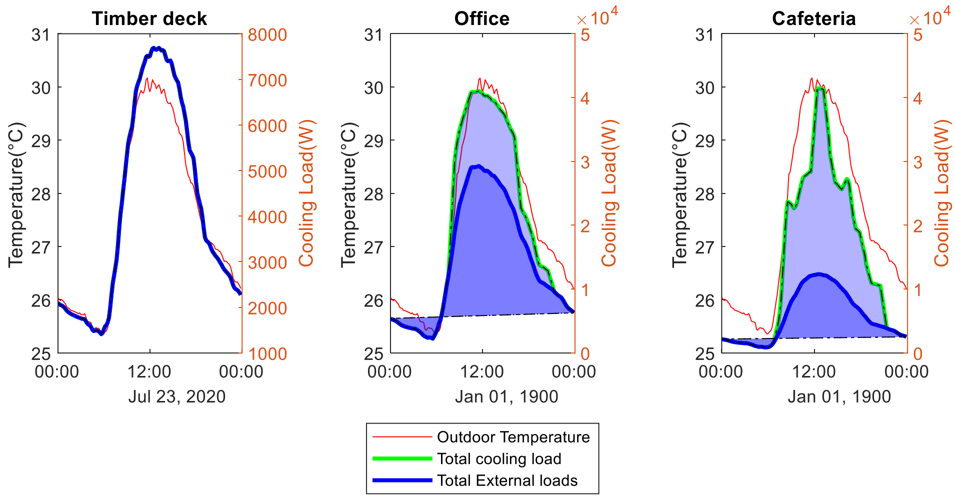

Fig. 4.3: Average External Cooling Load, average total load, and average outdoor temperature variation for a day with time for (a) Office, (b) Cafeteria, and (c) Timber Deck

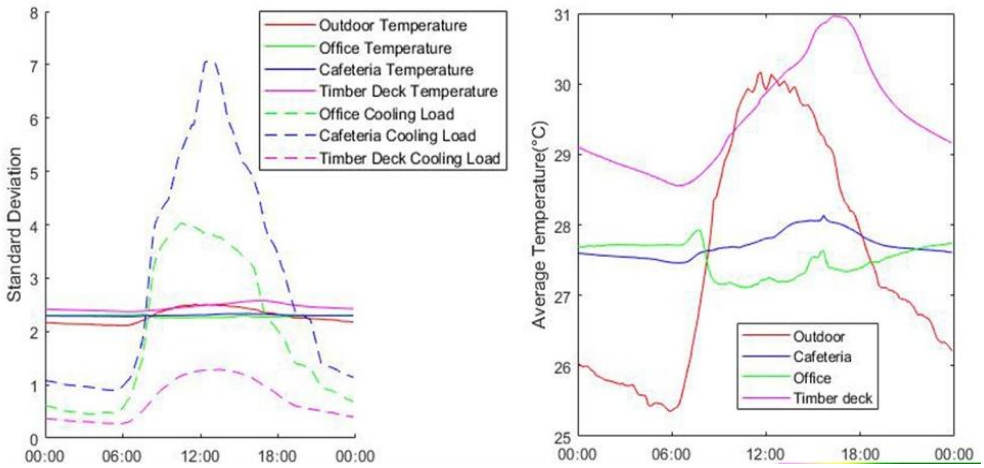

Fig. 4.4: Standard deviation plot of the selected areas (left) average indoor and outdoor temperature plot for an average day (right)

4.1.2 Daily maximums and hottest and coldest days

The external loads of the timber deck followed the exact variation of the outdoor temperature with its zero internal loads while the external loads of the office area also followed the variation of the outdoor temperature, but the inconsistency of internal loads make the total load variation differ from the outdoor temperature variation. As opposed to this, cafeteria internal loads and temperatures show very little sensitivity to outdoor temperature. This can be also observed in the daily peaks of these values plotted against the day of the month as given in Figure 4.5. This observation can be further verified by studying the variation of the hottest and coldest days of the month for three rooms which is depicted in Figure 4.6.

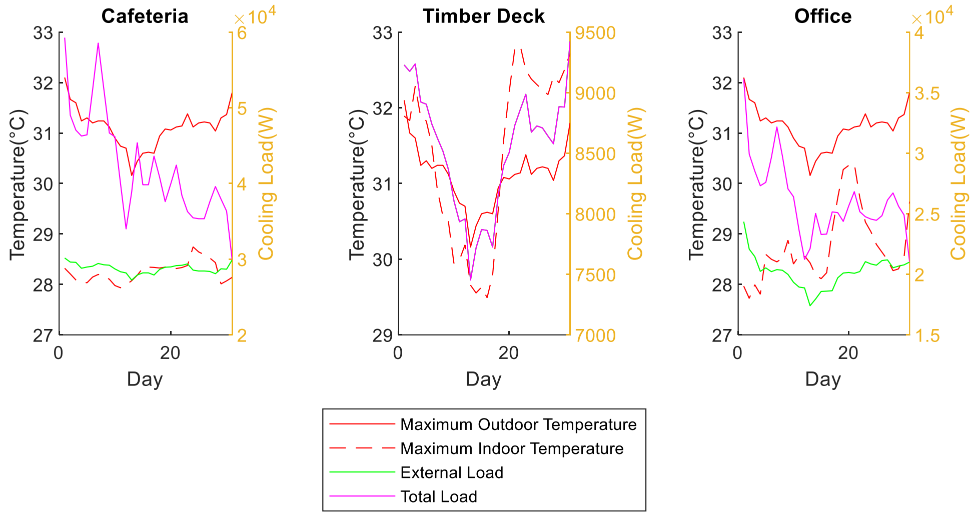

Fig. 4.5: Plot of maximum daily values for 31 days for Cafeteria (a.), Timber Deck (b.) and Office (c.)

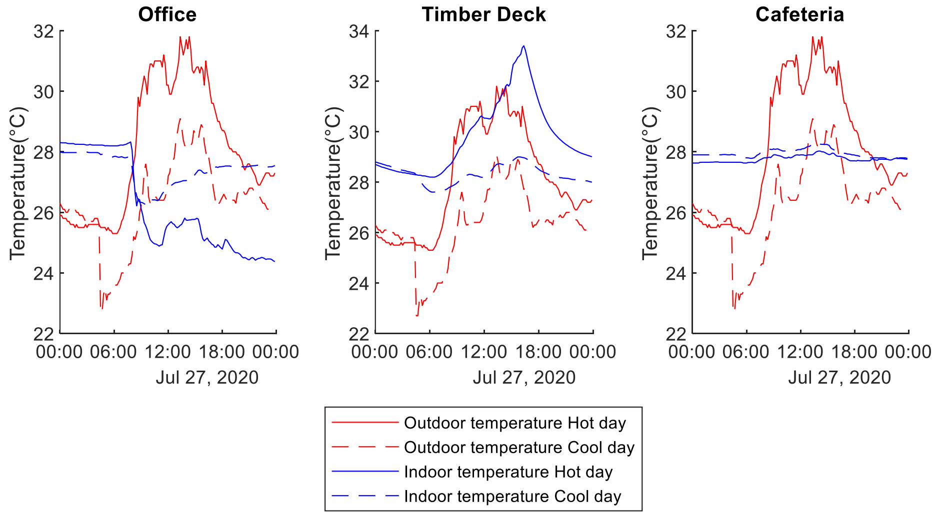

Fig. 4.6: Plot of values for the warmest and coldest days for Office (a.), Timber Deck (b.) and Cafeteria (c.)

4.1.3 Sensitivity analysis of cooling load to outdoor temperature

The outdoor temperature variation and related indoor cooling load increase was calculated considering the previously found time lag. The results were plotted with outdoor temperature variation percentage vs. cooling load increase percentage which is shown in Figure 4.7. The results were fitted to a linear curve with 95% confidence bounds which can be used to interpolate the percentage increase of cooling load per 1°C increase of outdoor temperature as given in the study by Watkins and Levermore

[100]. It was observed that the timber deck has the highest sensitivity and the cafeteria with lowest sensitivity as given in Table 4.1. This regression model can be used to predict the future energy demand of the selected zones of the building due to the future temperature increase.

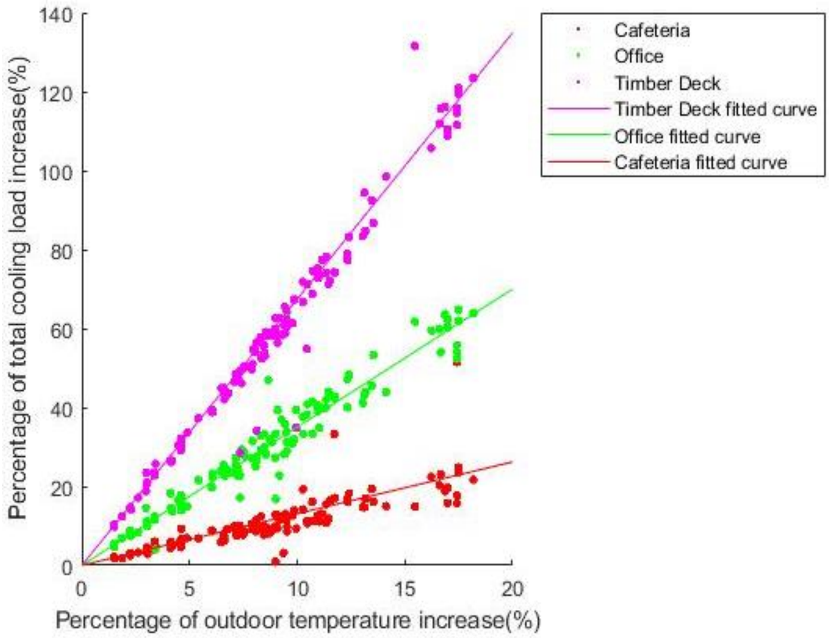

Fig. 4.7: Plot of variation between increases of outdoor temperature to increase of cooling load (sensitivity analysis)

TABLE 4.1: CALCULATED SENSITIVITY OF ZONES TO OUTDOOR TEMPERATURE

Property	Zone		
	Cafeteria	Office	Timber Deck
Gradient of the linear curve	1.31	3.5	6.744
R^2 of fitted curve	0.6302	0.9053	0.9645
Percentage increasee of cooling load per 1°C increase of outdoor temperature	5.038%	13.462%	25.938%

4.1.4 Cooling Load Prediction

In predicting the future cooling energy demand patterns for a building, three main scenarios that contribute to the increase in energy demand should be taken into consideration: the demand changes due to the average outdoor temperature rise, the demand due to the increase of the number of hot days or cold days and the demand increase due to the aging of the building. According to the literature [49], it is predicted that on average under the current emission conditions, the global temperature will increase by 2°C by the year 2050 which is an increase of 8.69% compared to 27°C in 2020. Using the above-discussed linear regression model for the building zones, this increase of outdoor temperature in 2050 will approximately return an increase of around 10.076%, 26.924%, and 51.876% of cooling load in the cafeteria, office and timber deck, respectively.

The Cooling Degree days (CDD) is another important parameter when calculating/predicting the monthly energy consumption of the building using average values. The number of Cooling Degree Days (CDD) is calculated by Equation 39 where, T_P is the preferred temperature and T_A is the hourly average outdoor temperature and d is the number of days in the month.

$$CDD = \sum_{1}^{31} \left(\frac{\sum_{1}^{24}(T_A - T_P)}{24}\right) \tag{39}$$

Although the number of CDD will not directly affect the peak cooling energy demand of a building, it will affect the total energy consumption of the air conditioners. Currently the office area is the only directly air-conditioned area which is taken into consideration in this study. It is equipped with four 36,000 btuhr (10.551 KW) split air conditioners, with a rated COP of 3.6 for cooling. This accounts for a total maximum cooling load of 42.2 KW extractable by the air conditioning system. The calculated maximum cooling load of this area is 36.14 KW. Therefore, the air conditioning system is sufficient to cool the area under current conditions. With an average calculated cooling load of 19.56KW for working hours between 8.00 a.m. to 5 p.m., which is roughly 54.12% of the rated cooling load of the air conditioning system, by adapting the works of Wang, Zhang and Xia [101], the average electrical energy consumption can be calculated by using Equation 40 which returns an average total energy consumption per month (P_C) as 1268.93 KWh.

$$P_C = \left(\frac{Cooling\ capacity\ of\ air\ conditioning\ system * 0.5412}{COP}\right) * Operating\ time \tag{40}$$

The month used in this study (August of 2020) has a CDD value of 292.8. Therefore, the above calculated average energy consumption is for a month with 292.8 CDD.

According to a study conducted by the Department of Meteorology, Sri Lanka, it is found that in Sri Lanka the number of cold nights and days will decrease while the number of hot nights and days increase in the coming year. The works of Newman (2018) predicts that following the global CDD increase for past years, the CDD increase trend of roughly 33% for the last 30-year time span (1985 to 2015) and it is predicted to continue throughout the 21st century which will give an estimated 392.4 of CDD in the year 2050 (taking CDD of 292.8 in 2020). Adapting from the works Krese, Prek and Butala [102], converting this to electrical power consumption, it is notable that the power consumption is projected increase to 1700.57 KWh in 2050 from 1268.93 KWh in 2020 for the month considered in the current study. Also, this increase is only considering the increase of the number of CDDs. The increase due to the other two factors should also be added on top of this for the full energy demand prediction.

The selected building is relatively new (built in 2018), hence it was assumed that there is no additional infiltration of heat and outside air into the building due to the age of the building. The heat load added due to added infiltration sums up to a significant value as the building ages [103]. The building considered in the current study will age by 32 years in 2050. A new building will have an increase of around 0.42 ACH (Air Changes per Hour) for 30-year time span [104]. By cooling load calculations, this returns an average increase of 1.89KW, 12.81KW and 5.91KW of cooling load for timber deck, cafeteria and office, respectively in the year 2050.

As observed in the above cooling load predictions the timber deck area has the most sensitivity to outdoor temperature with office and cafeteria following with 25.94%, 13.46% and 5.04% increase of cooling load with 1°C increase of outdoor temperature. With the increase of average global temperature within the next 30 years an additional 40.57%, 41.7% and 55.66% of load could be added on to the cooling loads for cafeteria, office and timber deck, respectively while an estimated additional 431.64KWh of electrical energy will be required for August 2050 for office area due to the increase of CDD. Therefore, on average, 41.7% of cooling load + 431.64KWh of additional energy per month will be needed for the office area alone, which is a significant increase.

4.1.5 Occupant survey results and indoor temperature set point calculation

Although ASHRAE standards give an internal temperature set point, occupants in hot and humid countries are comfortable in a higher temperature. As discussed in section 3.3.2, an occupant survey was conducted to identify the thermal comfort of the occupants of the selected buildings. The results of the survey given in Figure 4.8 indicate that an average man experiences a slightly warmer sensation than an average women which is justified by the calculated average clo values (0.67 for men and 0.58 for women)

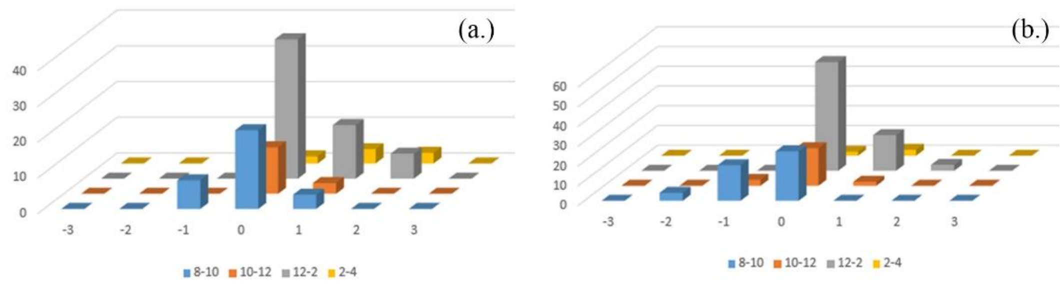

Fig. 4.8: Occupant survey results: PMV values for (a) men,(b) women

The calculated clo values were then used to calculate the ASHRAE standard comfort zone for both men and women. The maximum indoor temperatures and humidity levels were plotted on the graph of Relative Humidity vs. Indoor Temperature on which the two comfort zones were identified. As depicted in Figure 4.9 all the points related to 31 days of the selected months lie well right to the ASHRAE standard comfort zone indicating that occupants in these areas have PMV values closer to 1 (should experience slightly warm to warm sensation). Because of adaptive thermal comfort, the occupants are feeling more comfortable as opposed to the ASHRAE standard comfort level [27], [105]. The main reason for this change in the comfort zone is that people have been used to hot and humid environments in tropical countries like Sri Lanka, thus they prefer slightly warmer environments. As can be observed from Figure 4.9, it can be concluded that people were more comfortable in indoor temperature set points of 24°C - 25°C. Fanger's equation was used to obtain this set point using PMV values [16]. Therefore, the set point internal temperatures of 24°C was used for the further cooling load calculations.

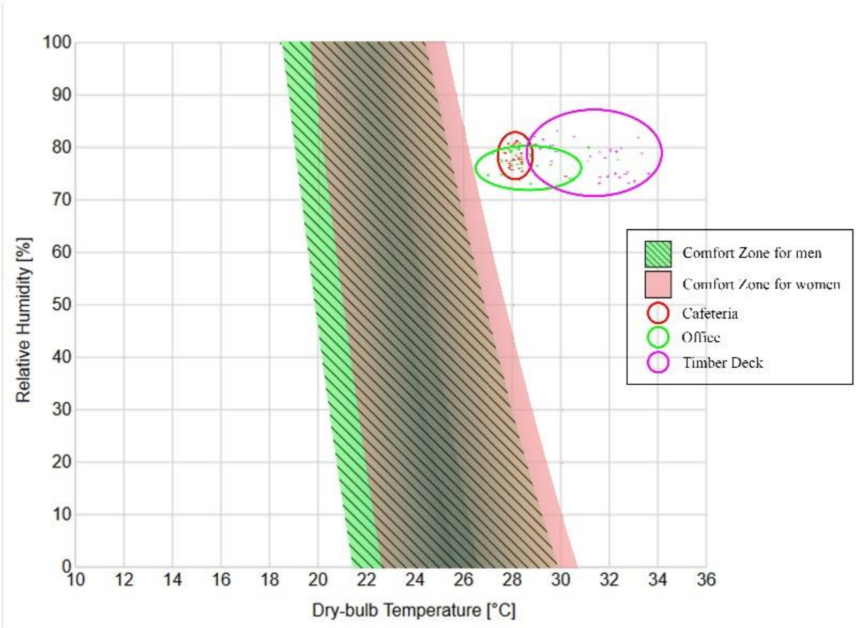

Fig. 4.9: ASHRAE standard comfort zone for men and women: the shaded area indicates the standard zone while the scatter plot indicates the measured values of the office area

4.2 Data collection results

With building 1 showing high sensitivity to increasing outdoor temperatures, a detailed analysis was done for all three buildings. This section details the results of the data collection presented in section 3.4. Figure 4.10 illustrates the results of the data collection for three buildings with Figure 4.11 illustrating the average daily variation of the temperature of each zone. A total of 6048 data points each having indoor temperature, indoor relative humidity, outdoor temperature, and outdoor relative humidity have been obtained during data collection for all the eight zones.

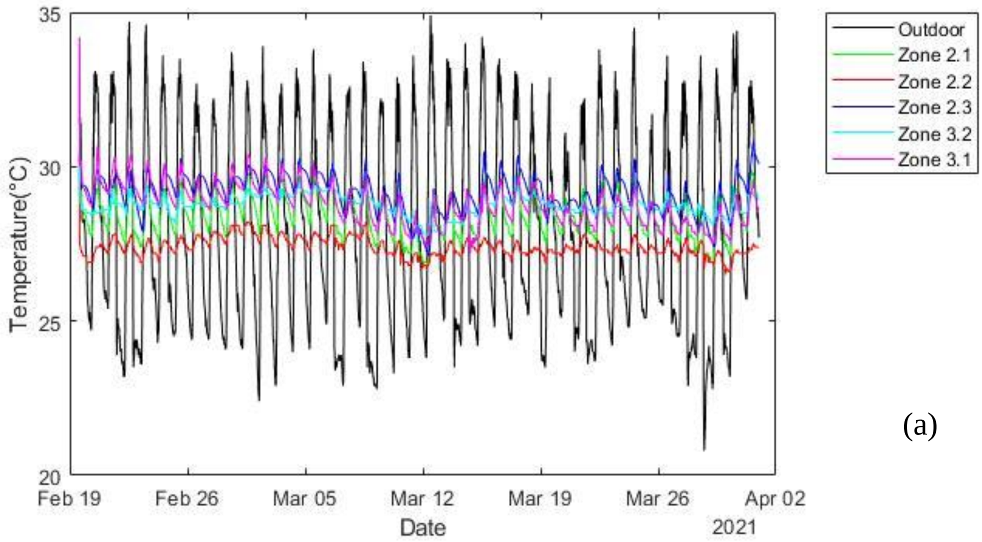

(a)

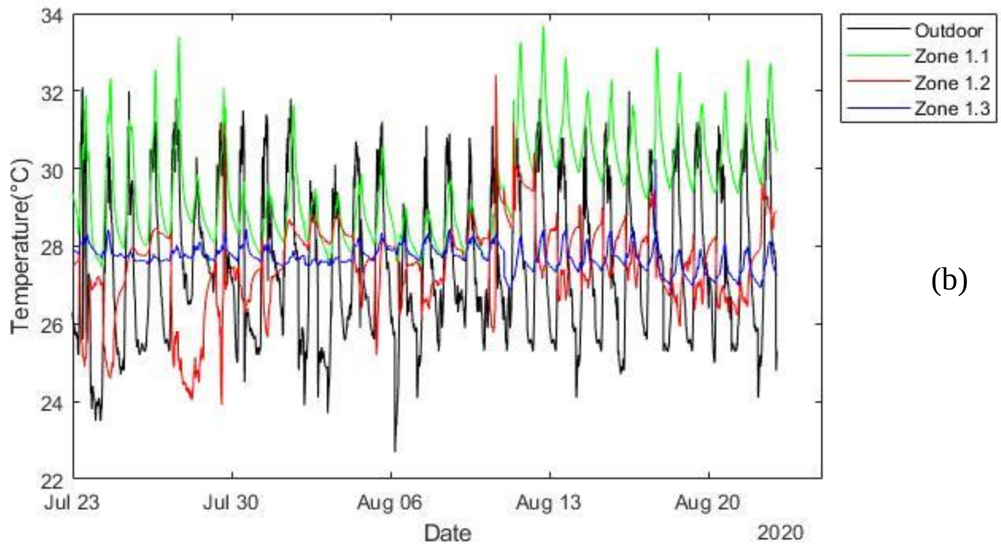

(b)

Fig. 4.10: A The variation of internal temperature and outdoor temperature of different zones in: (a) building 2 and 3, (b) building 1.

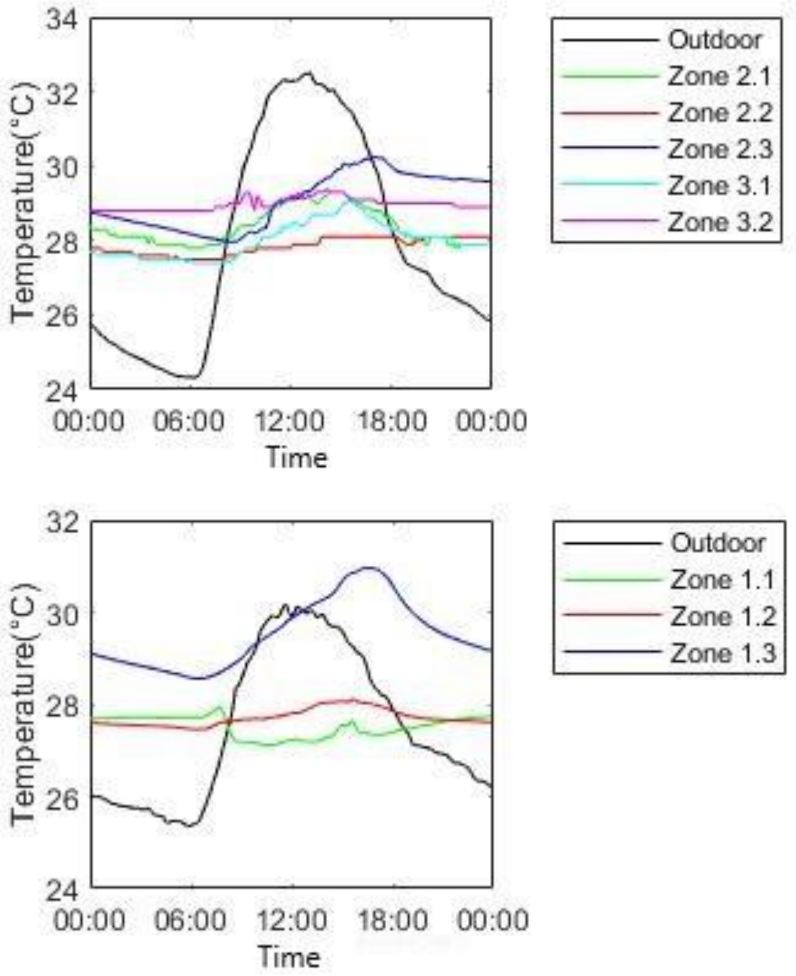

(c)

(d)

Fig. 4.11: Average daily variation of indoor temperature of (c) buildings 2 and 3, (d) average daily variations of building 1.

4.3 Neural network model performance

The simple regression model discussed in section 4.1.3. has the limitation that they use linear assumption in predicting the indoor temperature increase due to the outdoor temperature increase. Any deviation from the linear assumption is not captured in the model. Thus, a data-driven mode (black box model) would more accurately capture the indoor temperature variation with outdoor conditions. Hence, a data-driven model of NARX type was developed as discussed in section 3.5. The results of the testing stage of the neural network are given in Annex III (sample for zone 1.1 is given in Figure 4.12) for each building zone and a comparison of performance in terms of RMSE and correlation coefficient R of data driven models developed for each zone building zone are given in Table 4.2.

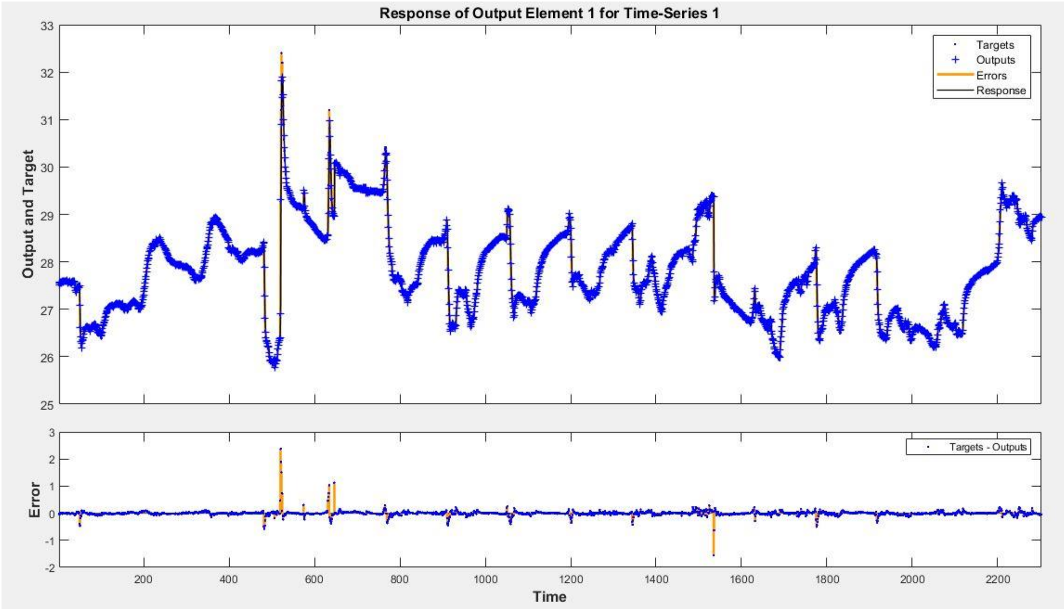

Fig. 4.12: Sample test results of data-driven models for zone 1.1

TABLE 4.2: PERFORMANCE OF NARX MODELS OF DIFFERENT ZONES

Zone	MSE	R
1.1	2.9271×10^{-3}	0.9431
1.2	2.2775×10^{-3}	0.8435
1.3	3.3660×10^{-3}	0.8202
2.1	3.3514×10^{-3}	0.7453
2.2	1.4409×10^{-3}	0.7981
2.3	1.0250×10^{-3}	0.8052
3.1	4.9567×10^{-3}	0.8320
3.2	1.8877×10^{-3}	0.7359

The correlation coefficient (R) was selected as a measure of the relationship between outdoor conditions and indoor temperature. An R-value of zero indicates a random relationship and an R-value of 1 indicates a complete relationship between inputs and outputs. Comparing the R values and error plots given in Figure 4.12 (Annex III), it was observed that all zones in building 1 showed relatively higher correlation. Zone 1.1 with a high window-to-external wall ratio, low area, unshaded glass facing west, no internal heat gains, and absence of furniture showed a high correlation between indoor temperature and outdoor conditions. In comparison, Zone 1.3 situated on the first floor of the building with a high floor area, low window-to-wall ratio, and internal heat gains showed a relatively low correlation. All zones in building 2 showed relatively low correlation indicating that the internal temperature is not as much dependent on the outdoor conditions as in building 1. This was observed through the error plots of the zones as indicated in Figure 4.12 (Annex III). Zone 2.3 showed a high correlation in comparison to other zones of the same building due to low area, and high external wall-to-window ratio. Building 3 showed a moderate correlation. Although the selected areas of building 3 were non-air conditioned, the building was designed to be cooled by a mechanical cooling system and therefore the adjacent areas were air conditioned which partly cools down the zones selected.

In addition to the above analysis, the network trained for zone 2.1 has been tested using a two-week data set collected in 2010. The peak outdoor temperature for an average day for the data collection period (March- April) has almost been unchanged but the temperature at night has shown an average increase of nearly $1^{o}C$. Similarly, the peak indoor temperature of the zone was observed to be relatively unchanged but the average indoor temperature throughout the day had a significant increase in 2021 compared to 2010 as shown in Figure 4.13.

The testing of the network using the 2010 data set yielded an MSE of 6.7814×10^{-3} and an R-value of 0.713. The MSE has shown an increase, and R has shown a slight decrease as compared with the testing results in 2021. The Testing results also showed that the model has relatively high error values when the targets are relatively low (low indoor temperatures) however accuracy has improved for high targets (high indoor temperatures). This test with the 2010 data set further confirms that the models can be used to predict future indoor conditions as it can be assumed that due to an increase in outdoor temperatures, indoor temperatures will also increase.

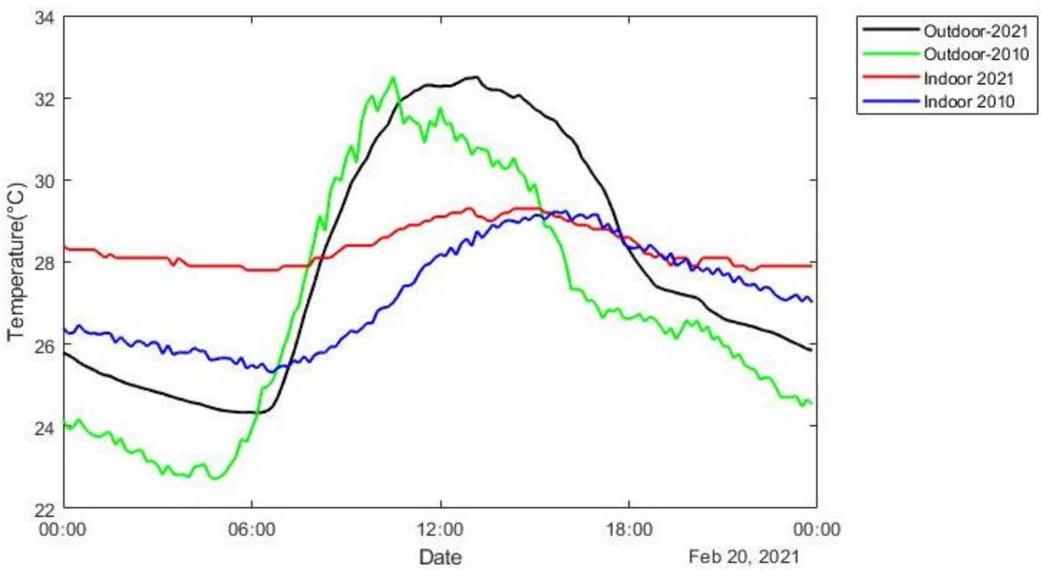

Fig. 4.13: Plots of temperature comparison of temperature data for years 2010 and 2021

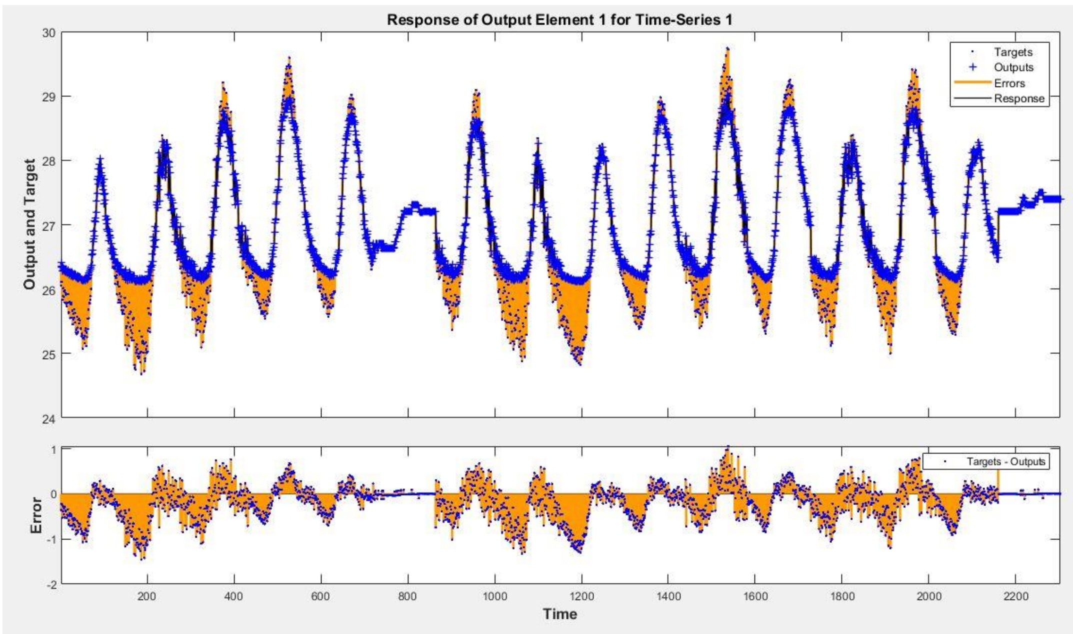

Fig. 4.14: Comparison of testing the model for years 2010 and 2021 for Zone 2.1

4.3.1 Indoor temperature prediction using neural network models

The models were used to predict the indoor temperature as given in section 3.7. IPCC has predicted the change in global average surface temperatures considering different emission scenarios. These scenarios are the Representative Concentration Pathways

(RCP) which are distinguished by the radiative forcing value of the different emission conditions. The four emission scenarios are listed below [48], [49], [50], [88],

1. RCP 2.6 – Radiative forcing of 2.6 W/m^2 is considered to be one of the best-case scenarios. Surface warming will be less than 2 °C by the year 2100.
2. RCP 4.5 – One of the two intermediate scenarios predicted with radiative forcing of 4.5 W/m^2. Emissions peak by 2040 and then decline. Surface warming will be less than 3°C by the year 2100.
3. RCP 6.0 – One of the two intermediate scenarios predicted with radiative forcing of 6 W/m^2. Surface warming will be less than 3.5°C by the year 2100.
4. RCP 8.5 – Worst case scenario predicted with radiative forcing of 8.5 W/m^2. Surface warming will be less than 5°C by the year 2100.

The created models have been used to predict the indoor temperature of the selected zones for years 2035 and 2090. As the outdoor temperature and relative humidity are exogenous inputs to the network, outdoor conditions have been estimated using the RCP 4.5 and 8.5 emission scenarios [50].

The maximum, minimum, and daily variation of the outdoor conditions for the year 2035 and 2090 has been obtained using the Weather Shift™[95] tool which uses morphing techniques to estimate future climate conditions [94]. The related simulation weather file (EPW) has been selected from the closest geometrical location to Colombo, Sri Lanka [93]. The results of the temperature predictions under the two climate scenarios for the selected zones are illustrated in Figure 4.15.

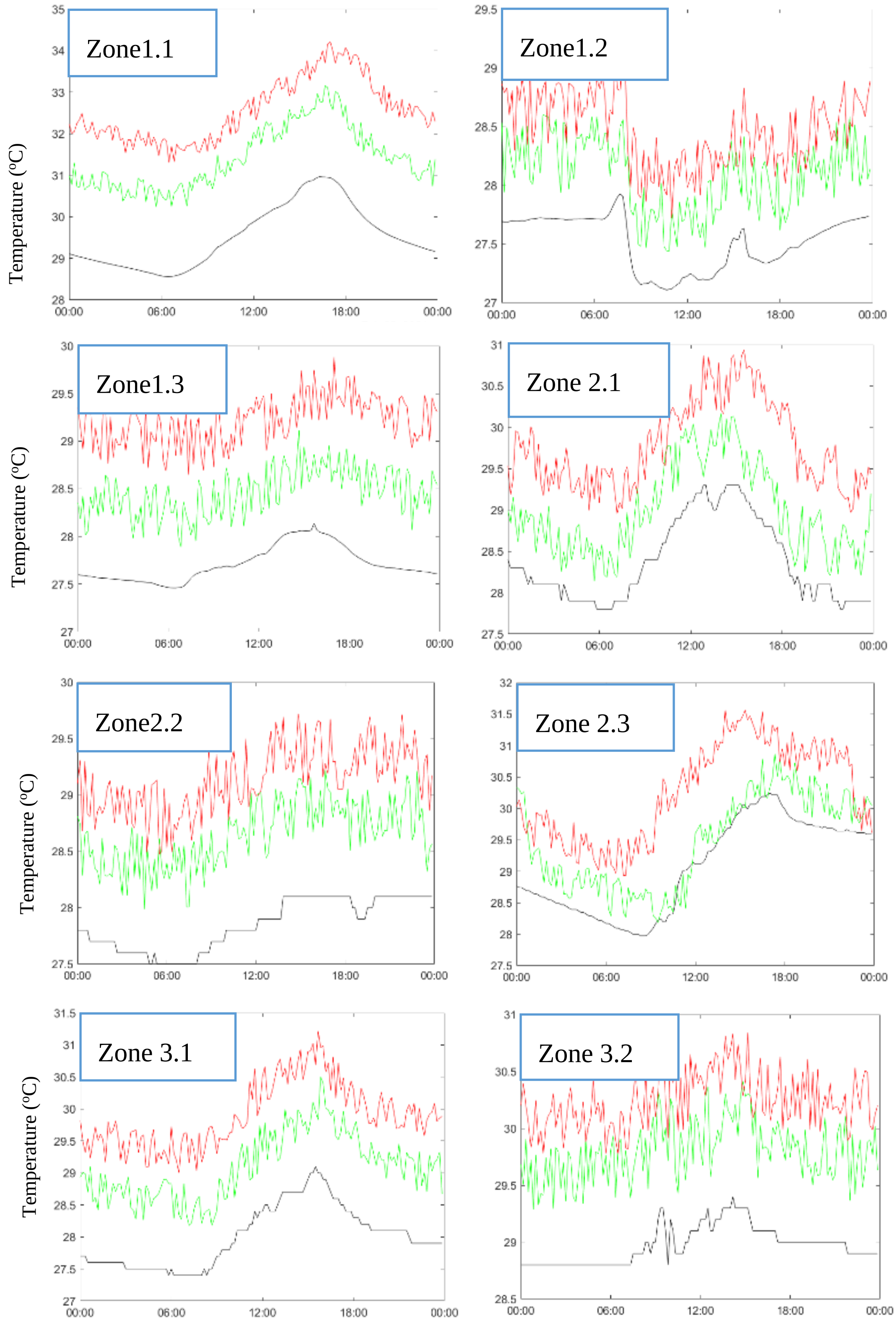

Fig. 4.15: Plot of predicted indoor temperatures for the zones for 2090 under RCP 4.5 (green) and 8.5 (red) scenarios and measured average daily variation of indoor temperature in 2021 (black)

IES VE tool was used to simulate the cooling load of each selected zone with a preconditioning period of one month. The RCP 4.5 and RCP 8.5 scenarios were used in predicting the cooling loads for the years 2035 and 2090. The results obtained from the analysis showed a clear and significant increase in the indoor temperature of the selected zones under both climate change scenarios as indicated in Table 4.3 A and B. Zone 1.1 showed the highest increase in cooling load with 31.25% increase by RCP 4.5 emission scenario and by 52.34% by RCP 8.5 emission scenario for 2035. A similar trend can be seen for predictions up to 2090. The same zone showed the highest increase in indoor temperature by 2090. This zone has an unshaded west-facing window with a high external wall-to-window ratio. Also, the zone does not have internal heat gains and furniture which is the cause of the high sensitivity of cooling loads to outdoor temperature changes. Similarly, zone 1.3 showed the least increase in cooling load due to the smaller number of internal walls. This zone also has a high ratio of internal heat gains to total heat gain. Notably, all zones in building 2 showed relatively less increase in cooling load as opposed to the other two buildings, mainly because it is a building originally designed for natural ventilation. Based on the analysis it can be concluded that on average 10% and 25% of cooling load increase can be predicted for all three buildings under RCP 4.5 and 8.5 climate change scenarios by the year 2035 while for 2090 the values can be up to 30% and 50%.

TABLE 4.3 - A: PREDICTED CHANGE OF INDOOR TEMPERATURE AND COOLING LOAD IN 2035 COMPARED TO 2021

Zone	Peak indoor temperature (ºC)			Peak cooling load (kW)			% increase of indoor temperature		% increase of cooling load	
	2021	2035		2021	2035					
		RCP 4.5	RCP 8.5		RCP 4.5	RCP 8.5	RCP 4.5	RCP 8.5	RCP 4.5	RCP 8.5
1.1	30.9	32.6	33.4	5.328	6.993	8.117	5.502	8.091	31.250	52.340
1.2	27.9	28.1	28.3	9.430	11.584	12.542	0.717	1.434	22.840	32.997
1.3	28.1	28.6	29.1	87.450	92.424	96.198	1.779	3.559	5.688	10.004
2.1	29.3	29.7	30.1	22.491	24.123	25.263	1.365	2.730	7.256	12.324
2.2	28.1	28.7	28.9	6.945	7.824	8.866	2.135	2.847	12.654	27.654
2.3	30.2	30.4	30.8	1.724	1.889	2.051	0.662	1.987	9.542	18.963
3.1	29.1	30.0	30.4	4.951	5.621	6.465	3.093	4.467	13.540	30.587
3.2	29.4	29.9	30.1	4.881	5.598	6.445	1.701	2.381	14.680	32.037

TABLE 4.3 - B: PREDICTED CHANGE OF INDOOR TEMPERATURE AND COOLING LOAD IN 2090 COMPARED TO 2021

Zone	Peak indoor temperature (ºC)			Peak cooling load (kW)			% increase of indoor temperature		% increase of cooling load	
	2021	2090		2021	2090					
		RCP 4.5	RCP 8.5		RCP 4.5	RCP 8.5	RCP 4.5	RCP 8.5	RCP 4.5	RCP 8.5
1.1	30.9	33.1	34.2	5.328	9.123	11.317	7.079	10.498	71.240	112.40
1.2	27.9	28.6	29.1	9.430	12.490	13.987	2.408	4.333	32.451	48.324
1.3	28.1	29.1	29.9	87.450	97.405	104.81	3.475	6.207	11.384	19.851
2.1	29.3	30.2	30.9	22.491	25.101	27.967	2.958	5.586	11.609	24.348
2.2	28.1	29.2	29.7	6.945	9.0616	10.087	3.986	5.765	30.478	45.241
2.3	30.2	30.9	31.6	1.724	2.0415	2.276	2.080	4.380	18.421	32.019
3.1	29.1	30.5	31.2	4.951	6.3601	7.797	4.811	7.262	28.461	57.483
3.2	29.4	30.4	30.9	4.881	6.5565	7.530	4.989	4.989	34.327	54.272

4.4 Grey box model validation results

A grey box model, which is a combination of both physics-based models and data-driven models provides the advantage of changing some building parameters in simulations compared to completely data-driven models. Hence, the grey box model was developed as described in section 3.6. As described in the methodology, unmolded parameters need to be evaluated during the model training and a cross-validation process was used for this. The results of the cross-validation procedure were averaged to obtain a single value for the parameters and the RMSE, NRMSE, and R values, which are given in Table 4.4. Model identification and validation results with error plots for zone 1.1 are shown in Figure 4.16.

TABLE 4.4: RESULTS OF IDENTIFICATION AND VALIDATION

Zone	Identification			Validation			Parameters				
	RMSE	NRMSE	R	RMSE	NRMSE	R	X1	X2	X3 (x 10^{-4})	X4 (x 10^{-4})	X5 (x 10^{-4})
1.1	0.387	18.895	0.867	0.398	19.462	0.789	1.365	0.833	1.281	0.723	0.257
1.2	0.266	12.134	0.864	0.331	15.046	0.789	0.926	0.725	0.815	0.639	0.215
1.3	0.253	11.968	0.818	0.464	21.902	0.763	0.807	0.981	0.962	0.681	0.229
2.1	0.272	9.100	0.771	0.446	14.925	0.698	1.322	0.563	1.024	0.610	0.299
2.2	0.099	3.915	0.853	0.160	6.303	0.787	1.077	0.724	0.814	0.709	0.243
2.3	0.199	9.655	0.831	0.271	13.131	0.780	0.883	0.610	1.375	0.653	0.285
3.1	0.106	3.827	0.773	0.185	6.697	0.716	1.364	0.575	0.971	0.695	0.314
3.2	0.243	11.630	0.851	0.337	16.166	0.770	0.921	0.872	0.898	0.624	0.201

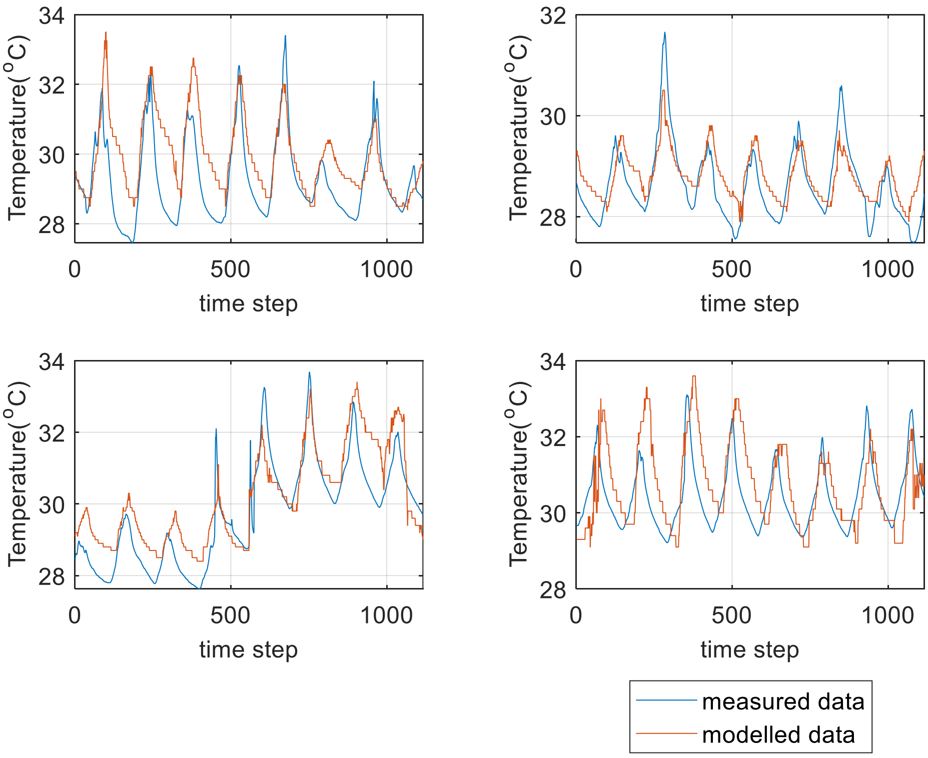

Fig. 4.16: Results of four-fold cross validation for zone 1.1.

The grey box model for each zone showed acceptable results with correlation coefficients greater than or equal to 0.7 in both identification and validation

(Correlation coefficients higher than 0.65 are considered “good” [106]). Zone 1.1 with a higher window-to-external wall ratio (WWR), unshaded glass facing west, no internal heat gains, and absence of furniture showed a high correlation between indoor temperature and outdoor conditions. In comparison, Zone 1.3 situated on the first floor of the building showed a relatively low correlation as the window-to-wall ratio is low. All zones in building 2 showed relatively low correlation indicating that the internal temperature is not dependent on the outdoor conditions. Zone 2.3 showed a high correlation in comparison to other zones of the same building due to low floor area, and high external wall-to-window ratio. Building 3 showed a moderate correlation although the selected areas were non-air conditioned, the building has been designed to be cooled by a mechanical cooling system, and the adjacent areas are air-conditioned which partly cools down the zones selected. It was also noted that zones with high ratio of external heat gains to internal heat gains have shown relatively higher model performance and consistent parameter identification when the model training was done at different times.

The results from the model predictions using developed grey box models for 2035 and 2090 for indoor temperatures together with the measured indoor temperature of 2020 for selected building zones are illustrated in Annex IV (Sample for zone 1.1 shown in Figure 4.17). Average predicted daily indoor temperature variations were calculated and shown in Table 4.5.

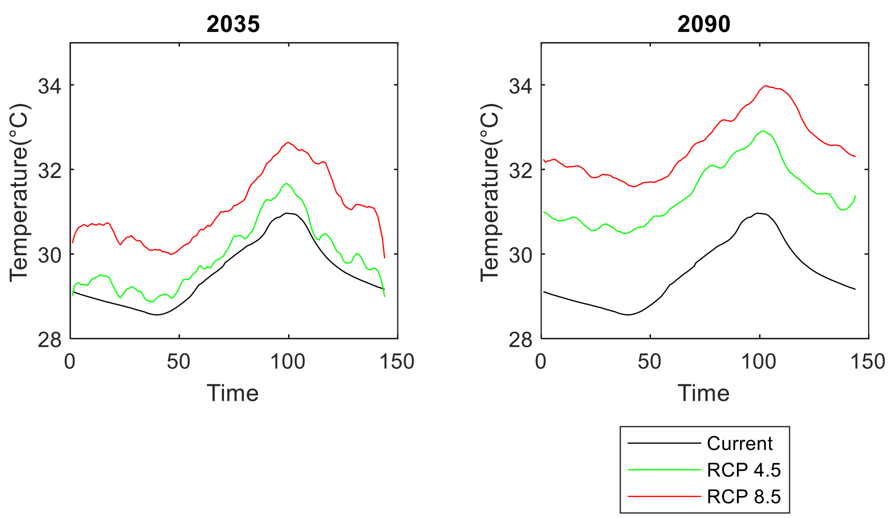

Fig. 4.17: Plots of prediction of indoor temperature from grey box models for zone 1.1. The results are averaged for a single day.

TABLE 4.5 - A: PEAK OF AVERAGE INDOOR TEMPERATURE PREDICTION RESULTS FOR TWO TYPES OF MODELS FOR 2035

Zone	Peak indoor temperature (°C)						Predicted increase of peak indoor temperature (°C)			
	Grey box model			Black box model			Grey box model		Black box model	
	2021	2035		2021	2035		2035			
		RCP 4.5	RCP 8.5		RCP 4.5	RCP 8.5	RCP 4.5	RCP 8.5	RCP 4.5	RCP 8.5
1.1	30.9	32.6	33.2	5.328	32.6	33.4	5.536	7.299	5.502	8.091
1.2	27.9	27.8	28.6	9.43	28.1	28.3	1.227	2.457	0.717	1.434
1.3	28.1	28.8	29.3	87.45	28.6	29.1	2.614	4.435	1.779	3.559
2.1	29.3	30.0	30.3	22.491	29.7	30.1	2.224	3.320	1.365	2.73
2.2	28.1	28.5	29.2	6.945	28.7	28.9	1.326	4.007	2.135	2.847
2.3	30.2	30.5	30.6	1.724	30.4	30.8	0.949	1.255	0.662	1.987
3.1	29.1	30.0	30.6	4.951	30	30.4	3.194	5.136	3.093	4.467
3.2	29.4	29.6	30.1	4.881	29.9	30.1	0.835	2.491	1.701	2.381

TABLE 4.5 - B: PEAK OF AVERAGE INDOOR TEMPERATURE PREDICTION RESULTS FOR TWO TYPES OF MODELS FOR 2090

Zone	Peak indoor temperature (°C)						Predicted increase of peak indoor temperature (°C)			
	Grey box model			Black box model			Grey box model		Black box model	
	2021	2090		2021	2090		2090			
		RCP 4.5	RCP 8.5		RCP 4.5	RCP 8.5	RCP 4.5	RCP 8.5	RCP 4.5	RCP 8.5
1.1	30.9	33.1	34.2	5.328	9.123	11.317	7.079	10.498	71.240	112.40
1.2	27.9	28.6	29.1	9.430	12.490	13.987	2.408	4.333	32.451	48.324
1.3	28.1	29.1	29.9	87.450	97.405	104.81	3.475	6.207	11.384	19.851
2.1	29.3	30.2	30.9	22.491	25.101	27.967	2.958	5.586	11.609	24.348
2.2	28.1	29.2	29.7	6.945	9.0616	10.087	3.986	5.765	30.478	45.241
2.3	30.2	30.9	31.6	1.724	2.0415	2.276	2.080	4.380	18.421	32.019
3.1	29.1	30.5	31.2	4.951	6.3601	7.797	4.811	7.262	28.461	57.483
3.2	29.4	30.4	30.9	4.881	6.5565	7.530	4.989	4.989	34.327	54.272

It was observed that the zones with models having high correlation coefficients (both black box and grey box) had smooth indoor temperature predictions for 2090 while the prediction values of both models were fluctuating for zones with relatively lower correlation coefficients. This indicates the importance of refining the models for better correlation values for the model predictions to be smooth and reliable.

The prediction results from both models showed a considerable increase in indoor temperature by 2090 under both climate change scenarios. Zone 1.1 showed the highest increase in indoor temperature for both models. Overall both models showed relatively similar results showing the highest increase for zone 1.1 and the lowest increase for zone 2.1. Figure 4.19 shows the predicted percentage increase of cooling load for all zones from both model types for two selected climate change scenarios for 2090. The percentage increase in cooling load is calculated as the difference between the predicted cooling load and cooling load in 221 divided by the cooling load in 2021. The results showed consistency in predicting the indoor conditions using both models. Cooling load predictions from the black box model have been higher than the cooling load predictions from the grey box model for the RCP 4.5 emission scenario while it has been the other way around for the RCP 8.5 emission scenario. The grey box model error plot showed relatively high error for high-temperature differences when training the model indicating that the model accuracy reduces with increasing temperature. With RCP 8.5 scenario temperatures higher than the temperature from RCP 4.5, the grey box model results might have been skewed in these higher temperatures which need to be studied further.

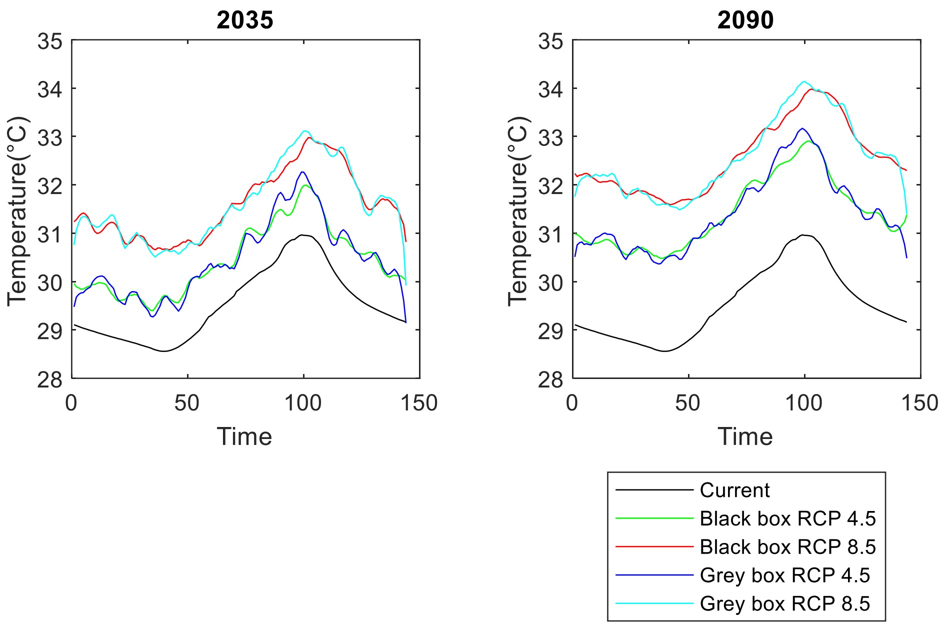

Fig. 4.18: The indoor temperature predictions (averaged to a single day) for the zone with the best correlation (zone 1.1) and the worst correlation (zone 1.3)

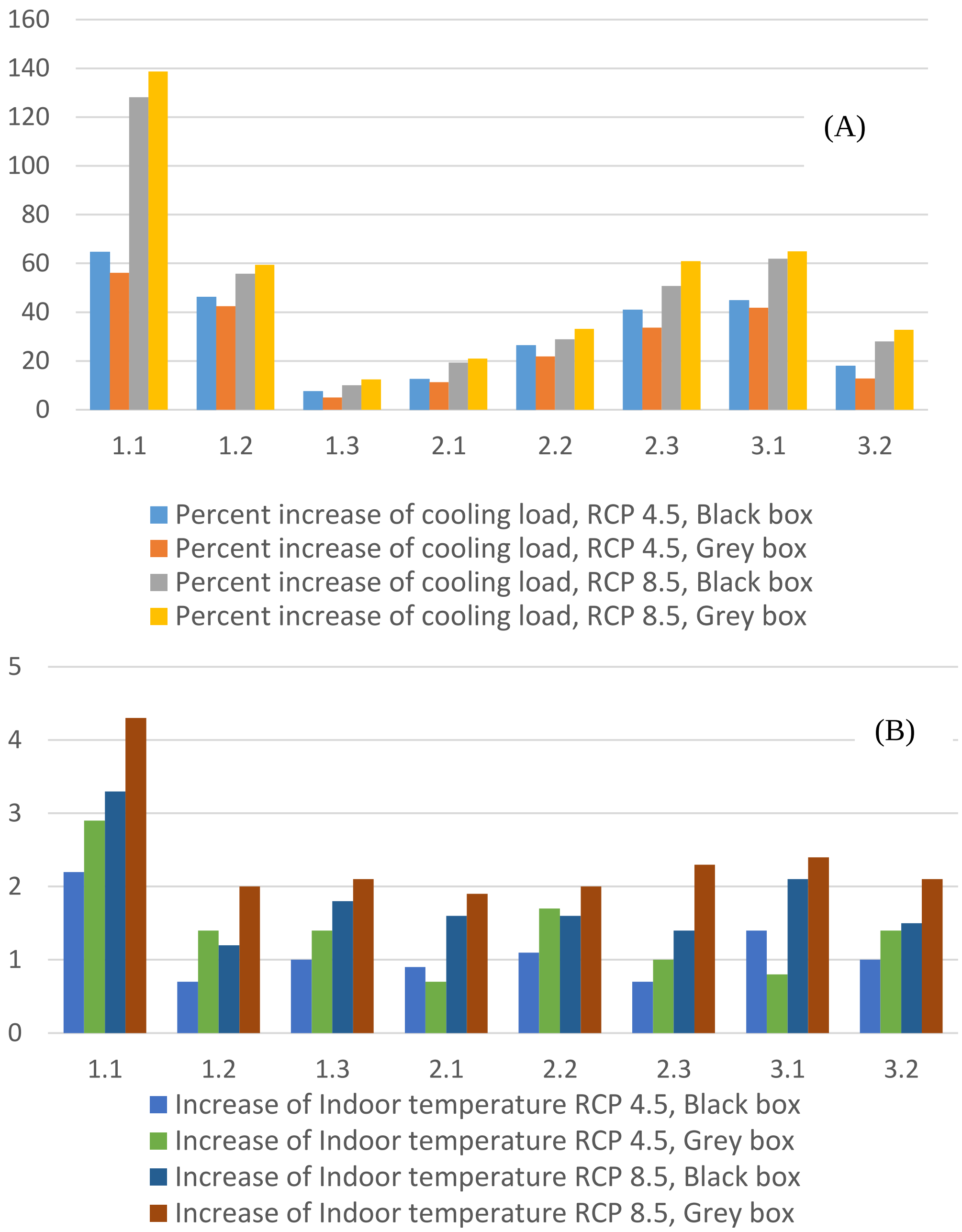

Fig. 4.19: Predicted percentage increase of cooling load (A) and predicted increase of indoor temperature (B) for all zones under RCP 4.5 and 8.5 climate change scenarios using both models for 2090

To further analyze the deviations of two model predictions the difference of percentage increase of cooling load by both models (Percentage increase of cooling load black box – percentage increase of cooling load grey box) was compared with different input parameters. The external cooling load to total cooling load ratio showed a pattern that correlated to the difference in percentage increase of cooling load. This is illustrated in Figure 4.20. The difference in percentage increase of cooling load by both models

The difference between the predicted cooling load increase by the two models of a zone increased with increasing external heat gain/total heat gain ratio of the zone. This can be explained by the previously observed model performance of black box models. Black box models showed high correlation coefficients during testing for models in zones with a higher ratio of external heat loads. Therefore, the black box model performance is better than the grey box model performance for zones with a high external heat gain ratio. In these zones, the black box model predictions and grey box model predictions have a larger difference than in zones with low external heat gain ratios. Thus, black box models are more reliable in predicting the indoor temperature for the building zones for which the models were trained compared to grey box models. However, grey box models provide flexibility in changing the different physical parameters during the prediction period while providing reasonable accuracy. The accuracy of the grey box models could be further improved by adding more physical parameters to the model.

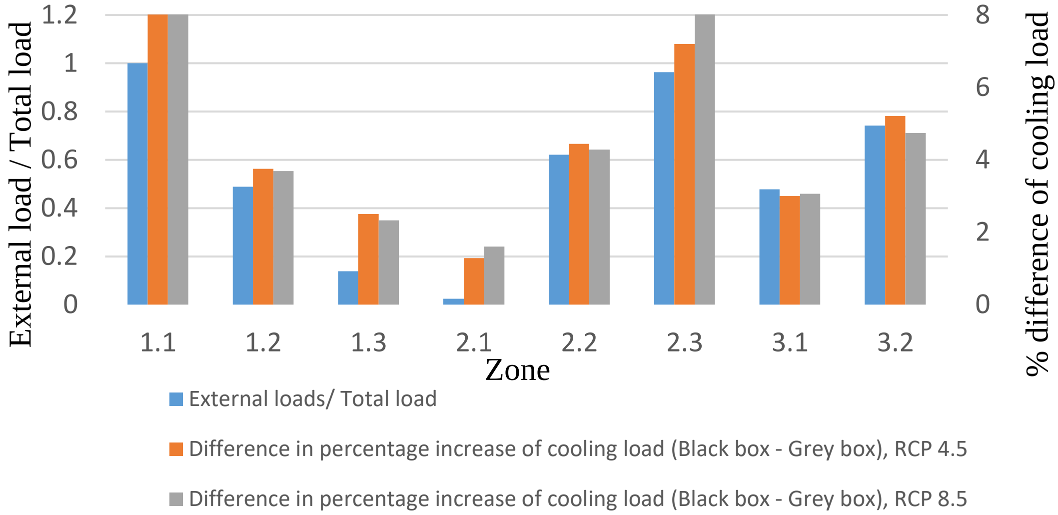

Fig. 4.20: Change in model predicted cooling loads compared with the difference of external loads to internal loads for 2090

4.5 Evaluation of cooling load increase mitigation tactics

This section of the chapter shows the results of the analysis of different cooling load mitigation strategies and their effectiveness in mitigating climate change impacts. The developed grey box model together with CFD simulations were used for the analysis as described in section 3.8.

4.5.1 Effect of thermal mass optimization on indoor temperature and cooling load

The trained grey box models were used to evaluate the variation of the indoor temperatures for the selected zones changing the thermal mass of the zones. The thermal capacity (C) values were changed for each zone to calculate the indoor temperatures. Figure 4.21 shows the predicted indoor temperature variation with increasing and decreasing C by 1% increments.

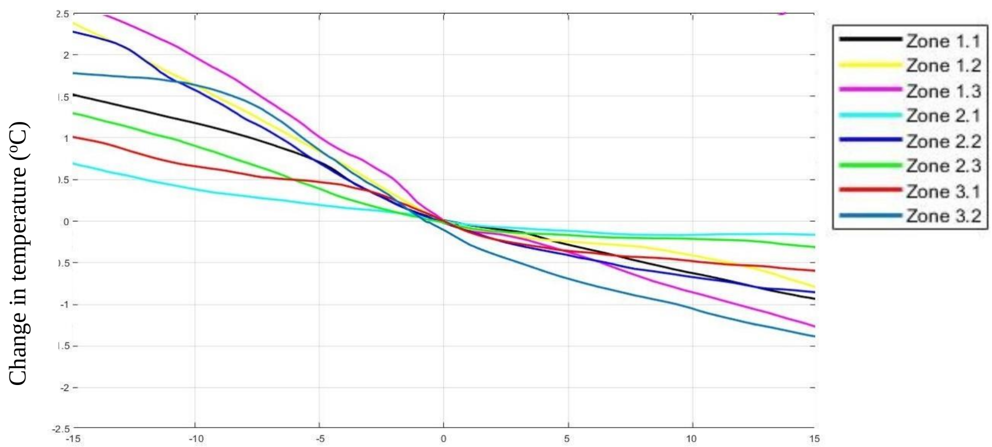

Fig. 4.21: Prediction of indoor temperature varying with different C values for different building zones

An effective night-time cooling method is required for the total cooling energy to have an effective reduction. The zones were simulated by IES VE with an increase of 10% thermal mass for each of the zones. Two simulation instances were calculated as follows,

1. Without any night-time ventilation.
2. Opening the windows at night (7.00 p.m ot 7.00 a.m). MacroFlo module of IES VE was used to simulate the ventilation of the zones.

The results of the simulations are given in Table 4.6.

Although the peak indoor temperatures showed a reduction in both scenarios, the peak cooling load has little to no difference in the instance where the nigh-time ventilation was not available. With night-time ventilation, the zones showed significant cooling load reductions as shown in Table 4.6.

TABLE 4.6: SIMULATED COOLING LOADS FOR DIFFERENT ZONES FOR 10% INCREASE IN THE THERMAL MASS

Zone	Without night-time ventilation		With night-time ventilation	
	Peak indoor temperature (^oC)	Peak cooling load (kW)	Peak indoor temperature (^oC)	Peak cooling load (kW)
1.1	30.9	5.328	30.4	4.819
1.2	27.9	9.430	28.1	9.024
1.3	28.1	87.450	28.0	84.257
2.1	29.3	22.491	29.1	18.541
2.2	28.1	6.945	28.1	6.12
2.3	30.2	1.724	30.1	1.711
3.1	29.1	4.951	29.2	3.947
3.2	30.9	5.328	30.4	4.819

4.5.2 Effect of optimized solar design on indoor temperature

The effect of optimum solar design was simulated by changing the emissivity values as described in section 3.8.2. Figure 4.22 shows the indoor temperature variation of different zones calculated by using different emissivity values.

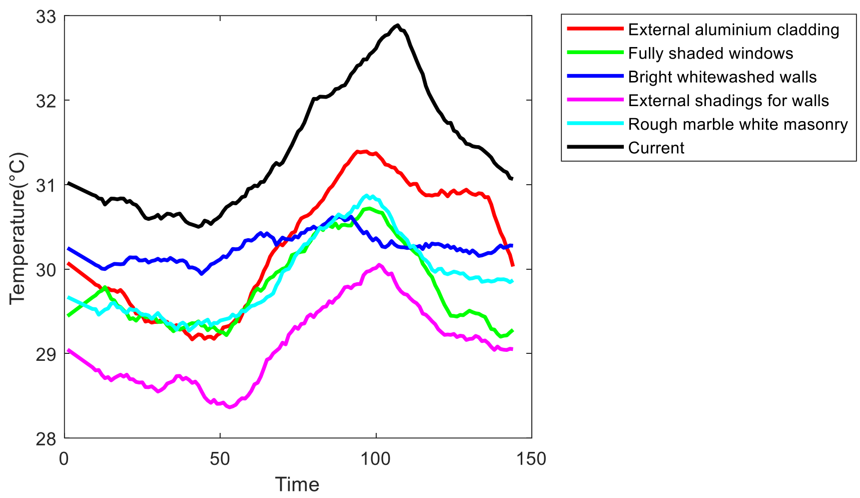

Fig. 4.22: Prediction of indoor temperature varying with different emissivity values for Zone 2.3

The combined optimized solar designs identified from the above graphs were implemented in IES VE cooling load calculations to calculate the peak cooling load of each zone and the results are given in Table 4.7.

TABLE 4.7: COOLING LOADS OF DIFFERENT ZONES UNDER OPTIMIZED SOLAR DESIGN

Zone	Used strategies	Cooling load (kW)	Percentage decrease in cooling load (%)
1.1	Fully shaded glass	3.124	61.24
1.2	Fully shaded glass with aluminium cladding for walls	8.849	12.11
1.3	Fully shaded glass	84.211	3.14
2.1	Fully shaded glass with white enamel paint for external walls	20.98	10.24
2.2	Fully shaded glass with white enamel paint for external walls	5.247	15.25
2.3	Fully shaded glass, white enamel paint for external walls, roofing or shadings for external walls/windows	0.987	30.84

3.1	Roofing or shadings for external walls/windows	3.984	18.02
3.2	White enamel paint for external wall	4.105	6.78

Zone 1.1 has the highest heat addition due to the west-facing unshaded windows which has the highest benefit from the optimized solar designs. Zone 1.3 having a majority of heat addition from internal sources has the lowest benefit from optimized solar designs.

As shown in Figure 4.23, all zones showed benefits from the proposed passive solar designs to mitigate the predicted cooling load increase. Zone 1.1 showed the highest percentage decrease in cooling load the zone managing to reduce nearly 60% of the cooling load increase through passive solar designs. Zones in building 2 did not show significant demand increase mitigation by passive solar designs as the building already has many passive cooling strategies such as external shadings and the building is well shaded from all sides by trees. Zone 1.3 has a very small area exposed to outdoor conditions and therefore the demand mitigation through passive solar designs is minimal.

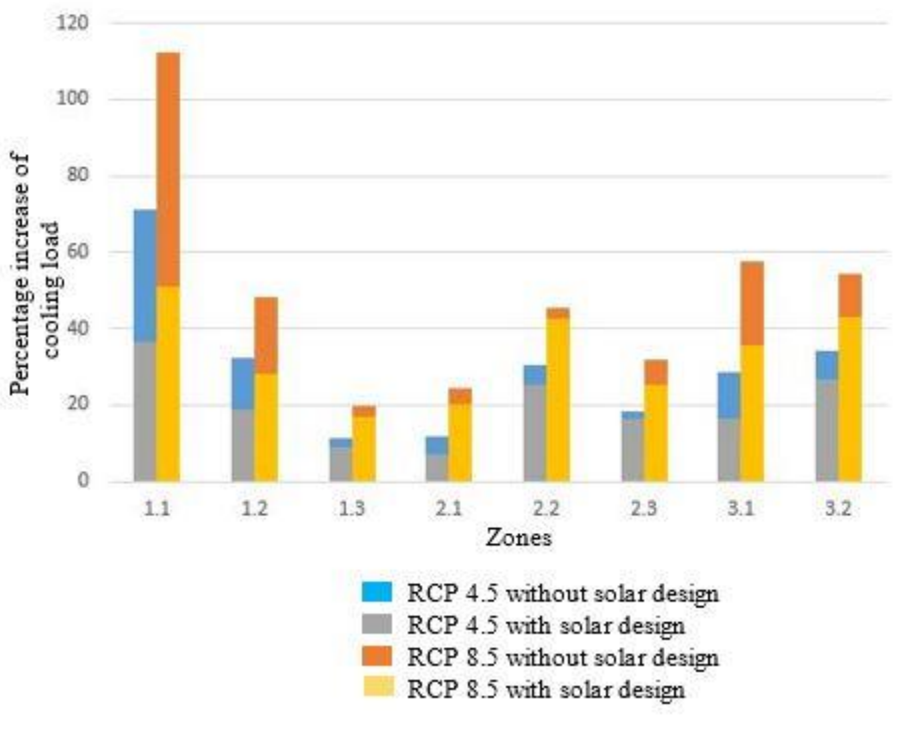

Fig. 4.23: Effect of passive solar deign on the predicted cooling energy demand

4.5.3 Effect of natural and induced ventilation

The developed CFD model for ventilation was compared with the published results. Position 6 in Figure 3.6 in section 3.8 was used for the validation, where the velocity plots for three directions were compared, and the relative error values were calculated. The plots of comparison between published experimental results [78] and the current simulation results are shown in Figure 4.24.

Table 4.8 shows the different error values, and the simulation times calculated for position 6, for different grid sizes.

TABLE 4.8: ERROR VALUES OF DIFFERENT GRID SIZES USED

Grid size	Calculated Error (RMSE)	Computation time
36x36x36	5.825x10-2	1 hr 58 minutes
44x44x44	1.331x10-2	2 hr 12 minutes
72x72x72	8.501x10-3	4 hr 24 minutes

Considering the difference between the calculated RMSE and computational time, grid size of 44x44x44 was selected, which provide a reasonable accuracy without significantly increasing the computational time. Also, the Figure 4.24 depicts that this grid resolution provided a good match with the experimental and previous simulation results.

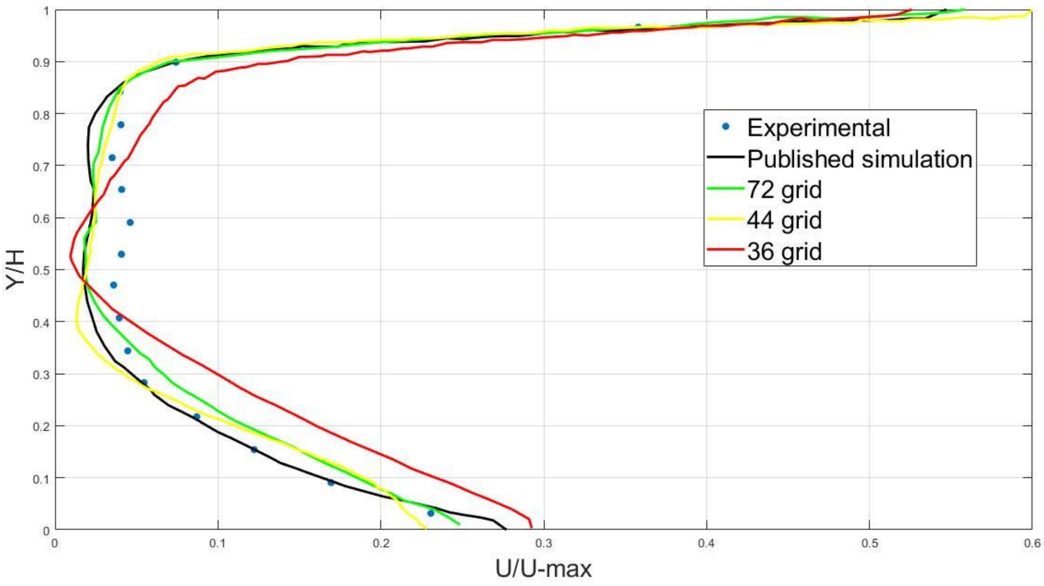

Fig. 4.24: Comparison of simulated and experimental results of [78]

This grid resolution with simulation parameters discussed in section 3.8.3 was used to simulate the natural and induced ventilation for each zone. It was observed that natural ventilation had different effects on the indoor temperature variation of different zones. Zone 1.3 which has a low window-to-floor area ratio did not show any significant change in indoor temperatures with natural ventilation while zone 2.3 with a very high window-to-floor area ratio showed a significant decrease in indoor temperature peaks. Zone 1.2 which was originally air-conditioned showed an increase in indoor temperature when the windows were opened (natural ventilation) and fans turned on (induced ventilation). The indoor temperature variations of zones 1.2 and 2.3 are shown in Figure 4.25 and Figure 4.26 under normal conditions, natural ventilation, and induced ventilation.

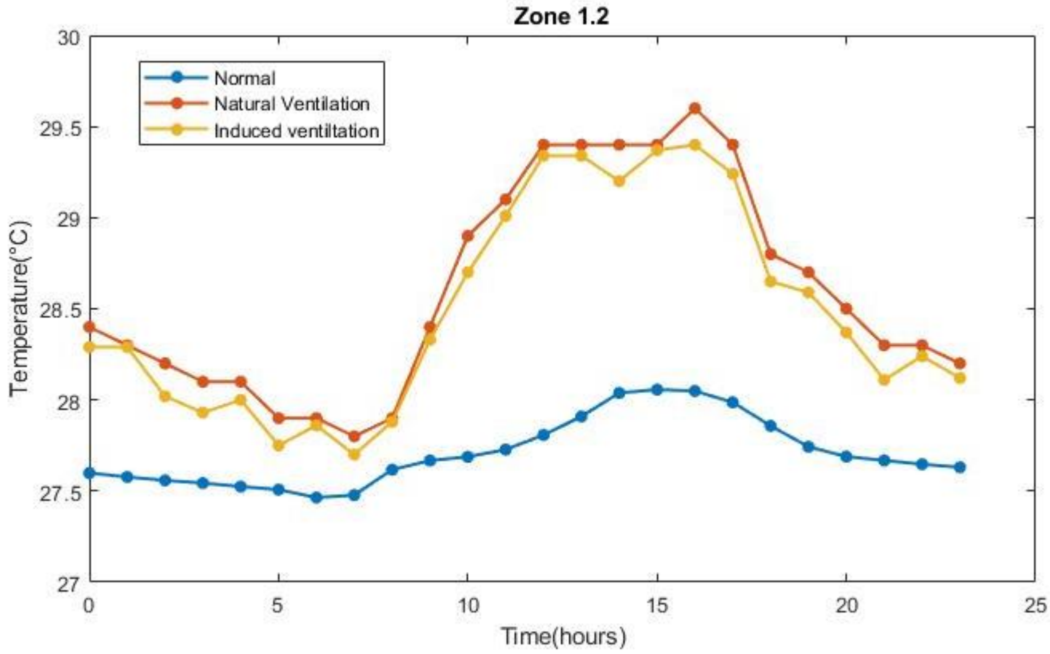

Fig. 4.25: Average indoor temperature variation of Zone 1.2 with natural and induced ventilation

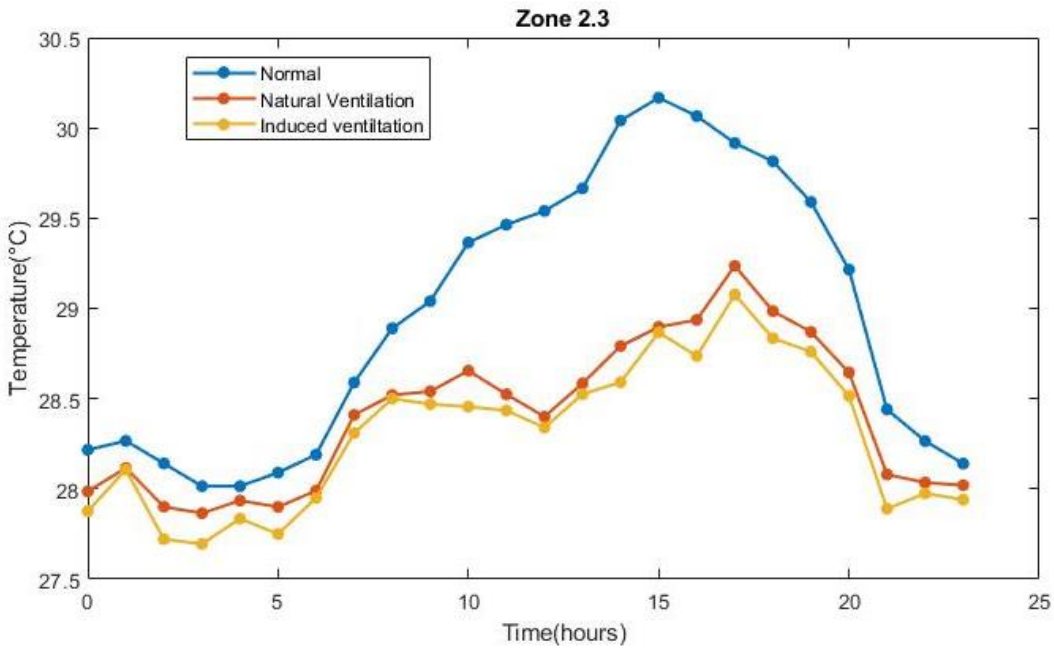

Fig. 4.26: Average indoor temperature variation of Zone 2.3 with natural and induced ventilation

It was observed that induced ventilation using ceiling fans did not have a significant impact on indoor temperature variation when compared to natural ventilation. However, induced ventilation increased the average flow velocity of the zones. An increase in the average flow velocity of the zones increased the thermal comfort of the occupants inside the zones. The flow variation of each zone at 2.00 p.m. is shown in Figure 4.27. The calculated PMV values for all zones at 2.00 p.m. with natural and induced ventilation are shown in Figure 4.28.

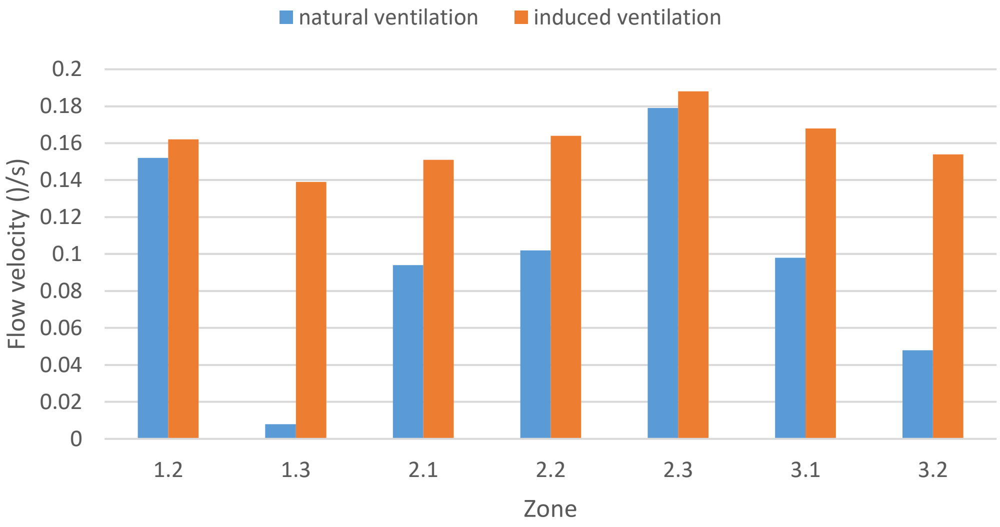

Fig. 4.27: Flow velocity with natural and induced ventilation for each zone at 2.00 p.m.

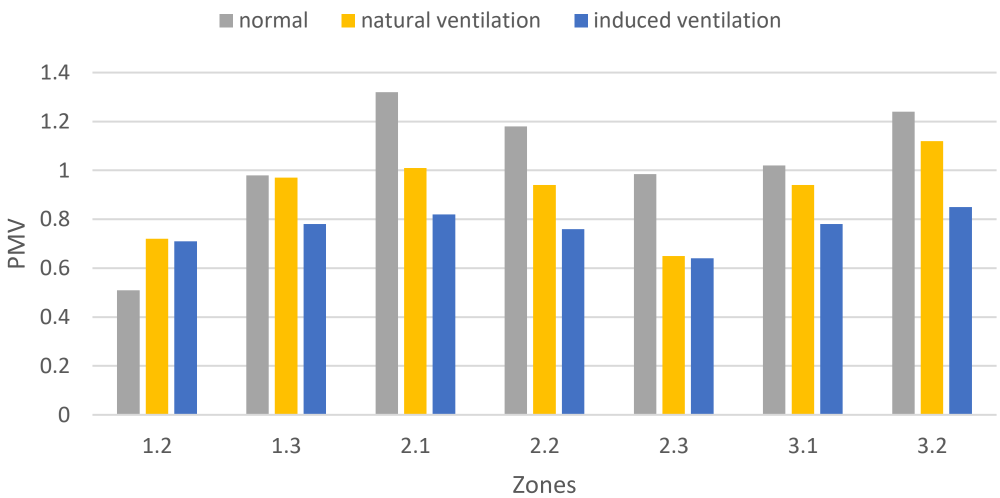

Fig. 4.28: Flow velocity with natural and induced ventilation for each zone at 2.00 p.m.

All zones except zone 1.2 showed the potential to reduce the PMV significantly by natural and induced ventilation. A reduction in PMV reflects that an average occupant is more comfortable with a reduction in warm sensation. (A zero PMV is comfortable while a PMV of 1 is a warm sensation). Zone 1.2, which is air-conditioned showed an increase in PMV as in the normal data collected period. It should be noted that the PMV of air-conditioned zone 1.2 is around 0.45 while the non-air-conditioned zone 2.3 showed the ability to have just a slightly higher PMV of around 0.6 just by natural ventilation. Therefore, most of these zones have the ability to reduce the warm thermal sensation of the occupants just by natural ventilation or by the use of ceiling fans which consumes far less energy than a typical air conditioner.

4.6 Economic benefit analysis

The above-calculated values from each passive cooling strategy were used to calculate the electrical energy saved and quantify the money saved over 10 years. The results are shown in Table 4.9.

Since there is no data about the baseline total cost of electricity or baseline total cooling energy usage for the whole building when calculating the predicted money saved for the whole building, an averaging method by zone placement, usage and floor area was used. It was assumed that the effectiveness of the mitigation tactics is lower in interior zones. It should be noted that the usage, internal loads, and loads due to occupants can vary from the selected zones for analysis.

Following the same trend in the cooling load mitigations, Sumanadasa building has the highest payback period for an initial cost of 1,000,000 LKR. The Western Provincial Council building overall had the most benefit from the selected passive cooling method and will recover the same initial cost within 1 year and 1 month.

This economic analysis is based on limited data and based on several simplifications, to show the economic benefits of the proposed technical improvements through natural ventilation methods. To generate a proper conclusion on economic viability, a more comprehensive analysis is required for individual buildings, which is beyond the scope of this study.

TABLE 4.9: PREDICTED ECONOMIC BENEFIT AND PAYBACK PERIOD FROM THE SUGGESTED PASSIVE COOLING STRATEGIES

Building	Zone	Predicted building averaged cooling load reduction (%)	Predicted peak cooling load reduction in zones (kW)	Predicted electrical energy saved per day	Money saved over 10 years (per zone) (LKR)	Predicted money saved over 10 years (per building averaged by floor area) (LKR)	Payback period for a cost of 1,000,000 LKR
Western Provincial Council Building	1.1	32.94%	3.263	5.438	258,757.16	9,881,449.05	1 year 1 month
	1.2		1.142	1.523	72,450.07		
	1.3		2.746	4.577	217,762.17		
Sumanadasa Building	2.1	23.82%	2.303	3.838	182,642.44	5,558,366.80	3 years 9 months
	2.2		1.059	1.765	83,991.45		
	2.3		0.532	0.886	42,164.27		
ENTC building	3.1	34.06%	0.892	1.487	70,752.32	8,363,420.22	1 year 8 months
	3.2		4.967	8.278	393,882.14		

CHAPTER 5

CONCLUSION

In this study, two models, a black box NARX model and a grey box model based on Newton's cooling law and radiation were used to model the relationship between indoor and outdoor temperatures of some selected existing buildings in tropical climates. The models were used to predict the indoor temperature of the selected building zones by 2035 and 2090 using existing climate change models. The predictions from both models showed a high increase in indoor temperature in the selected zones. The grey box models showed results with slightly higher Mean Square Error (MSE) and slightly lower correlation coefficients (R) than the black box models for each zone. It can be concluded that data-driven black box models show slightly higher accuracy in modeling indoor temperature than grey box models, for the buildings that the model was trained in. However, the accuracy of the grey box models can be increased by adding more parameters and physical relationships to the model build-up. When using the built models for temperature predictions, it was observed that zones with models (black box and grey box) having higher correlation coefficients between indoor and outdoor temperatures had relatively similar predictions by both types of models. Zones with lower correlation showed slight differences in indoor temperature predictions. It can be concluded that the indoor temperature of zones with a higher correlation between indoor and outdoor temperatures is more predictable. The predicted increase in indoor temperature by the models can be used to calculate the increase of cooling loads in these areas and thereby calculate and predict the electrical consumption for cooling of the selected zones for 2035 and 2090.

Currently developed models showed good accuracy in predicting indoor temperature using existing modelled outdoor temperature data. All models showed acceptable R values greater than 0.7 and nearly identical MSE values each time the networks were trained. The models were then used in their closed-loop form to predict the indoor temperature in 2035 and 2090. Outdoor conditions predicted by RCP 4.5 and RCP 8.5 emission scenarios were used as network inputs to calculate the indoor temperatures of these zones. The heat loads of the zones were calculated using a heat balance method and the results were compared for both emission scenarios. On average around 10% and 30% of cooling load increase can be predicted for all three buildings under RCP

4.5 and 8.5 climate change scenarios, respectively for 2035. The increase can be as high as 50% by 2090 as predicted by the models. This is a significant increase in cooling load and the relative increase in electrical consumption for space cooling of the building that could be a threat to the electrical infrastructure of these geographical regions.

The developed grey box models were then used in the evaluation of passive cooling strategies, where three types of passive cooling strategies, optimized thermal mass strategy, optimized solar design, and natural ventilation were used for the study. These passive cooling design strategies showed a significant reduction in predicted cooling load. The optimized thermal mass strategy showed a significant reduction in cooling load when combined with night-time cooling. Additionally, natural ventilation as a passive cooling method was evaluated. The CFD model required for the evaluation of natural ventilation was developed and validated using a published set of experimental and computational results. Natural and induced ventilation showed the ability to increase the thermal comfort of the occupants inside the zones by significantly reducing the PMV of all zones.

The suggested cooling load mitigation tactics showed the potential of reducing the predicted increase of cooling load by up to 30% depending on the zones. Passive solar design is observed to be the most effective and reliable method to reduce the cooling load increase of the selected zones.

5.1 Future directives

The research outcomes from the study can be used widely in many different aspects in improving the electrical infrastructure.

- The numerical models can be trained for different data sets from other buildings and zones to predict the cooling demand increase. The study can be extended to generalize the results by grouping the buildings in a city-wide scale to different architectural types and training the models to different sample buildings of architectural type categories. This can yield a demand prediction on a city-wide scale which will be important for the future energy generation and distribution plans of a country.
- Generalization of the model can be achieved by training more models on different types of buildings in the same geographical region. Then the

optimized physical parameters of the model equations can be tied down to building properties and can be used as a database when modelling other buildings. A similar approach has been tested successfully for German building stock in the TEASER program [107], but these results are highly sensitive to the environmental conditions and the building stock type. Therefore, developing more models for different buildings and creating a database of optimized parameters to create a wider dataset for buildings in hot and humid areas will be an interesting area of research. The ability to use these models as a connected model is a major advantage of developing grey box models over purely mathematical physics-based models.

- The grey box models are simplified models and they can be connected to developing multi-zone building models and multi-building community models. These community energy models are useful in calculating energy predictions in a collection or a community of buildings that are operated together. These models can be used to predict community energy predictions for future climate scenarios.
- The suggested demand mitigation tactics can be tested experimentally in the buildings to validate the results. The buildings can then be modified accordingly to reduce the predicted demand increase.

REFERENCES

[1] Asian Development Bank, *Sri Lanka: Energy Sector Assessment, Strategy, and Road Map*, no. December. 2019.

[2] Ministry of Power and Energy, "SRI LANKA ENERGY SECTOR DEVELOPMENT PLAN FOR A KNOWLEDGE-BASED ECONOMY 2015-2025," 2015.

[3] Sri Lanka Sustainable Energy Authority, "Sri Lanka Sustainable Energy Authority," 2010.

[4] Liam Critchley, "How are Thermal Power Plants Polluting the Environment?" [Online]. Available: https://www.azocleantech.com/article.aspx?ArticleID=861

[5] D. Geekiyanage and T. Ramachandra, "A model for estimating cooling energy demand at early design stage of condominiums," *Journal of Building Engineering*, vol. 17, no. February, pp. 43–51, 2018, doi: 10.1016/j.jobe.2018.01.011.

[6] H. Wu, D. Wang, Y. Liu, and Y. Wang, "Study on the effect of building envelope on cooling load and life-cycle cost in low latitude and hot-humid climate," *Procedia Engineering*, vol. 205, pp. 975–982, 2017, doi: 10.1016/j.proeng.2017.10.153.

[7] C. Younes, C. A. Shdid, and G. Bitsuamlak, "Air infiltration through building envelopes: A review," *Journal of Building Physics*, vol. 35, no. 3, pp. 267–302, 2012, doi: 10.1177/1744259111423085.

[8] H.M.H. Abed, "Effect of Building Form on the Thermal Performance of Residential Complexes in the Mediterranean Climate of the Gaza Strip," Islamic University of Gaza, 2012.

[9] K. Yeang, "The Green Skyscraper," Prestel, Munich, 1999.

[10] D. Geekiyanage and T. Ramachandra, "A model for estimating cooling energy demand at early design stage of condominiums in Sri Lanka A model for estimating cooling energy demand at early design stage of condominiums," *Journal of Building Engineering*, vol. 17, no. February, pp. 43–51, 2018, doi: 10.1016/j.jobe.2018.01.011.

[11] S. Magli, C. Lodi, L. Lombroso, A. Muscio, and S. Teggi, "Analysis of the urban heat island effects on building energy consumption," *International Journal of Energy and Environmental Engineering*, vol. 6, no. 1, pp. 91–99, 2015, doi: 10.1007/s40095-014-0154-9.

[12] "Sustainable Window Design - Green Garage Detroit." [Online]. Available: http://www.greengaragedetroit.com/index.php/Sustainable_Window_Design

[13] Z. Huifen, Y. Fuhua, and Z. Qian, "Research on the Impact of Wind Angles on the Residential Building Energy Consumption," *Mathematical Problems in Engineering*, vol. 2014, 2014, doi: 10.1155/2014/794650.

[14] E. A. Arens and P. B. Williams, "The effect of wind on energy consumption in buildings," *Energy and Buildings*, vol. 1, no. 1, pp. 77–84, 1977, doi: https://doi.org/10.1016/0378-7788(77)90014-7.

[15] A. A. Bakar and N. A. M. Ariffin, "the Impact of External Environment on the Internal Thermal Environment of the Main Prayer of Putra ....," no. October 2015, 2017.

[16] Arena 3050, "Predicting Thermal Comfort," *AREN 3050 Environmental Systems for Buildings I*, vol. 42, no. 1971, pp. 3–6, 2005.

[17] Sri Lanka Sustainable Energy Authority, *Code of practice for energy efficient buildings in SrI Lanka*. 2010.

[18] A. Bhatia, "HVAC Made Easy : A Guide to Heating & Cooling Load Estimation," *PDH Online*, vol. 196, 2012.

[19] "EnergyPlus." Accessed: Sep. 21, 2023. [Online]. Available: https://energyplus.net/

[20] "Welcome | TRNSYS : Transient System Simulation Tool." Accessed: Sep. 21, 2023. [Online]. Available: http://www.trnsys.com/

[21] R. Kramer, J. van Schijndel, and H. Schellen, "Simplified thermal and hygric building models: A literature review," Dec. 01, 2012, *Higher Education Press Limited Company*. doi: 10.1016/j.foar.2012.09.001.

[22] Y. Li, Z. O'Neill, L. Zhang, J. Chen, P. Im, and J. DeGraw, "Grey-box modeling and application for building energy simulations - A critical review," *Renewable and Sustainable Energy Reviews*, vol. 146, no. April, p. 111174, 2021, doi: 10.1016/j.rser.2021.111174.

[23] A. T. Nguyen, S. Reiter, and P. Rigo, "A review on simulation-based optimization methods applied to building performance analysis," 2014. doi: 10.1016/j.apenergy.2013.08.061.

[24] H. OKTAY, R. YUMRUTAŞ, and M. Z. IŞIK, "Comparison of Cltd and Tetd Cooling Load Calculation Methods for Different Building Envelopes," *Mugla Journal of Science and Technology*, no. February, 2020, doi: 10.22531/muglajsci.631222.

[25] K. G. \\Acharya\, G. P. Yewale, M. V. Tendolkar, and S. H. Kulkarni, "Estimation and Analysis of Cooling Load for Indian Subcontinent by CLD/SCL/CLF method at part load conditions," *Journal of Physics: Conference Series*, vol. 1240, no. 1, 2019, doi: 10.1088/1742-6596/1240/1/012031.

[26] J. D. Spitler, F. C. McQuiston, and K. Lindsey, "the Cltd / Scl / Clf Cooling Load Calculation Method," *ASHRAE Transactions*, vol. 99, no. 1, pp. 183–192, 1993.

[27] G. Paliaga *et al.*, "Thermal environmental conditions for human occupancy," *ASHRAE Standard*, vol. 8400, no. 55, 2013.

[28] S. C. Turner *et al.*, "Ashrae 55-2010," *Encyclopedia of Finance*, vol. 2010, pp. 227–227, 2008, doi: 10.1007/0-387-26336-5_1680.

[29] Ansi/Ashrae, "ANSI/ASHRAE 55:2004 Thermal Environmental Conditions for Human Occupancy," *Ashrae*, vol. 2004, p. 30, 2004, doi: 10.1007/s11926-011-0203-9.

[30] ASHRAE, *Pocket Guide for Air Conditioning, Heating, Ventilation, refrigeration*. 1993.

[31] F. Feng and Z. O'neill, "Identifying Models of HVAC Systems Using ARIMAX."

[32] Y. Zhang, Z. O'Neill, B. Dong, and G. Augenbroe, "Comparisons of inverse modeling approaches for predicting building energy performance," *Build Environ*, vol. 86, pp. 177–190, Apr. 2015, doi: 10.1016/j.buildenv.2014.12.023.

[33] Z. Ma, C. Ye, H. Li, and W. Ma, "Applying support vector machines to predict building energy consumption in China," in *Energy Procedia*, Elsevier Ltd, 2018, pp. 780–786. doi: 10.1016/j.egypro.2018.09.245.

[34] X. Tian, J. Yan, Y. Yang, C. Xiao, and Q. Zhou, "Parameter identification of a nonlinear model using an improved version of simulated annealing," *Int J Distrib Sens Netw*, vol. 15, no. 2, 2019, doi: 10.1177/1550147719832788.

[35] C. Sun, S. Shu, G. Ding, X. Zhang, and X. Hu, "Investigation of time lags and decrement factors for different building outside temperatures," *Energy Build*, vol. 61, pp. 1–7, Jun. 2013, doi: 10.1016/j.enbuild.2013.02.003.

[36] C. Fan, F. Xiao, and Y. Zhao, "A short-term building cooling load prediction method using deep learning algorithms," *Appl Energy*, vol. 195, no. June, pp. 222–233, 2017, doi: 10.1016/j.apenergy.2017.03.064.

[37] Q. Zhou, S. Wang, X. Xu, and F. Xiao, "A grey-box model of next-day building thermal load prediction for energy-efficient control," *Int J Energy Res*, vol. 32, no. 15, 2008, doi: 10.1002/er.1458.

[38] Y. Zhao, J. Wen, and S. Wang, "Diagnostic Bayesian networks for diagnosing air handling units faults - Part II: Faults in coils and sensors," *Appl Therm Eng*, vol. 90, pp. 145–157, Jul. 2015, doi: 10.1016/j.applthermaleng.2015.07.001.

[39] S. Li and J. Wen, "A model-based fault detection and diagnostic methodology based on PCA method and wavelet transform," *Energy Build*, vol. 68, no. PARTA, pp. 63–71, 2014, doi: 10.1016/j.enbuild.2013.08.044.

[40] A. Bagheri, V. Feldheim, and C. S. Ioakimidis, “On the evolution and application of the thermal network method for energy assessments in buildings,” Apr. 01, 2018, *MDPI AG*. doi: 10.3390/en11040890.

[41] R. Kramer, J. van Schijndel, and H. Schellen, “Inverse modeling of simplified hygrothermal building models to predict and characterize indoor climates,” *Build Environ*, vol. 68, pp. 87–99, 2013, doi: 10.1016/j.buildenv.2013.06.001.

[42] A. Li, Y. Sun, and X. Xu, “Development of a simplified resistance and capacitance (RC)-network model for pipe-embedded concrete radiant floors,” *Energy Build*, vol. 150, pp. 353–375, Sep. 2017, doi: 10.1016/j.enbuild.2017.06.011.

[43] A. Bagheri, V. Feldheim, D. Thomas, and C. S. Ioakimidis, “The adjacent walls effects in simplified thermal model of buildings,” *Energy Procedia*, vol. 122, pp. 619–624, Sep. 2017, doi: 10.1016/J.EGYPRO.2017.07.359.

[44] C. Klemm and P. Vennemann, “Modeling and optimization of multi-energy systems in mixed-use districts: A review of existing methods and approaches,” Jan. 01, 2021, *Elsevier Ltd*. doi: 10.1016/j.rser.2020.110206.

[45] L. Nazarenko *et al.*, “Future climate change under RCP emission scenarios with GISS ModelE2,” *Journal of Advances in Modeling Earth Systems*, vol. 7, no. 1, pp. 244–267, 2015, doi: 10.1002/2014MS000403.

[46] H. Le Treut, U. Cubasch, and M. Allen, “Historical Overview of Climate Change Science,” *Notes*, vol. 16, 2005.

[47] D. T. King, J. D. Macdougall, and G. Tapper, “A Short History of Planet Earth,” *Palaios*, vol. 14, no. 2, p. 192, 1999, doi: 10.2307/3515375.

[48] Richard. Moss *et al.*, *Towards new scenarios for analysis of emissions, climate change, impacts, and response strategies : IPCC Expert Meeting report : 19-21 September, 2007, Noordwijkerhout, the Netherlands*. 2008.

[49] G. Krinner *et al.*, “Long-term climate change: Projections, commitments and irreversibility,” *Climate Change 2013 the Physical Science Basis: Working Group I Contribution to the Fifth Assessment Report of the Intergovernmental Panel on Climate Change*, vol. 9781107057, pp. 1029–1136, 2013, doi: 10.1017/CBO9781107415324.024.

[50] IPCC, “Climate System Scenario Tables,” in *Climate Change 2013 - The Physical Science Basis*, 2014, pp. 1395–1446. doi: 10.1017/cbo9781107415324.030.

[51] L. Clarke *et al.*, “Effects of long-term climate change on global building energy expenditures,” *Energy Economics*, vol. 72, pp. 667–677, 2018, doi: 10.1016/j.eneco.2018.01.003.

[52] A. Newman, “Heat stress : Threatens to undermine export economies and disrupt global supply chains,” no. August, pp. 1–9, 2018.

[53] K. P. MOUSTRIS, P. T. ZACHARIA, I. K. LARISSI, P. . T. NASTOS, and A. G. PALIATSOS, “Cooling and Heating Degree-Days Calculation for Representative Locations Within the Greater Athens Area, Greece,” *Proceedings of the 12th International Conference on Environmental Science and Technology*, no. September, pp. 8–10, 2011.

[54] A. R. Katili, R. Boukhanouf, and R. Wilson, “Space Cooling in Buildings in Hot and Humid Climates—A Review of the Effect of Humidity on the Applicability of Existing Cooling Techniques,” *Proceedings of 14th International Conference on Sustainable Energy Technologies (SET)*, no. August, pp. 25–27, 2015, doi: 10.13140/RG.2.1.3011.5287.

[55] T. Lundgren, K. and Kjellstrom, “Sustainability challenges from climate change and air conditioning use in urban areas,” *Sustainability, 5(7), pp.3116-3128,* 2013.

[56] L. W. Davis and P. J. Gertler, “Contribution of air conditioning adoption to future energy use under global warming,” *Proceedings of the National Academy of Sciences of the United States of America*, vol. 112, no. 19, pp. 5962–5967, 2015, doi: 10.1073/pnas.1423558112.

[57] L. Clarke *et al.*, “Effects of long-term climate change on global building energy expenditures,” *Energy Economics*, vol. 72, pp. 667–677, 2018, doi: 10.1016/j.eneco.2018.01.003.

[58] V. Chaturvedi, J. Eom, L. E. Clarke, and P. R. Shukla, “Long term building energy demand for India: Disaggregating end use energy services in an integrated assessment modeling framework,” *Energy Policy*, vol. 64, pp. 226–242, 2014, doi: 10.1016/j.enpol.2012.11.021.

[59] M. Tewari, F. Salamanca, A. Martilli, L. Treinish, and A. Mahalov, “Impacts of projected urban expansion and global warming on cooling energy demand over a semiarid region: Impacts of projected urban expansion and global warming,” *Atmospheric Science Letters*, vol. 18, pp. 419–426, Nov. 2017, doi: 10.1002/asl.784.

[60] A. Kitous and J. Després, *Assessment of the impact of climate change on residential energy demand for heating and cooling*. 2018. doi: 10.2760/96778.

[61] W. Goetzler, M. Guernsey, J. Young, J. Fuhrman, and O. Abdelaziz, “The Future of Air Conditioning for Buildings,” *Department of Energy Office of Energy Efficiency and Renewable Energy Building Technologies Office*, no. July, p. 94, 2016.

[62] F. T. Wu *et al.*, “Evaluation and projection of summer extreme precipitation over east Asia in the regional model inter-comparison project,” *Climate Research*, vol. 69, no. 1, pp. 45–58, 2016, doi: 10.3354/cr01384.

[63] Intergovernmental Panel on Climate Change and Intergovernmental Panel on Climate Change, “Residential and commercial buildings,” *Climate Change 2007*, pp. 387–446, 2012, doi: 10.1017/cbo9780511546013.010.

[64] H. Rogner, D. Zhou, R. Bradley, P. Crabbé, O. Edenhofer, and B. Hare, “Mitigation. Contribution of Working Group III to the Fourth Assessment Report of the Intergovernmental Panel on Climate Change,” *Introduction. In Climate Change 2007*, Jan. 2007.

[65] N. D. Dogne, “PASSIVE COOLING TECHNIQUES, DESIGN CONCEPT AND VENTILATION TECHNIQUES,” 2014.

[66] V. K. Venkiteswaran, J. Liman, and S. A. Alkaff, “Comparative Study of Passive Methods for Reducing Cooling Load,” *Energy Procedia*, vol. 142, pp. 2689–2697, 2017, doi: 10.1016/j.egypro.2017.12.212.

[67] H. Y. Levine, M., D. Ürge-Vorsatz, K. Blok, L. Geng, D. Harvey, S. Lang, G. Levermore, A. Mongameli Mehlwana, S. Mirasgedis, A. Novikova, J. Rilling, “Residential and commercial buildings. In Climate Change 2007: Mitigation,” *Contribution of Working Group III to the Fourth Assessment Report of the Intergovernmental Panel on Climate Chan*, 2007.

[68] R. Vasaturo, T. van Hooff, I. Kalkman, B. Blocken, and P. van Wesemael, “Impact of passive climate adaptation measures and building orientation on the energy demand of a detached lightweight semi-portable building,” *Building Simulation*, vol. 11, no. 6, pp. 1163–1177, 2018, doi: 10.1007/s12273-018-0470-8.

[69] X. Zhou, D. Yan, and X. Shi, “Comparative research on different air conditioning systems for residential buildings,” *Frontiers of Architectural Research*, vol. 6, no. 1, pp. 42–52, 2017, doi: 10.1016/j.foar.2016.11.004.

[70] Leifer. D. Rajapaksha. U1, 2, Hyde. R1, Rajapaksha.I1, 2, “Developing a framework of interventions for retrofitting high-rise office buildings in warm climates”.

[71] S. A. Nada and M. A. Said, “Performance and energy consumptions of split type air conditioning units for different arrangements of outdoor units in confined building shafts,” *Applied Thermal Engineering*, vol. 123, no. May, pp. 874–890, 2017, doi: 10.1016/j.applthermaleng.2017.05.104.

[72] J. Liu and Q. Q. Pei, “Numerical simulation and experiment study of indoors thermal environment in summer air-conditioned room,” *Procedia Engineering*, vol. 52, pp. 230–235, 2013, doi: 10.1016/j.proeng.2013.02.132.

[73] Y. Li, P. Fazio, and J. Rao, “Numerical modeling of hygrothermal response in a full-scale experimental room and through the envelope,” *Thermal Performance of the Exterior Envelopes of Whole Buildings - 11th International Conference*, no. 2007, 2010.

[74] C. Fan, F. Xiao, and Y. Zhao, "A short-term building cooling load prediction method using deep learning algorithms," *Applied Energy*, vol. 195, no. June, pp. 222–233, 2017, doi: 10.1016/j.apenergy.2017.03.064.

[75] X. Li, T. Zhao, J. Zhang, and T. Chen, "Predication control for indoor temperature time-delay using Elman neural network in variable air volume system," *Energy and Buildings*, vol. 154, pp. 545–552, 2017, doi: 10.1016/j.enbuild.2017.09.005.

[76] F. Ascione, N. Bianco, R. F. De Masi, G. M. Mauro, and G. P. Vanoli, "Design of the building envelope: A novel multi-objective approach for the optimization of energy performance and thermal comfort," *Sustainability (Switzerland)*, vol. 7, no. 8, pp. 10809–10836, 2015, doi: 10.3390/su70810809.

[77] A. Boodi, K. Beddiar, Y. Amirat, and M. Benbouzid, "Simplified building thermal model development and parameters evaluation using a stochastic approach," *Energies*, vol. 13, no. 11, 2020, doi: 10.3390/en13112899.

[78] S. M. M. Rahman, "Simplified 3R2C Building Thermal Network Model: A Case Study," *International Journal of Structural and Construction Engineering*, vol. 13, no. 6, pp. 288–294, 2019.

[79] K. Chow and Arne. Holdø, "Numerical prediction of indoor temperature stratification," *The International Journal of Multiphysics*, vol. 2, no. 4, pp. 355–366, 2008, doi: 10.1260/1750-9548.2.4.355.

[80] IPCC, *Foreword Technical and Preface*. 2019.

[81] S. I. Edition, *Fundamentals*. 2017.

[82] *2017 ASHRAE® Handbook - Fundamentals (SI Edition)*. American Society of Heating Refrigerating and Air-Conditioning Engineers Inc., 2017.

[83] S. I. Edition, *Fundamentals*. 2017.

[84] ANSI/ASHRAE, "ANSI/ASHRAE Standard 55-2017 : Thermal Environmental Conditions for Human Occupancy," *ASHRAE Inc.*, vol. 2017, p. 66, 2017, doi: ISSN 1041-2336.

[85] M. M. Gouda, S. Danaher, and C. P. Underwood, "Application of an artificial neural network for modelling the thermal dynamics of a building's space and its heating system," *Mathematical and Computer Modelling of Dynamical Systems*, vol. 8, no. 3, pp. 333–344, 2002, doi: 10.1076/mcmd.8.3.333.14097.

[86] P. Hietaharju, M. Ruusunen, and K. Leivisk, "A dynamic model for indoor temperature prediction in buildings," *Energies*, vol. 11, no. 6, 2018, doi: 10.3390/en11061477.

[87] T. Lu and M. Viljanen, "Prediction of indoor temperature and relative humidity using neural network models: Model comparison," *Neural Computing and Applications*, vol. 18, no. 4, pp. 345–357, 2009, doi: 10.1007/s00521-008-0185-3.

[88] L. Nazarenko *et al.*, "Future climate change under RCP emission scenarios with GISS ModelE2," *Journal of Advances in Modeling Earth Systems*, vol. 7, no. 1, pp. 244–267, 2015, doi: 10.1002/2014MS000403.

[89] F. J. S. De La Flor, R. O. Cebolla, J. L. M. Félix, and S. Á. Domínguez, "Solar radiation calculation methodology for building exterior surfaces," *Solar Energy*, vol. 79, no. 5, pp. 513–522, 2005, doi: 10.1016/j.solener.2004.12.007.

[90] O. M. Brastein, D. W. U. Perera, C. Pfeifer, and N. O. Skeie, "Parameter estimation for grey-box models of building thermal behaviour," *Energy and Buildings*, vol. 169, pp. 58–68, 2018, doi: 10.1016/j.enbuild.2018.03.057.

[91] X. Tian, J. Yan, Y. Yang, C. Xiao, and Q. Zhou, "Parameter identification of a nonlinear model using an improved version of simulated annealing," *International Journal of Distributed Sensor Networks*, vol. 15, no. 2, 2019, doi: 10.1177/1550147719832788.

[92] P. Bacher and H. Madsen, "Identifying suitable models for the heat dynamics of buildings," *Energy and Buildings*, vol. 43, no. 7, pp. 1511–1522, 2011, doi: 10.1016/j.enbuild.2011.02.005.

[93] R. Dickinson and B. Brannon, "Generating future weather files for resilience," *36 th International Conference on Passive and Low Energy Architecture. Cities, Buildings, People: Towards Regenerative Environments*, 2016.

[94] L. Troup and D. Fannon, "Morphing climate data to simulate building energy consumption," *ASHRAE and IBPSA-USA Building Simulation Conference*, pp. 439–446, 2016.

[95] "No Title." [Online]. Available: https://www.weathershift.com/heat

[96] T. Catalina, J. Virgone, and F. Kuznik, "Evaluation of thermal comfort using combined CFD and experimentation study in a test room equipped with a cooling ceiling," *Building and Environment*, vol. 44, no. 8, pp. 1740–1750, 2009, doi: 10.1016/j.buildenv.2008.11.015.

[97] A. A. Youssef, E. M. Mina, A. R. ElBaz, and R. N. AbdelMessih, "Studying comfort in a room with cold air system using computational fluid dynamics," *Ain Shams Engineering Journal*, vol. 9, no. 4, pp. 1753–1762, 2018, doi: 10.1016/j.asej.2016.07.005.

[98] M. Wang and Q. Chen, "Assessment of various turbulence models for transitional flows in an enclosed environment (RP-1271)," *HVAC and R Research*, vol. 15, no. 6, pp. 1099–1119, 2009, doi: 10.1080/10789669.2009.10390881.

[99] C. Sun, S. Shu, G. Ding, X. Zhang, and X. Hu, "Investigation of time lags and decrement factors for different building outside temperatures," *Energy and Buildings*, vol. 61, pp. 1–7, Jun. 2013, doi: 10.1016/j.enbuild.2013.02.003.

[100] R. Watkins and G. J. Levermore, “Quantifying the effects of climate change and risk level on peak load design in buildings,” *Building Services Engineering Research and Technology*, vol. 32, no. 1, pp. 9–19, 2011, doi: 10.1177/0143624409357122.

[101] N. Wang, J. Zhang, and X. Xia, “Energy consumption of air conditioners at different temperature set points,” *IEEE AFRICON Conference*, no. September 2018, 2011, doi: 10.1109/AFRCON.2011.6072174.

[102] G. Krese, M. Prek, and V. Butala, “Analysis of building electric energy consumption data using an improved cooling degree day method,” *Strojniski Vestnik/Journal of Mechanical Engineering*, vol. 58, no. 2, pp. 107–114, 2012, doi: 10.5545/sv-jme.2011.160.

[103] K. Gowri, D. Winiarski, and R. Jarnagin, “Infiltration Modeling Guidelines for Commercial Building Energy Analysis,” *Contract*, no. September, p. 21, 2009, doi: PNNL-18898.

[104] M. H. Sherman, “Building Airtightness: Research and Practice,” no. January 2004, 2014.

[105] M. a. J. F. N. Humphreys, “1998 H&N Understandng the adaptive approach.pdf,” 1998.

[106] P. Schober and L. A. Schwarte, “Correlation coefficients: Appropriate use and interpretation,” *Anesthesia and Analgesia*, vol. 126, no. 5, pp. 1763–1768, 2018, doi: 10.1213/ANE.0000000000002864.

[107] P. Remmen, M. Lauster, M. Mans, M. Fuchs, T. Osterhage, and D. Müller, “TEASER: an open tool for urban energy modelling of building stocks,” *J Build Perform Simul*, vol. 11, no. 1, 2018, doi: 10.1080/19401493.2017.1283539.

ANNEX I – THERMAL COMFORT SURVEY

E1. THERMAL ENVIRONMENT POINT-IN-TIME SURVEY

1. **Record the approximate outside air temperature _____ and seasonal conditions:**

   ☐ Winter ☐ Spring ☐ Summer ☐ Fall

2. **What is your general thermal sensation? (Check the one that is most appropriate)**

*(**Note to survey designer:** This scale must be used as-is to keep the survey consistent with ASHRAE Standard 55.)*

☐ Hot
☐ Warm
☐ Slightly Warm
☐ Neutral
☐ Slightly Cool
☐ Cool
☐ Cold

3. **Either (a) place an "X" in the appropriate place where you are located now:**

*(**Note to survey designer:** Provide appropriate sketch for your space or building.)*

or (b) **place an "X" in the check box that best describes the area of the building where you are located now.**

☐ North
☐ East
☐ South
☐ West
☐ Core
☐ Don't know

4. **On which floor of the building are you located now?**

☐ 1st
☐ 2nd
☐ 3rd
☐ Other (provide the floor number): ______________

5. **Are you near an exterior wall (within 15 ft)?**

☐ Yes
☐ No

6. **Are you near a window (within 15 ft)?**

☐ Yes
☐ No

7. **Using the list below, please check each item of clothing that you are wearing right now. (Check all that apply):**

*(**Note to survey designer:** This list can be modified at your discretion.)*

☐ Short-Sleeve Shirt	☐ Dress	☐ Nylons
☐ Long-Sleeve Shirt	☐ Shorts	☐ Socks
☐ T-shirt	☐ Athletic Sweatpants	☐ Boots
☐ Long-Sleeve Sweatshirt	☐ Trousers	☐ Shoes
☐ Sweater	☐ Undershirt	☐ Sandals
☐ Vest	☐ Long Underwear Bottoms	
☐ Jacket	☐ Long Sleeve Coveralls	
☐ Knee-Length Skirt	☐ Overalls	
☐ Ankle-Length Skirt	☐ Slip	

☐ Other: (Please note if you are wearing something not described above, or if you think something you are wearing is especially heavy.) ________________

8. **What is your activity level right now? (Check the one that is most appropriate)**

☐ Reclining
☐ Seated
☐ Standing relaxed
☐ Light activity standing
☐ Medium activity standing
☐ High activity

Figure X1 Thermal Environment Point-in-Time Survey

E2. THERMAL ENVIRONMENT SATISFACTION SURVEY[1]

1. Either (a) place an "X" in the appropriate place where you spend most of your time:

(Note to survey designer: Provide appropriate sketch for your space or building.)

or (b) place an "X" in the check box that best describes the area of the building where your space is located.

☐ North
☐ East
☐ South
☐ West
☐ Core
☐ Don't know

2. On which floor of the building is your space located?

☐ 1st
☐ 2nd
☐ 3rd
☐ Other (provide the floor number)________________

3. Are you near an exterior wall (within 15 ft)?

☐ Yes
☐ No

4. Are you near a window (within 15 ft)?

☐ Yes
☐ No

5. Which of the following do you personally adjust or control in your space? (Check all that apply.)

(Note to survey designer: This list can be modified at your discretion.)

☐ Window blinds or shades
☐ Room air-conditioning unit
☐ Portable heater
☐ Permanent heater
☐ Door to interior space
☐ Door to exterior space
☐ Adjustable air vent in wall or ceiling
☐ Ceiling fan
☐ Adjustable floor air vent (diffuser)
☐ Portable fan
☐ Thermostat
☐ Operable window
☐ None of these
☐ Other: ________________________

Please respond to the following questions based on your overall or average experience in the past [six] months.

(Note to survey designer: The above statement can be modified for a different span of time.)

6. How satisfied are you with the temperature in your space? (Check the one that is most appropriate)

7. If you are dissatisfied with the temperature in your space, which of the following contribute to your dissatisfaction:

a. In warm/hot weather, the temperature in my space is (check the most appropriate box):

(Note to survey designer: Include a scale or, as shown below, check boxes.)

☐ Always too hot
☐ Often too hot
☐ Occasionally too hot
☐ Occasionally too cold
☐ Often too cold
☐ Always too cold

b. In cool/cold weather, the temperature in my space is (check the most appropriate box):

(Note to survey designer: Include a scale or, as shown below, check boxes.)

☐ Always too hot
☐ Often too hot
☐ Occasionally too hot
☐ Occasionally too cold
☐ Often too cold
☐ Always too cold

c. When is this most often a problem? (check all that apply):

☐ Morning (before 11am)
☐ Mid-day (11am–2pm)
☐ Afternoon (2pm–5pm)
☐ Evening (after 5pm)
☐ Weekends/holidays

[1] This survey has been adapted from the CBE occupant IEQ survey developed by the Center for the Built Environment at the University of California at Berkeley.

Figure X2 Thermal Environment Satisfaction Survey

- ☐ Monday mornings
- ☐ No particular time
- ☐ Always
- ☐ Other:

d. **How would you best describe the source of this discomfort? (Check all that apply):**

*(**Note to survey designer:** This list can be modified at your discretion.)*

- ☐ Humidity too high (damp)
- ☐ Humidity too low (dry)
- ☐ Air movement too high
- ☐ Air movement too low
- ☐ Incoming sun
- ☐ Heat from office equipment
- ☐ Drafts from windows
- ☐ Drafts from vents
- ☐ My area is hotter/colder than other areas
- ☐ Thermostat is inaccessible
- ☐ Thermostat is adjusted by other people
- ☐ Clothing policy is not flexible
- ☐ Heating/cooling system does not respond quickly enough to the thermostat
- ☐ Hot/cold surrounding surfaces (floor, ceiling, walls or windows)
- ☐ Deficient window (not operable)
- ☐ Other: ____________________

e. **Please describe any other issues related to being too hot or too cold in your space:**

Figure X2 (continued) Thermal Environment Satisfaction Survey

ANNEX II – EQUIPMENT SURVEY RESULTS FOR BUILDING 1

Room	**Equipment**	**No. of equipment**	**Rated Wattage (W)**	**Heat gain**				**Usage Factor**	**Radiant factor**
				Sensible Convective (W)	*Sensible Radiant (W)*	*Latent (W)*	*Total(W)*		
Cafeteria	Microwave oven	3	1700	0	0	0	0	0	0
	Serving cabinet	8	1993	205	821	0	1026	0.51	0.2
	Coffee brewer	5	3810	59	88	205	352	0.08	0.17
	Freezer	6	790	147	176	0	323	0.41	0.45
	Oven	2	5000	718	3214	0	3932	0.79	0.18
	Reach in refrigerat	5	1407	88	264	0	352	0.25	0.25
	Rice cooker	2	1550	14	68	0	82	0.05	0.17
	Boiler (hooded)	8	2450	822	0	0	822	0.84	0.35

	Computers	5	750	83	-	-	83	1	1
	Television	5	240	26	-	-	26	1	1
	Speakers	6	220	15	-	-	15	1	1
	Cash register	5	25	9	-	-	9	1	1
	Mobile phones	35	NA	3	-	-	3	1	1
Office	Coffee brewer	5	3810	59	88	205	352	0.08	0.17
	Computers	36	750	83	-	-	83	1	1
	Television	4	240	26	-	-	26	1	1
	Speakers	6	220	15	-	-	15	1	1
	Phone charger	10	NA	5	-	-	5	1	1
	Mobile phones	41	NA	3	-	-	3	1	1

	Photo copier	2	250	28.5	-	-	28.5	1	1
	Printer	4	200	14.5	-	-	14.5	1	1
	Top mounted	1	1200	172	-	-	172	1	1
Timber Deck	-	-	-	-	-	-	-	-	-

ANNEX III – NARX MODEL TRAINING AND ERROR PLOTS

Zone 1.1

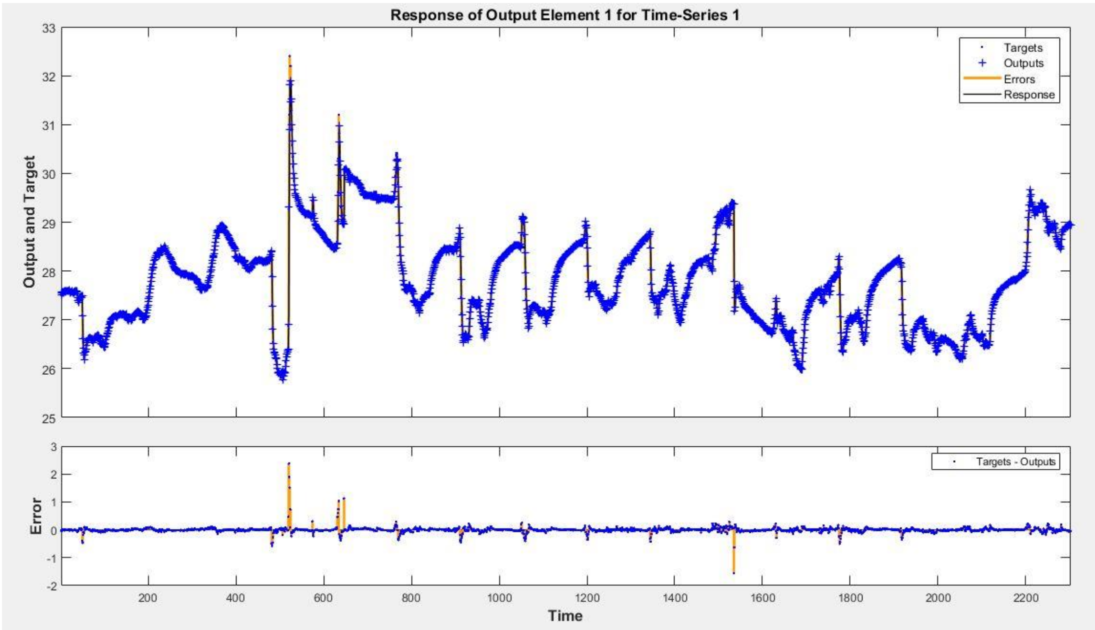

Zone 1.2

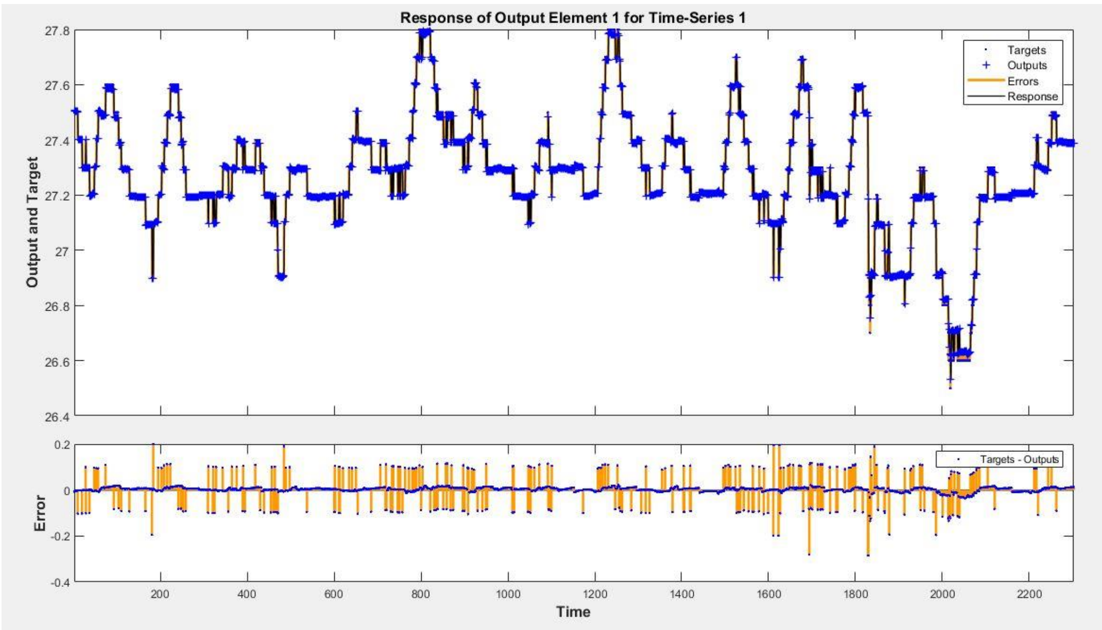

Zone 1.3

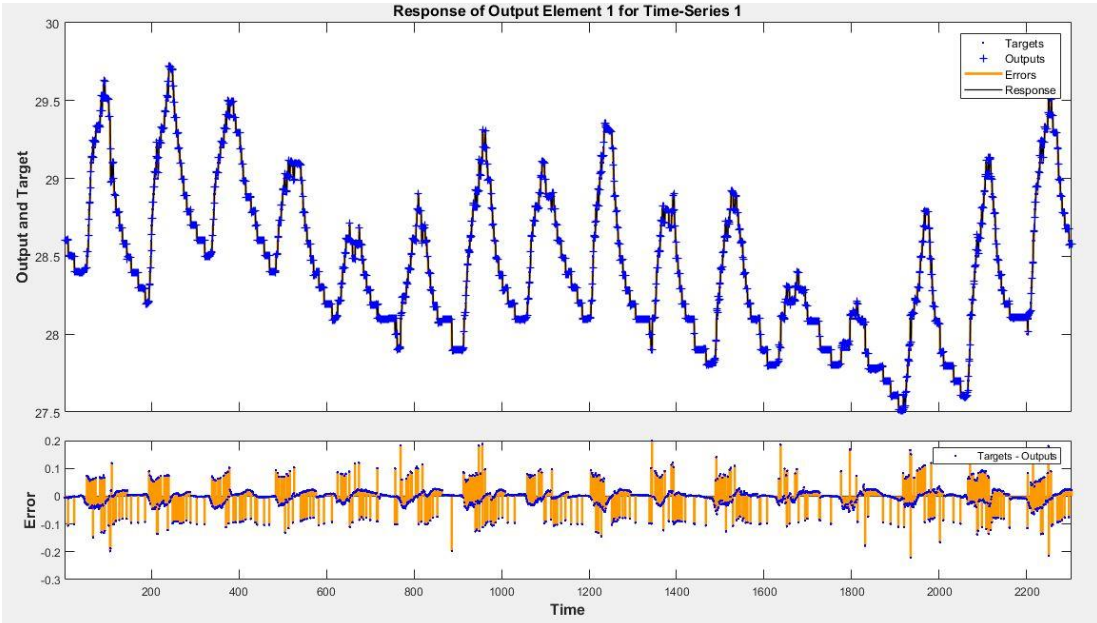

Zone 2.1

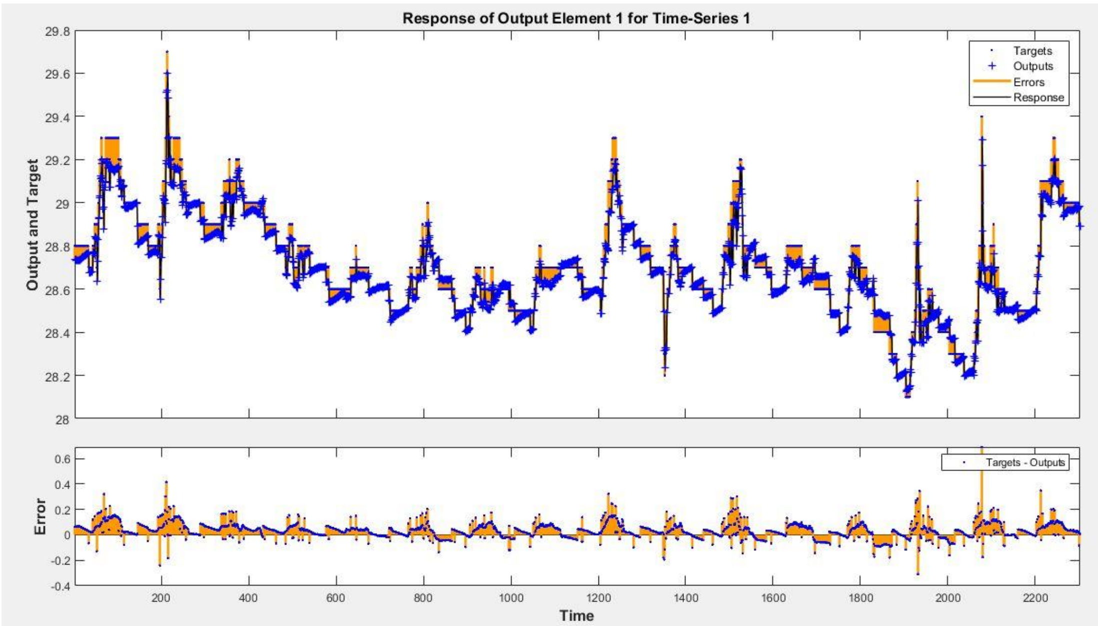

Zone 2.2

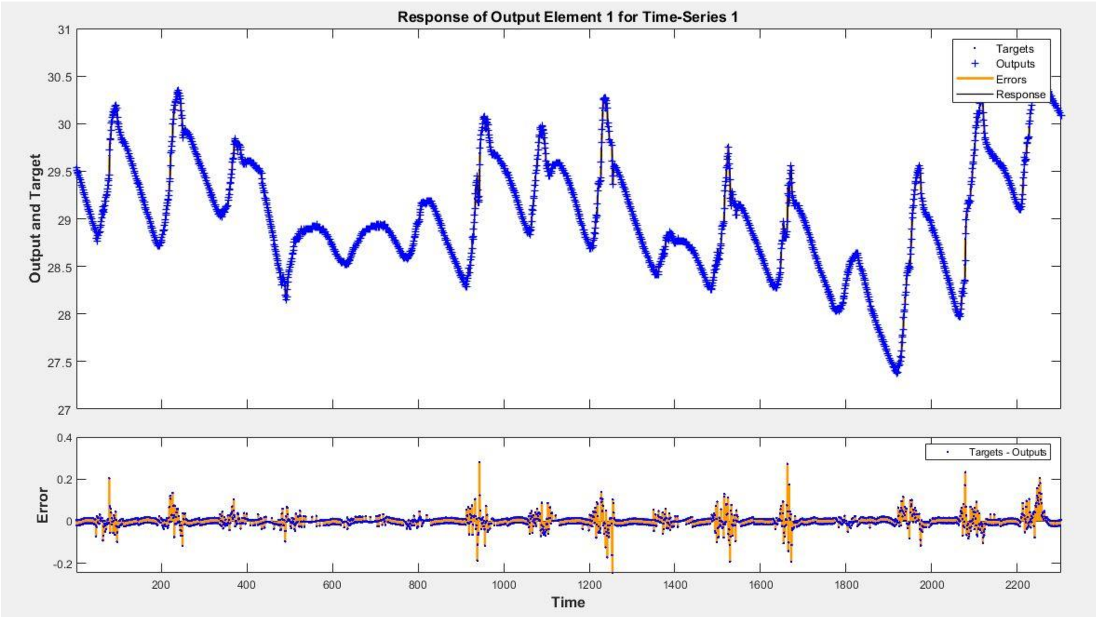

Zone 2.3

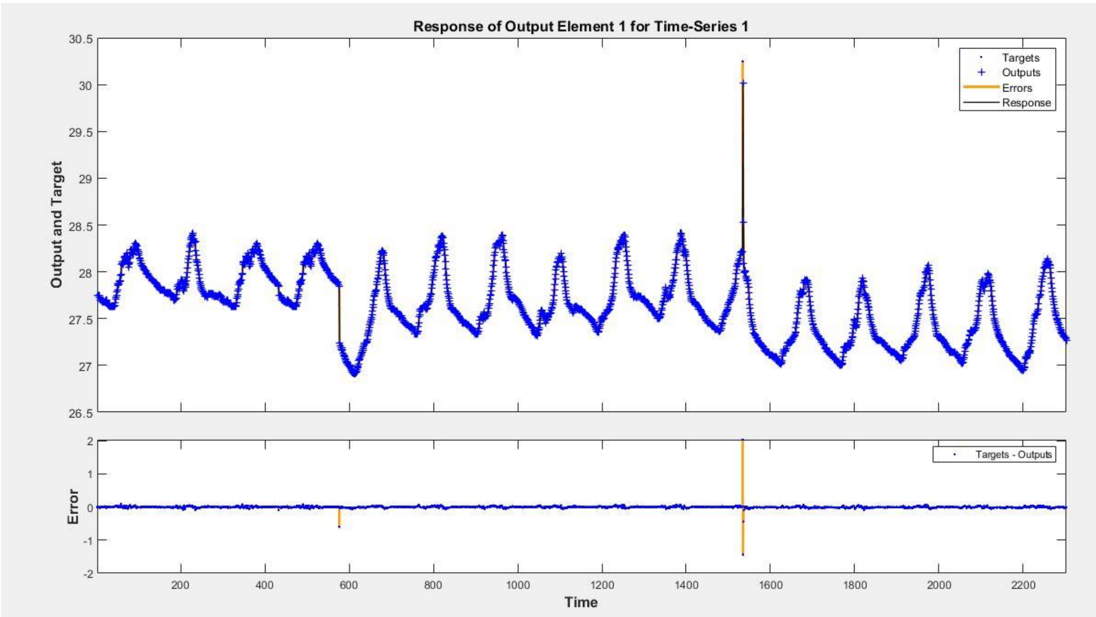

Zone 3.1

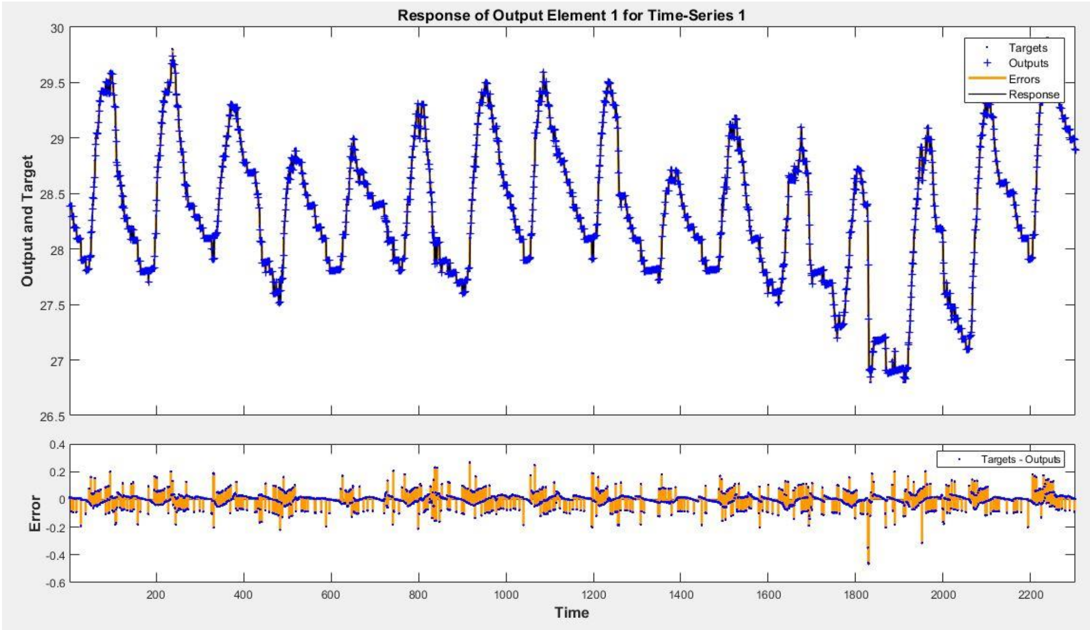

Zone 3.2

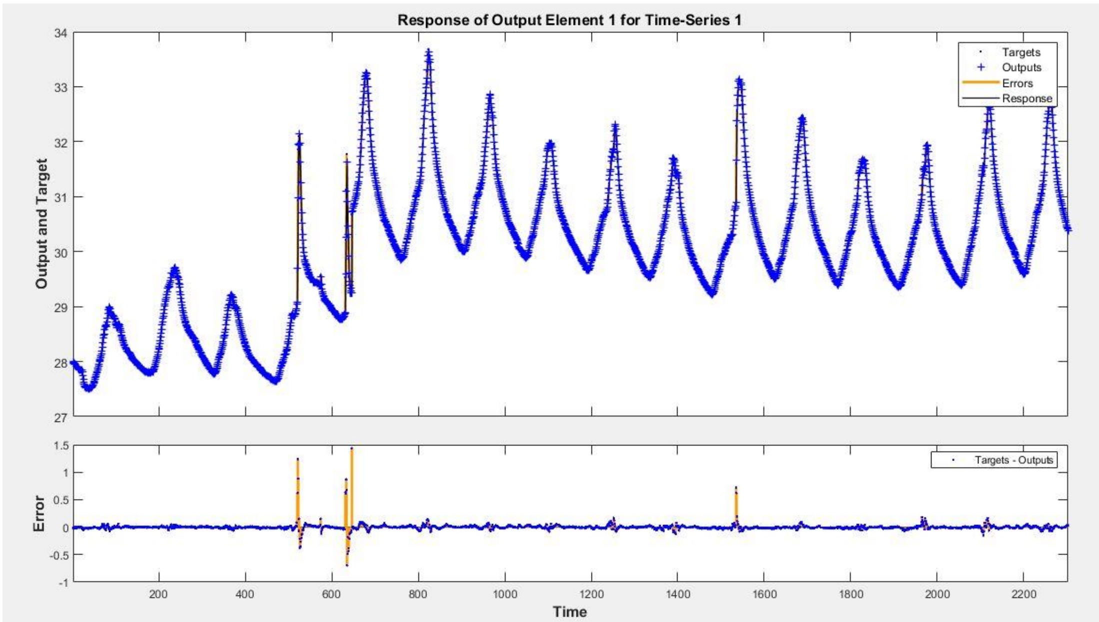

ANNEX IV – GREY BOX MODEL INDOOR TEMPERATURE PREDICTIONS FOR 2090

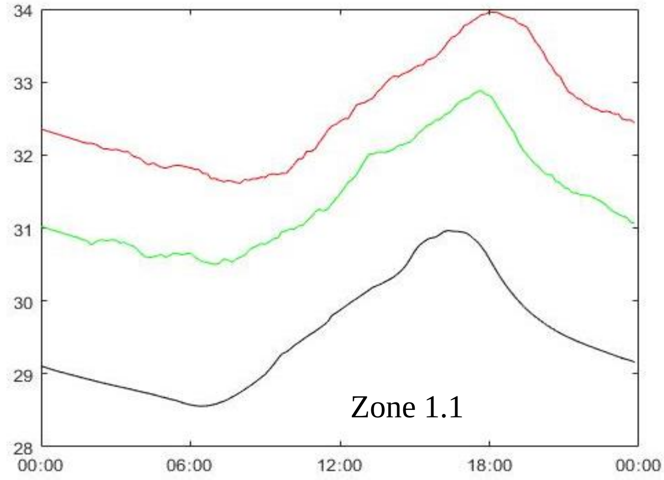

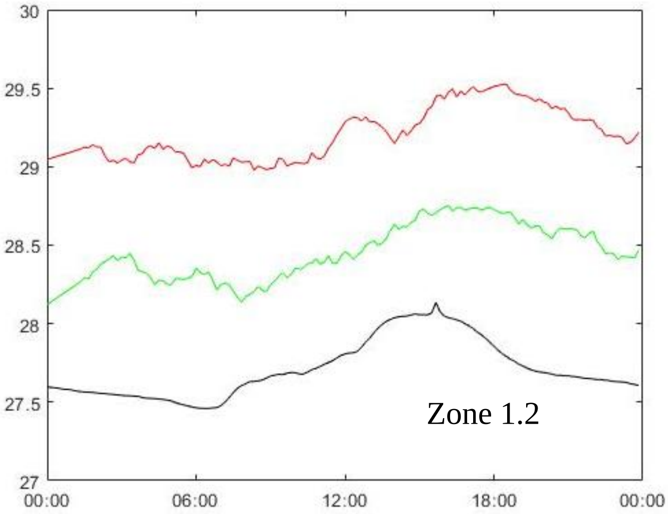

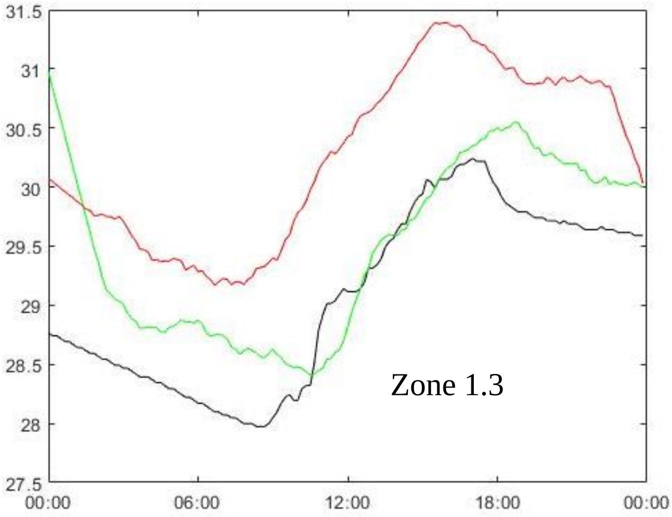

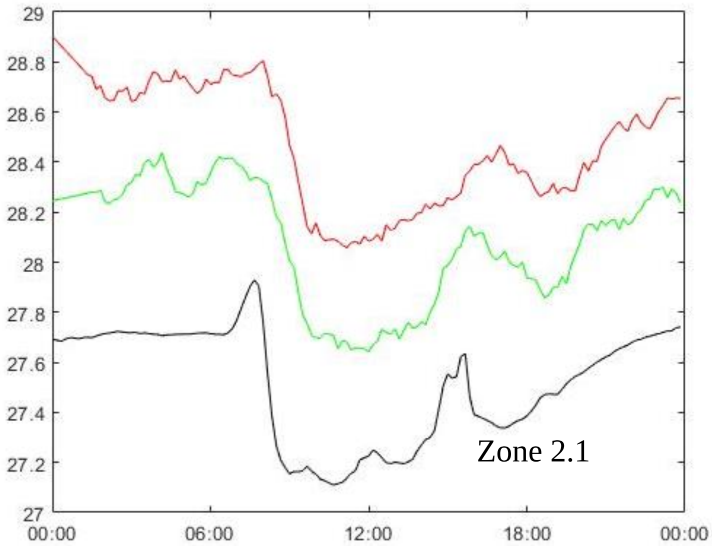
29
28.8
28.6
28.4
28.2
28
27.8
27.6
27.4
27.2
27
00:00
06:00
12:00
18:00
00:00
Zone 2.1

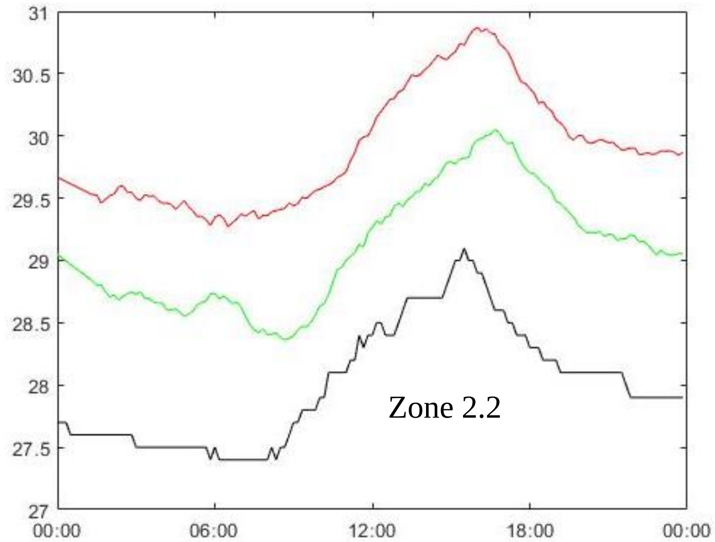
31
30.5
30
29.5
29
28.5
28
27.5
27
00:00
06:00
12:00
18:00
00:00
Zone 2.2

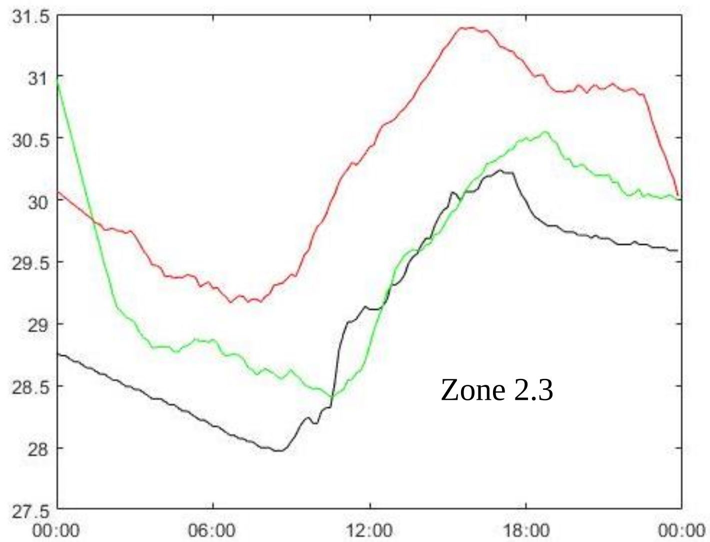
31.5
31
30.5
30
29.5
29
28.5
28
27.5
00:00
06:00
12:00
18:00
00:00
Zone 2.3

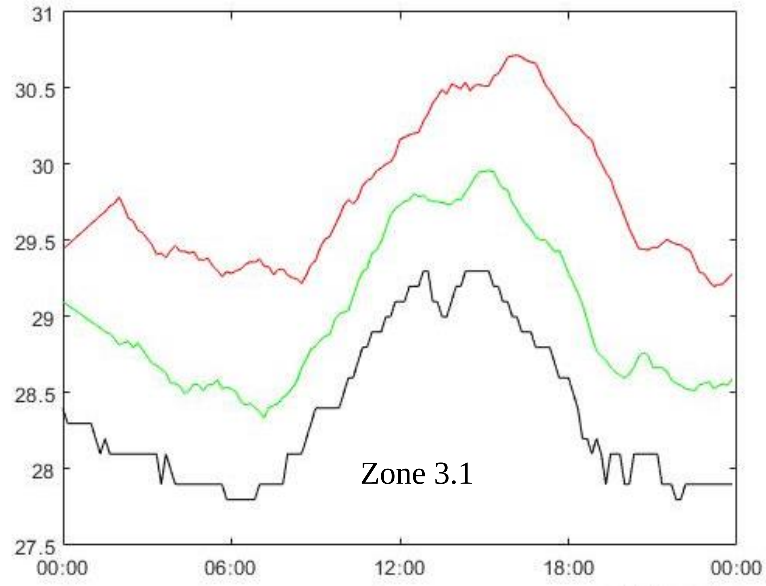
31
30.5
30
29.5
29
28.5
28
27.5
00:00
06:00
12:00
18:00
00:00
Zone 3.1